SOL-GEL ROUTES TO TRANSPARENT CONDUCTIVE COATINGS

by

Maria Sugrue

A thesis submitted in partial fulfilment of the requirements of Kingston University for the degree of Doctor of Philosophy

December 1999

This research was carried out in collaboration with the Defence Evaluation and Research Agency, Farnborough, under Contract number SMCFU/599

Sol-Gel Routes to Transparent Conductive Coatings

Abstract

A novel sol-gel process has been developed for producing transparent conductive tin dioxide films and for their application to polymer substrates.

Initially, tin oxide was produced by hydrolysis of tin tetrachloride using amended versions of methods found in the literature. The tin oxide produced from the procedure did not adhere well to glass and was not transparent. The procedure was also very time consuming.

Preliminary experiments using tin bis (acetylacetonate) dichloride as a precursor were very promising and all efforts were soon concentrated on that route. After a lot of experimentation optimising the method, it was found that colloids capable of producing conductive transparent tin oxide coatings were obtained approximately 10 days after beginning the procedure.

Indium and antimony dopants were added to the tin oxide at the sol-gel stage in order to investigate their effect on the DC conductivities of the tin oxide coatings. Bulk conductivities in the ranges 1 to 100 Sm^{-1} and 13 to 800 Sm^{-1} were obtained for p- and n-type doped annealed tin oxide coatings on glass substrates respectively. The percentage transparencies of the coatings remained high for unannealed coatings (~80%) but decreased to ~ 40% after annealing.

Polymer pre-treatments were carried out on the poly (methyl methacrylate), polycarbonate and poly (ethylene terephthalate) substrates. The contact angles and surface energies of the substrates were studied to investigate the effects of the surface pre-treatment techniques. Treatment of the poly (methyl methacrylate) and poly (ethylene terephthalate) substrates consisted of hydrolysis by aqueous sodium hydroxide. A combination of UV/ozone oxidation was used for the polycarbonate substrates.

The tin oxide coatings were applied to the polymer substrates by spin-coating, solvent casting and spray coating. From optical microscopy studies, it was shown that the spin-coated films were the most uniform and least cracked. To further increase the adhesion of the coatings on the polymeric substrates, a systematic study was made of the effects of coupling agents, both on the substrate surfaces and in the sol-gel solutions themselves. Short pulses of heating were given to the coatings in an infrared furnace. The annealing did not increase the bulk conductivities greatly but the coatings retained a very high transparency (greater than 90%). To investigate the effect of infrared annealing on tin oxide powder, it was shown from X-ray diffraction that the crystallinity of the tin oxide increased significantly as a result of annealing in the infrared furnace.

ACKNOWLEDGEMENTS

First and foremost I would like to thank my supervisor, Prof. Peter Foot for his supervision and expert guidance throughout this research. My gratitude also goes to my second supervisor, Dr. Richard Singer for his encouragement and helpful suggestions. Many thanks to the Defence Evaluation and Research Association (DERA) who funded this study.

At the DERA I would like to thank Mr. Ian Youngs and Dr. Eoin O'Keefe for many useful and constructive discussions. Thanks go to the lecturers and technical staff in the School of Applied Chemistry at Kingston University who have assisted me during my research. In particular Bill Edwards, Trisha Hill, Simon de Mars, Fred Quentin and June Falla. Thanks are also extended to the DERA for the use of their laboratory facilities.

Kingston wouldn't have been the same without the friends I made there. I want to thank them for giving me great memories of Kingston and for keeping me smiling. I thank Caroline, Slick, Denis, Neal, Jat, Greig, Jackie, Parissa and Cathriona. Also thanks to Ruth for the many phone calls and sisterly support. Thanks to the girls in Dublin: Rena, Anna-Marie, Paula and Jean for putting up with me for the last six months. To Simon, extra special thanks for being there for me during the last year and a half and for being such a good friend.

Finally, to my parents, sister and brothers for all your love and support I am most heartfully grateful. Without your faith in me, none of this would have been possible.

GLOSSARY OF ABBREVIATIONS

acac	acetylacetonate
AES	Atomic emission spectroscopy
FTIR	Fourier transform infrared analysis
ICP	Inductively coupled plasma
IMS	Industrial methylated spirits
IPA	Isopropanol
ITO	Indium tin oxide
PC	Polycarbonate
PEN	Poly (ethylene naphthalate)
PET	Poly (ethylene terephthalate)
PMMA	Poly (methyl methacrylate)
SEM	Scanning electron microscopy
THF	Tetrahyrofuran
TG	Thermogravimetric analysis
XRD	X-ray diffraction

CONTENTS

1.1 Introduction

This chapter discusses the general background to the project and relevant work carried out in relation to it. Section 1.2 contains an introduction to some terms relating to colloids, followed by the history and main reactions of the sol-gel process. Some previous work using sol-gel processes to produce tin oxide and other metal oxides is reviewed. The properties and applications of tin oxide are then discussed in terms of its crystal structure and its energy band diagram. Finally, the objectives of the project are outlined, followed by the proposed plan of experimental work.

1.2 Colloids

The term "colloid" was originally used to describe particles of small dimension that could not pass through porous membranes with a pore size of approximately 10^{-6}m [1]. Nowadays however, colloids are defined as particles which fit within the size range 1 to 1000nm[2-4]. A colloidal system consists of two or more phases, where one phase is in colloidal dimensions. The particles of the dispersed phase are so small (1 - 1000nm) that gravitational forces are negligible and interactions are dominated by short-range forces, such as van der Waals attractions and surface charges. Some common everyday examples of colloidal dispersions are given in table 1.1 below.

In the last fifty years, interest has increased in colloidal processes due to advances in techniques such as small angle x-ray scattering, Raman spectroscopy, small angle neutron scattering and light scattering which allow detailed investigations of the processes in colloidal dimensions.

Table 1.1: Examples of Colloidal Dispersions

Colloidal Term	Dispersed Phase	Dispersion Medium	Examples
Solid aerosol	Solid	Gas	smoke, dust
Emulsion	Liquid	Liquid	milk, mayonnaise
Liquid aerosol	Liquid	Gas	Fog, liquid sprays
Foam	Gas	Liquid	Fire-extinguisher foam
Sol	Solid	Liquid	Toothpaste, dye
Solid suspension	Solid	Solid	Pigmented plastics
Solid Foam	Gas	Solid	Expanded polystyrene
Solid emulsion	Liquid	Solid	Opal, pearl

1.3 Sols and their Stability

The formation of sol particles involves the degradation of bulk matter or the aggregation of molecules or ions. The dispersion method usually requires the addition of an inert diluent or wet milling in the presence of a surfactant in order to avoid the tendency of the particles to re-unite. The aggregation method involves forming a molecularly dispersed supersaturated solution, from which the colloid precipitates in a suitably divided form. The aggregation method is a more favourable method as it results in more finely dispersed systems[3].

In the production of sols, the particle sizes produced depend upon the relative rates of nucleation and growth. In order to produce monodispersed sols, the crystallization of the nuclei must be rapid but the actual growth of the crystals must be slow. Polydispersed systems are more usual when the processes of crystallization and growth of particles occur simultaneously. Particles of a typical sol might consist of agglomerates of between 10^3 and 10^9 atoms, either in an elemental state or in the form of ions of molecules.

Sols are divided into two classes: lyophilic ("solvent loving") and lyophobic ("solvent hating"), depending on the ease with which the system can dispersed if it has been allowed to dry out. Lyophilic sols can be dispersed easily by adding a suitable solvent to the dry colloid. They will swell at first as they take up the liquid and finally form a homogeneous solution, a typical example of a lyophilic colloidal solution being the preparation of jelly from the protein gelatin. Most biological colloids are lyophilic in character e.g. proteins and polysaccharides. Lyophobic colloids, however can only be dispersed by vigorous mechanical agitation, or by the application of some other external source of energy. Most colloids used for technological applications are lyophobic[4].

The stability of a sol is determined by the relative magnitudes of the forces of attraction and repulsion between the particles. These depend on such factors as the nature and size of the particles, their distance apart and the ionic strength of the dispersion medium. Repulsion must exceed attraction if the system is to remain dispersed, otherwise agglomeration will take place. Lyophilic sols are not affected by electrolyte concentrations of the surrounding medium until it becomes quite high. Lyophobic colloids, on the other hand can be significantly affected by quite low concentrations of electrolyte ($< 10^{-2}$M). A natural occurrence illustrating the effect electrolytes can have on colloidal systems is the precipitation of colloidal mud at river mouths due to salinity.

1.4 The Sol-Gel Process

As the name suggests, the sol-gel process involves the conversion of a sol to a gel. It is mostly used for materials applications, in the production of multi-component metal oxide coatings. The multi-component oxide produced can take the form of a glass, a glass ceramic or a crystalline substance[5]. The main advantage of the sol-gel process over traditional methods of producing ceramics and glasses is that it is a low temperature process. Another important advantage is its usefulness in coating large and unusually-shaped objects through dip-coating[6]. The metal oxides produced have good homogeneity and stoichiometry due to the fact that the main starting materials, metal alkoxides can be subjected to high purification operations e.g. distillation, crystallization or electrolysis.

Also, due to the low processing temperatures involved in the sol-gel process, additional impurities are minimized[7-10].

Historically the first paper reporting a sol-gel synthesis was in 1846, describing Ebelmann and Grahams' studies on silica gels[6]. They observed that under acidic conditions the hydrolysis of tetraethyl orthosilicate (TEOS), $Si(OC_2H_5)_4$ yielded SiO_2 in the form of a "glass-like material". However, extremely long drying times of over 1 year were required in order to avoid the silica gels becoming fine powders. It wasn't until almost a century later that more significant interest was taken in the sol-gel process.

The first dip-coating patents appeared in 1939 when Geffcken and Berger reported using a sol-gel process to prepare single oxide coatings[11]. In 1953 the first products from sol-gel processes appeared on the market and in 1959 large scale production of automotive rear-mirrors (TiO_2-SiO_2-TiO_2) began. Over the following ten years, commercial products of the sol-gel process included anti-reflection coatings (TiO_2/SiO_2-TiO_2-SiO_2) and sunshielding windows[5]. Another more unusual application of sol-gel technology is in the production of microspheres of crystalline nuclear waste forms in the safe disposal of "spent" nuclear fuel[12].

The main reactions involved in the sol-gel process are hydrolysis and condensation[13]. In the following scheme, M represents silicon or a metal which is attached through an oxygen atom to a hydrocarbon moiety, R.

$$\text{M-OR} + \text{H}_2\text{O} \rightarrow \text{M-OH} + \text{R-OH} \quad \ldots\ldots(1)$$

$$\text{M-OR} + \text{OH-M} \rightarrow \text{M-O-M} + \text{ROH} \quad \ldots\ldots(2)$$

$$\text{M-OH} + \text{OH-M} \rightarrow \text{M-O-M} + \text{H}_2\text{O} \quad \ldots\ldots(3)$$

Step (1) hydrolysis is followed by polycondensation reactions (2) and (3), which occur simultaneously, making it difficult to follow the process. The above reactions lead to mixed oxide hydroxides, of the general formula $[MO_{y-x}(OH)_{2x}]_n$, where y = metal

valency/2, x = fractional degree of hydration, n = an integer (degree of polymerisation). Figure 1.1 shows a scheme for the formation of tin oxyhydroxide during the ageing of a sol[14].

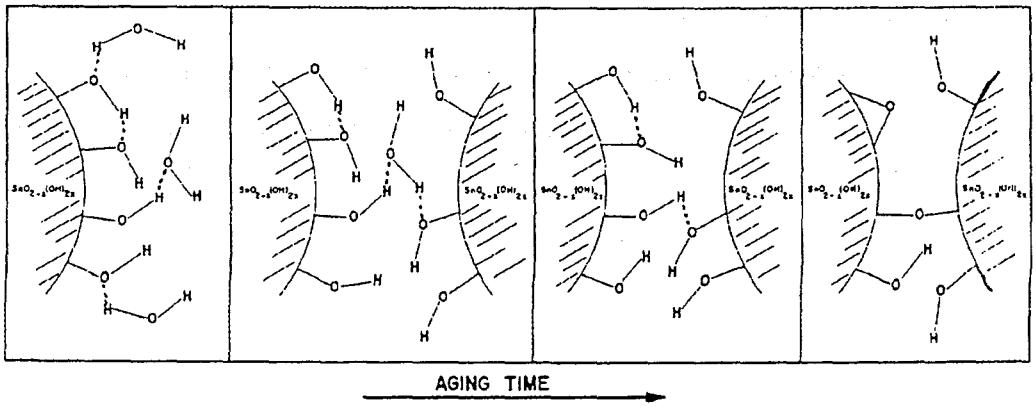

Figure 1.1: Ageing of a Sol

As above, in the formation of a gel, if the monomer can make more than 2 bonds, then there is no limit on the size of the molecule that can form. If one molecule reaches macroscopic dimensions so that it extends throughout the solution, the substance is said to be a gel. Thus, a gel is a substance that contains a continuous solid skeleton enclosing a continuous liquid phase. The *gel point* is the time at which the last bond is formed that completes the giant molecule[15]. Bond formation does not stop at the gel point however, segments of the gel network can still move close enough together to allow further condensation (or other bond formation processes).

Ageing is a term applied to the process of change in structure and properties after gelation. It can involve condensation, dissolution and reprecipitation of monomers and oligomers, or phase transformations within the liquid or solid phases. Spontaneous shrinkage, or *syneresis* happens in some gels as bond formation or attraction between particles induces contraction of the network and expulsion of the liquid from the pores.

Drying of gels by evaporation under normal conditions gives rise to capillary pressure that causes shrinkage of the gel network. The resulting dried gel is called a *xerogel*, often

reduced in volume by a factor of 5 or 10. If the wet gel is placed in an autoclave and dried under supercritical conditions, there is no interface between liquid and vapour, therefore no capillary pressure and relatively little shrinkage. This process is called *supercritical drying*, and the result is called an *aerogel*. The aerogel is very porous and can mostly be air, having volume fractions of solid as low as 1%. Figure 1.2 below shows the various products that can be formed from a sol-gel process.

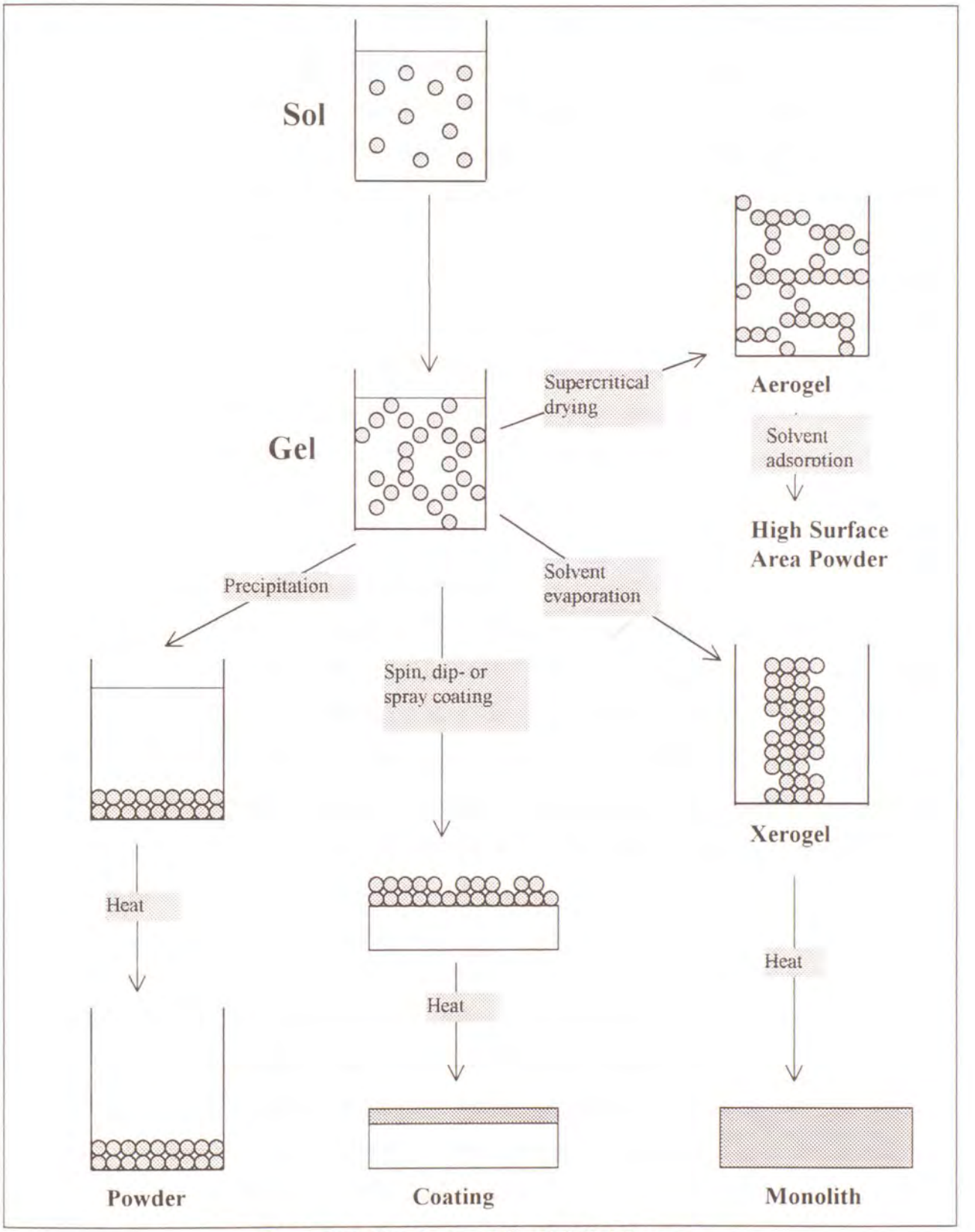

Figure 1.2: Products of the Sol-Gel Process

Alkoxides are the most common precursors in sol-gel research. Metal alkoxides are members of the family of metal organic compounds, which have an organic ligand attached to a metal or metalloid element e.g. tetra ethyl orthosilicate ($Si(OC_2H_5)_4$). Metal alkoxides are popular precursors because they react readily with water, hydrolysis. Also, because the metal alkoxides can be obtained in a very pure state, the products of the sol-gel process are also very pure[9, 16-19].

1.5 Metal Oxides Prepared from Sol-Gel Processes

This section is divided into two parts: the first sub-section deals with previous work carried out specifically in the area of sol-gel processes to produce tin oxide and the second sub-section describes some work carried out on the preparation of other metal oxides by sol-gel routes.

1.5.1 SnO_2 Prepared from Sol-Gel Processes

Over the last five to ten years, there has been a lot of interest in preparing tin oxide by sol-gel methods. Tin (IV) chloride ($SnCl_4$) is the most common starting material. The preparation typically starts with the hydrolysis of an aqueous solution of $SnCl_4$ using ammonium hydroxide (NH_4OH). The excess electrolyte ions (NH_4^+, Cl^-) in the resulting precipitate are removed (or partially removed) by dialysis or copious washing with water. Peptization of the sol then causes the formation of a gel, which can be used for coatings and other purposes.

W. Lada et al. prepared hydrous SnO_2 as described above, except that they added HNO_3 to peptize the sols[20]. Addition of HNO_3 (as a possible peptizing agent) was also tried in this work but it was unsuccessful. They also sometimes added ethanol to the colloidal suspensions, which resulted in coatings of better transparency than those not containing ethanol. They state that the addition of ethanol prevented agglomeration of the colloidal particles by the prevention of the formation of OH bridges, and that it can also have a positive effect in decreasing interfacial tension between the colloidal solution and the

recommendation of this reference to improve the transparency of the resulting gels but it did not have any effect on the transparency.

Hiratsuka *et al* used the same method to produce SnO_2 but their study was more concerned with the relationship between electrolyte concentration during the ageing of the gels and their resultant stability[14]. They found that the upper limit of stability for the colloidal suspensions was about 0.9mM Cl^-, and that above that value the aggregate size grows. Between concentrations of 9 and 20mM Cl^-, clusters grow slowly due to interactions among particles, and during ageing these clusters interact to form a gel. Above 20mM Cl^-, rapid aggregation occurs between the particles and gelation happens during ageing because of interactions between the aggregates. The authors' overall conclusion was that a gel which is formed more slowly is not destroyed when subjected to a small rate of shear. However, irrespective of electrolyte loading, condensation reactions occur to form Sn-O bonds. In agreement with Hiratsuka, de Souza Brito found that the degree of aggregation in the sols increases with the concentration of electrolyte[21]. This increase hinders condensation reactions during gelation, thus limiting the growth of crystalline regions which subsequently causes the formation of very porous films. On the basis of these findings, the chloride ion concentration of the tin oxide prepared in this study was kept as low as possible to minimize possible aggregation effects. The methods of removing the chloride ions and the results of the studies are discussed in chapter 2. De Souza Brito *et al.* also investigated the microstructural characteristics of SnO_2 xerogels as a function of electrolyte concentration and found that the mean crystallite size ranged from 3.2 to 2.1nm as the concentration of electrolyte in the suspensions increased from 0.05mM to 155mM Cl^-[21]. Their application for the SnO_2 xerogels was for ultrafiltration purposes, for which it is necessary to have pore sizes in the range of 1 to 100nm.

Dazhi *et al.* also studied the microstructure of SnO_2 prepared by a sol-gel process[22]. The tin oxide was prepared from $SnCl_4$ (as above), using distilled water to remove the Cl^- and NH_4^+ ions. They state that in general SnO_2 produced by sol-gel processes is a kind of nano-sponge material, consisting of many nanometre sized holes and nanocrystals. The

nanocrystals connect to each other in a random network which leads to a high concentration of surfaces and interfaces which could make it useful for catalysis. Tamaki *et al.* investigated the possibility of using ultrafine SnO_2 particles (prepared from $SnCl_4$ as above) in gas sensors[23]. Their work concentrated on trying to improve the sensitivity of the particles for such an application through the introduction of additives to stabilize the ultrafine particles. They found that the most effective additives were lanthanum, lead and zinc and that they could stabilize SnO_2 crystallites less than 10nm in size. Park *et al.* also report the production of tin oxide films for use as gas sensors. The tin oxide was prepared from tin (IV) isoproxide ($Sn(OC_3H_7)_4$) in isopropanol[24]. They added platinum and lanthanum oxide impurities to improve the response times of the sensors. It is reported that the La_2O_3 increased the surface area of the SnO_2 particles and the addition of platinum decreased the response time and increased sensitivity. The coatings which had the best overall response were Pt (0.5wt%)-La_2O_3(5wt%)-SnO_2 doubly loaded tin oxide coatings.

Crnjak-Orel and co-workers prepared antimony doped tin oxide from $SnCl_4.5H_2O$ and $SbCl_3$ dissolved in water[25]. Concentrated HCl was added to increase the solubility of the $SbCl_3$ and the resulting precipitates were washed with dilute NH_4NO_3 and H_2O until there was no trace of chloride ions. The highest conductivity was obtained for the sample containing 1.32 mol% antimony. They found that it was not possible to produce a gel with a concentration of antimony greater than 2.38 mol% although the initial concentration of antimony was a lot higher. Orel *et al.* used the same method of preparation as above to produce antimony doped tin oxide thin films on glass substrates[26]. However, they managed to increase the antimony dopant concentration in the coatings and found a minimum bulk resistivity of $1.2 \times 10^{-2}\Omega$cm for an antimony concentration of between 5 and 7mol% Sb in SnO_2. From this work, we also found that tin oxide gels could be produced with antimony concentrations up to 13 mol%.

Lin also prepared antimony doped SnO_2 from a mixture of $SnCl_4.5H_2O$ and $SbCl_3$ in ethanol[27]. The solutions were stirred, refluxed to form sols and aged in open beakers for 4 to 5 days to gel. Coatings were applied to glass substrates using spin-coating of the gel

suspensions and spraying of dried SnO_2 powders. It was found that increasing the doping concentration accelerates gelation. It also decreases the particle size and reduces the crystallinity of the dried gel. This is possibly because Sb could exist as Sb^{3+} or Sb^{5+} in solid solution and substitution of Sn^{4+} by Sb^{3+} or Sb^{5+} could generate vacancies and disturb local ordering of the crystal structure. The lowest surface resistance obtained was ~5 x 10^7 Ω/□ for a dopant concentration of 2.6mol%Sb. Terrier and co-workers also found evidence for slower crystallization in antimony doped tin oxide gels[28,29]. These SnO_2 powders were obtained from $SnCl_2.2H_2O$ and $SbCl_3$ precursors. It was found that higher temperatures and longer times were needed to reach densification for the doped samples since the introduction of dopant decreases the porosity of the gel. This porosity gave the Sb-doped layers a higher tendency to crack than undoped ones. It was found from XPS that a "competition" exists between the doping effects of Sb^{3+} and Sb^{5+} species substituted for Sn^{4+}. The best resistivity result was 3 x 10^{-3}Ωcm.

Maddalena prepared SnO_2 from $SnCl_2$ dissolved in absolute ethanol[30]. 3.0 mol% ZrO_2 and 3.0mol% TiO_2 dopants were added to improve the conductivity of the tin oxide powders. It was found that the zirconia and titania dopants increase the crystallization rate and cause an increase in electrical conductivity. The authors of reference 31 prepared undoped SnO_2 and antimony doped SnO_2 using the same procedure, and applied their coatings to pyrex[31]. They report that the undoped SnO_2 has a high resistivity of 1Ωcm, because they claim that there is no deviation from stoichiometry in undoped SnO_2 made by sol-gel methods. Their best resistivity result was 4.5 x 10^{-3}Ωcm, which was obtained for an antimony concentration of 10mol % in SnO_2. The band gap was calculated as 3.85eV for doped SnO_2 and 4 eV for undoped SnO_2.

Aegeter *et al.* prepared antimony doped SnO_2 coatings on silica and borosilicate slides from a coating solution of 5mol% $SbCl_3$ in a 0.5M ethanolic solution of $SnCl_2(OAc)_2$[32]. They did not achieve low resistivities for the coatings because they claim that sol-gel layers are built of small, almost spherical, loosely packed crystalline particles whereas coatings produced from spraying are composed of large, textured, densely packed particles

arranged in a columnar structure. However, they found that the resistivity decreases for multi-layer coatings, and that the coatings produced from sol-gel methods have better optical properties when compared to transparent conducting coatings prepared by other techniques. Mattox also did not have much success with preparing conductive undoped SnO_2 and antimony doped SnO_2 coatings by a sol-gel process[33]. Their starting materials were tin (IV) isoproxide ($Sn(OC_3H_7)_4$, indium (III) isopropoxide ($In(OC_3H_7)_3$ and liquid antimony butoxide ($Sb(III)(OC_4H_9)_3$. The SnO_2 films and Sb doped SnO_2 films showed no conductivity while the tin doped indium oxide (ITO) had a favourable result. They report that sodium from the substrate acts as a p-type doping agent, thus compensating in the case of both n-type SnO_2 and n-type Sb doped SnO_2. The average bulk resistivities obtained for their ITO coatings were 0.009Ωcm. However, Park *et al.* used the same starting materials as Mattox but applied the tin oxide coatings to ceramic cloths instead of glass substrates, and they achieved surface resistances of ~18Ω/□ for a 7mol% antimony solution[34]. In a non sol-gel method to prepare tin oxide, Davies and co-workers used a layer of silica on the substrate surfaces to minimize the effects of sodium diffusing into the tin oxide coatings[35]. They found that the thin silica coating reduces the amount of sodium found in the tin oxide layer by 2 orders of magnitude.

Puyane and Kato prepared their antimony-doped tin oxide films from butanoate and butoxide compounds of antimony and tin[36]. They report average surface resistances between 1.0 kΩ to 1.5 kΩ/□ for an antimony oxide doping concentration between 6 and 7 wt%. They also found that the addition of ethylene oxide to the dip-coating solutions made them more viscous without having detrimental effects on the resistances. Addition of ethylene oxide was tried in this work to increase the viscosity of some dip-coating solutions but it did not increase the viscosity of the colloidal solutions.

Finally Park prepared SnO_2 from tin(IV)ethylhexano-isoproxide ($Sn(OOC_8H_{15})_2(OC_3H_7)_2$ dissolved in isopropanol[37]. They report resistivities for annealed samples of 5.5×10^{-7} Ωcm to 5.7×10^{-3}Ωcm as the coating applications were increased from 1 to 10. The

band gap increased from 3.23 to 3.45eV by increasing the firing temperature from 300°C to 500°C.

1.5.2 Other Metal Oxides Prepared from Sol-Gel Processes

This section shows examples of other metal oxides prepared by sol-gel methods. Firstly, it has been successfully used to prepare indium tin oxide (ITO) coatings as shown by Furusaki and co-workers who prepared ITO from $In(NO_3)_3$ and $SnCl_4$[38]. For films fired at 500°C, they achieved resistivities of 500Ωcm and transmittances of approximately 90% over the visible range. Meanwhile, Nishio *et al.* also prepared their ITO coatings from a solution of $In(NO_3)_3$ and $SnCl_4$. They annealed their films at 700°C and had far superior resistivity values of approximately 9 x 10^{-3}Ωcm[39]. They found however, that it was necessary to keep the sols at a pH of 2.5 and that any minimal deviation from this pH caused the sols to destabilize. For Bel Hadj Tahar and co-workers, they report similar resistivity values of about 1 x 10^{-3}Ωcm for their ITO coatings, fired at 700°C and prepared from $InCl_3$ and $SnCl_4$[40]. They estimated the band gap of ITO to be 3.4eV which agrees closely with literature values[41].

Another metal oxide produced by a sol-gel work was aluminium oxide, which was prepared from $Al(OC_4H_9)_3$ and dilute HNO_3[42]. The relationship between the amount of acid added and the volume of solution when gelation occurred was investigated. It was found that the optimum concentration of acid to produce gels from the least volume of solution was 0.07M HNO_3. This concentration of acid also produced the most stable and coherent coatings on drying and firing. An example of a mixed oxide produced from sol-gel comes from Hayashi *et al.* who made $CaO\text{-}SiO_2$ mixed oxide glasses from calcium ethoxide ($Ca(OEt)_2$) and silicon ethoxide ($Si(OEt)_4$)[43]. They examined the effect of different modes of water addition (to effect hydrolysis) on the overall transparency of the glasses. They found that glasses prepared by the absorption of atmospheric moisture were transparent while those prepared by the direct addition of water were found to be translucent or opaque in appearance.

Hayashi and Saito prepared iron and copper oxide nanocomposites by a sol-gel route from the addition of salts of $FeCl_3.6H_2O$ and $Cu(NO_3)_2.3H_2O$ to solutions of tetraethyl orthosilicate in ethanol[44]. Another example of a metal oxide produced by a sol-gel process is that of zirconium oxide crystallites doped with lanthanum[45]. They found that crystallite formation occured at lower temperatures than normal due to the ease of oxygen diffusion in the nanoscale composites produced by sol-gel methods.

Finally, a problem which is often encountered in the preparation of metal oxides through sol-gel processes is that of cracking and fracturing of the gels as the liquid evaporates from the pores during the drying process[46]. A method of lessening this problem is through the gradual drying and densification of the xerogels, as described by Dahmouche *et al.* in the production of silicon dioxide[47]. Another technique for dealing with the cracking problem is that of supercritical drying as described by Canham and co-workers who prepared silicon dioxide with a porosity greater than 95% with this technique[48].

1.6 Properties of SnO_2

Tin occurs naturally as cassiterite or tin dioxide (SnO_2), the crystal structure of which is body-centred tetragonal, with each tin atom attached to 6 oxygens[49,50]. Figure 1.3 below shows one unit cell of the structure, the thicker lines representing the bonds between one tin atom and six oxygen atoms. Undoped tin oxide shows almost no deviation from stoichiometry and this accounts for the high resistvities of pure tin oxide[23,28,51,52].

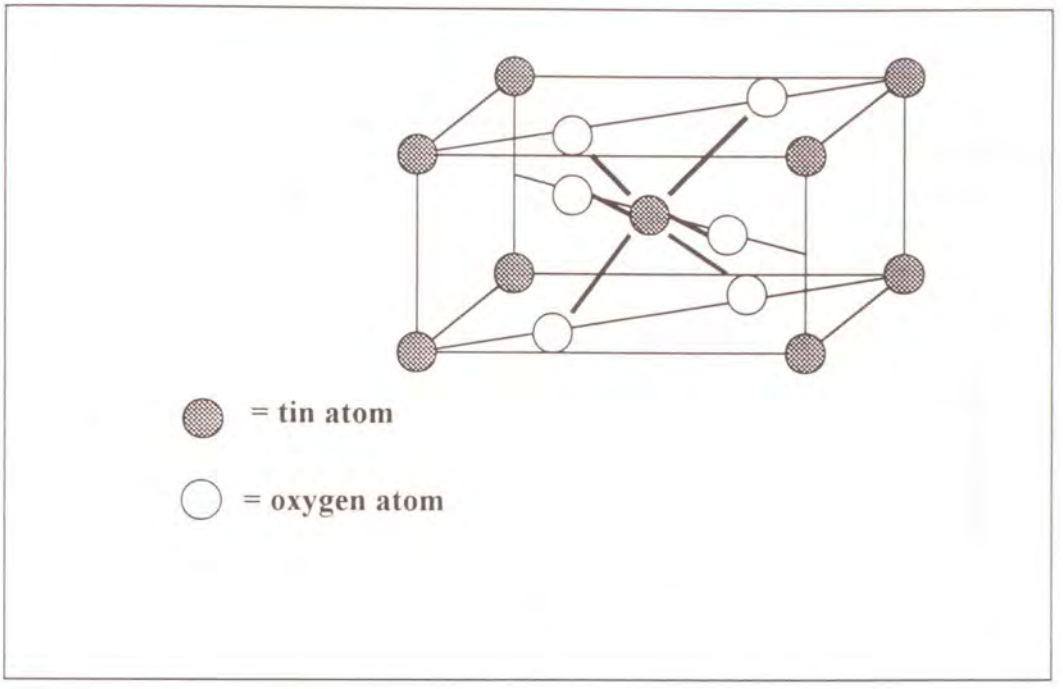

Figure 1.3: Body Centred Tetragonal Structure of Cassiterite

The optical properties of tin oxide are governed by the fact that it has a band gap energy of ~3 eV or greater, which means that it is transparent in the visible range[53,54]. Since it has a relatively large band gap, the promotion of just a few electrons can take place from the valence band to the conduction band through thermal excitation. Alternatively, impurity ions can be introduced which cause the formation of acceptor or donor levels in the band gap. At low dopant concentrations, the dopant atoms tend to occupy sites substitutionally by replacing tin atoms in the tin oxide lattice. At higher dopant concentrations, the dopant atoms occupy interstitial sites in the oxide. These dopants result in increased conductivity through the promotion of electrons from the donor level to the conduction band (n-type semiconductivity) or the acceptance of electrons from the valence band to the acceptor level which leaves holes in the valence band (p-type semiconductivity). Figure 1.4 below shows a band diagram for tin oxide, showing the donor and acceptor levels caused by the dopants.

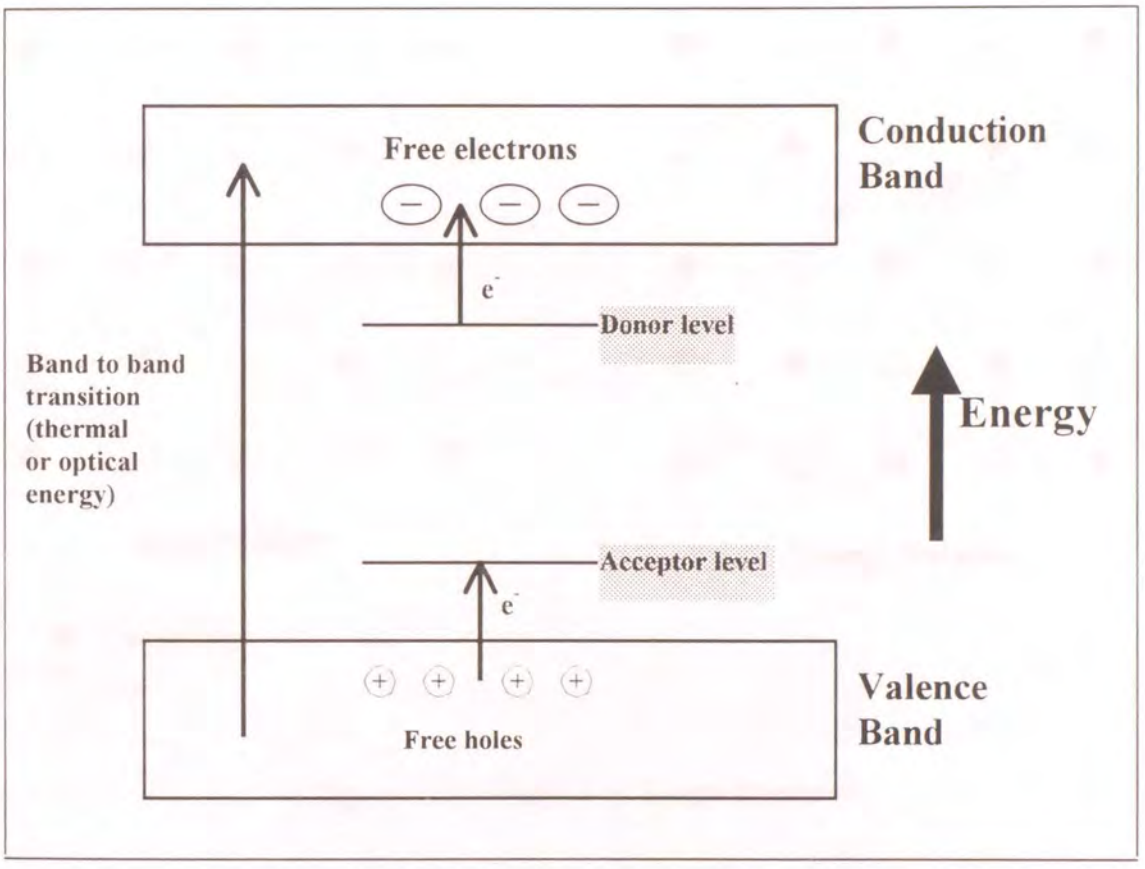

Figure 1.4: Energy Diagram for Tin Oxide

In ionic compounds such as tin oxide, single electrons or holes can also produce localized lattice distortions resulting from their electrostatic interaction with neighbouring ions. The distortion accompanies the electron or hole as it moves through the lattice and the result is known as a polaron[55]. The distortion may get trapped at a particular lattice site and can only move by thermally activated "hopping" through the solid.

Figure 1.5 below shows the formation of small and large polarons when a single electron is introduced into a metal oxide lattice. The introduction of an extra electron or hole changes the oxidation state of one atom in a solid. This changes the ionic radius which produces the local lattice distortion, thereby trapping the charge. When the radius of ionic polarization (R) is more than the lattice spacing, the result is a large polaron.

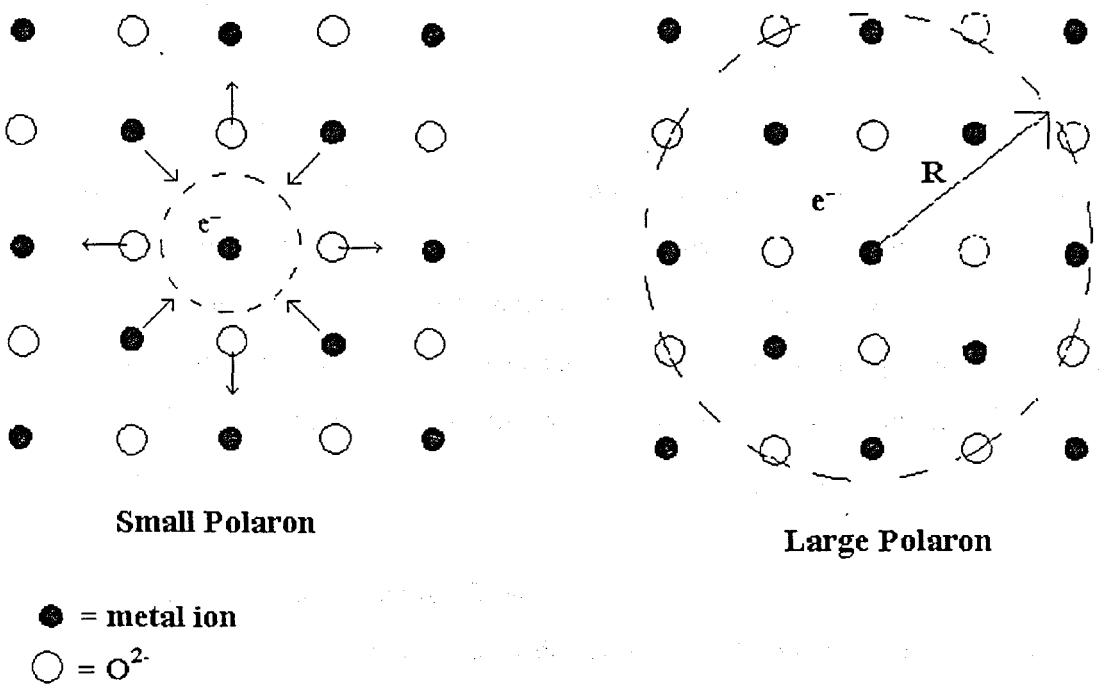

Figure 1.5: Small and Large Polarons

Small polarons have an activation energy for movement, which can be used in their characterisation. This is caused when the trapped positive hole (or electron) strongly distorts the surrounding lattice. This displacement create a potential of the form 1/r in ionic crystals which produces bound states. In order for a potential well to be set up, a hole must reside on a given site for a time longer than the vibrational period of the lattice which is of the order 10^{-13} second. Therefore the mobilities fall within the range 10^{-9} to 10^{-3} $cm^2/V/sec$[55]. The work required to move the neighbouring ions is the activation energy. The trapping process can only occur in polar crystals. In elemental crystals, such as Ge and Si, the potential has the form $1/r^4$ which cannot support bound states.

Polarons can also exhibit an absorption in the mid-infrared region[56] arising from oscillatory motion of the bound electrons or holes. The application of an infrared frequency electric field to the polarons is essentially the same as measuring an AC conductivity by conventional means, and it causes resonance of the polaron hopping

process. It can be shown that the absoption peak energy E=hv is equal to four times the polaron binding energy [57].

1.7 Applications of Tin Oxide

The optical and electrical properties of tin oxide described above give tin oxide many important applications in everyday life. It's commonly used in electrochromic devices, light emitting diodes and LCD display devices[41,47,57,58]. As mentioned in section 1.5, tin oxide ultrafine particles can be used in gas sensors, for ultrafiltration purposes and also in catalysts[21,22,23]. Other applications for tin oxide are in solar cells and in anti-reflective and anti-static coatings[59,60].

1.8 Objectives for Experimental Work

The main objective of this project was to develop a novel sol-gel process for producing conductive and transparent tin oxide, and to apply the tin oxide coatings to polymer substrates.

There are many different methods of producing tin oxide coatings e.g. chemical vapour deposition, sputtering techniques and spray pyrolysis. A sol-gel process was chosen over these more traditional methods of applying thin films because the other methods are more expensive and in the case of spray pyrolysis, it involves heating the substrate to high temperatures. The main advantage of the sol-gel route for this project was the fact that it's a low temperature process since the main substrates for the tin oxide were thermoplastic polymers.

For this study, it was thought advisable to use precursors which have a potential compatibility with polymers. Conventional sol-gel metal alkoxide precursors were ruled out because of their toxicity and their non-polarity which makes them incompatible with "polymer-friendly" solvents. $Sn(acac)_2Cl_2$ (tin (IV) bis acetylacetonate dichloride) was selected as a starting material because it has a low toxicity and it was hoped that residual

traces of chemically attached acetylacetonate remaining in the gel would aid binding of the gel to polyesters.

The advantages of putting a transparent conducting coating on a polymer substrate are endless, especially with an age of technology like flexible television screens and touch screen technology almost upon us. For this project it was decided to use poly (methyl methacrylate), polycarbonate, poly (ethylene terephthalate) and poly (ethylene naphthalate) as the polymer substrates. Unfortunately polymers of this kind do not lend themselves easily to coating with inorganic metal oxides. A means of making the polymer surfaces more compatible for coating with a metal oxide needed to be found. Another fundamental problem with the application of tin oxide to polymers is that it is not possible to heat the polymer substrates to temperatures usual for fully annealing the tin oxide. Therefore, a means of annealing the coatings without excessive damage to the substrates was required.

The proposed plan of experimental work was as follows:

1. To investigate the preparation of tin oxide using one aqueous sol-gel procedure from the literature. Also, to prepare tin oxide by a sol-gel using a novel precursor. In order to improve the conductivity of the tin oxide coatings, to add n-and p-type dopant impurity ions during the sol-gel processes.

2. Initially to apply the tin oxide coatings to glass substrates and to investigate the relationship between processing conditions and the resulting DC conductivity and percentage transparencies of the tin oxide coatings.

3. To find a way of making the polymer substrate surfaces more compatible for coating with an aqueous based solution and to successfully apply the tin oxide coatings to the polymer substrates.

4. To find a method of annealing the tin oxide coatings on the polymer surfaces without damaging the polymer substrates. Finally, to optimise the conductivity and transparency of the coatings on the polymers to give the best possible conductivity and transparency results.

References

1. P. J. Flory, *Principles of Polymer Chemistry,* Cornell University Press, Ithaca, New York (1953)
2. D. H. Everett, *Basic Principles of Colloid Science,* Royal Society of Chemistry, London (1988)
3. D. J. Shaw, *Introduction to Colloid and Surface Science,* Butterworth-Heinemann, Oxford (1992)
4. R. J. Hunter, J. Robert, *Introduction to Modern Colloid Science,* Oxford University Press, Oxford (1993)
5. H. Dislich, P. Hinz, *J. Non-Cryst. Solids,* **48** 11 (1982)
6. L. L. Hench, J. K. West, *Chem. Rev.*, **90** 33 (1990)
7. H. Dislich, *J. Non-Cryst. Solids,* **57** 371 (1983)
8. H. Dislich, *J. Non-Cryst. Solids,* **73** 599 (1985)
9. M. J. Hampden-Smith, T. A. Wark, C. J. Brinker, *Coordination Chem. Reviews,* **112** 81 (1992)
10. D. H. Uhlmann, T. Suratwala, K. Davidson, J. M. Boulton, G. Teowee, *J. Non-Cryst. Solids,* **218** 113 (1997)
11. L.L. Hench, J. K. West, *Chem. Rev.*, **90** 33 (1990)
12. D. P. Stinton, P. Angelini, A. J. Caputo, W. J. Lackey, *J. Am. Ceram. Soc.*, **65** 394 (1982)
13. M. Henry, J. P. Jolivet, J. Livage, *Structure and Bonding,* 77 153 (1992)
14. R. S. Hiratsuka, C. V. Santilli, D. V. Silva, S. H. Pulcinelli, *J. Non-Cryst. Solids,* **147** 67 (1992)
15. C. J. Brinker, G. W. Scherer, *The Physics and Chemistry of Sol-Gel Processing,* Academic Press Limited, London (1990)

16. L. G. Hubert-Pfalzgraf, *Applied Organometallic Chemistry,* **6** 627 (1992)
17. J. Livage, *Chemica Scripta,* **28** 9 (1988)
18. M. Guglielmi, G. Carturan, *J. Non-Cryst. Solids,* **100** 16 (1988)
19. C. D. E. Lakeman, D. A. Payne, *Materials Chem. and Phys.,* **38** 305 (1994)
20. W. Lada, A. Deptula, T. Olczak, W. Torbicz, D. Pijanowska, A. Di Bartolomeo, *J. Sol-Gel Sci. and Tech.,* **2** 551 (1994)
21. G. E. de Souza Brito, S. H. Pulcinelli, C. V. Santilli, *J. Sol-Gel Sci. and Tech.,* **2** 575 (1994)
22. W. Dazhi, W. Shulin, C. Jun, Z. Suyüan, L. Fangqing, *Phy. Rev. B,* **49** 14282 (1994)
23. J. Tamaki, N. Miura, N. Yamazoe, *J. Mat. Sci.,* **27** 963 (1992)
24. S-S. Park, H. Zheng, J. D. Mackenzie, *Materials Letters,* **17** 346 (1993)
25. Z. Crnjak-Orel, B. Orel, M. Hodoscek, V. Kaucic, *J. Mat. Sci.,* **27** 313 (1992)
26. B. Orel, U. Lavrencic-Stangar, A. Crjak-Orel, P. Bukovec, M. Kosec, *J. Non-Cryst. Solids,* **167** 272 (1994)
27. Y-J. Lin, C-J. Wu, *Surface and Coatings Tech.,* **88** 239 (1997)
28. C. Terrier, J. P. Chetelon, R. Berjoan, J. A. Roger, *Thin Solid Films,* **263** 37 (1995)
29. J. P. Chatelon, C. Terrier, G. Blanchin, H. Mugnier, J. A. Roger, *Materials Science Forum Vols,* **239** 81 (1997)
30. A. Maddalena, R. Dal Maschio, S. Diré, A. Raccanelli, *J. Non-Cryst. Solids,* **121** 365 (1990)
31. C. Terrier, J. P. Chatelon, J. A. Roger, *Thin Solid Films,* **295** 95 (1997)
32. M. A. Aegeter, A. Reich, D. Ganz, G. Gasparro, J. Pütz, T. Krajoewski, *J. Non-Cryst. Solids,* **218** 123 (1997)
33. D. Mattox, *Thin Solid Films,* **204** 25 (1991)
34. S.-S. Park, H. Zheng, J. D. Mackenzie, *Materials Letters,* **22** 175 (1995)
35. B. M. Davies, K. H. Panell, S. P. Albright, *J. Mat. Res.,* **9** 226 (1994)
36. R. Puyane, I. Kato, *Proc. Soc. Photo-Optical Instrumentation Engineering,* **401** 190 (1983)
37. S-S Park, J. D. Mackenzie, *Thin Solid Films,* **258** 268 (1995)
38. T. Furusaki, J. Takahashi, K. Koduira, *J. Cer. Soc. of Japan,* **102** 200 (1994)

39. K. Nishio, T. Sei, T. Tsuchiqa, *J. Mat. Sci.*, **31** 1761 (1996)

40. R. Bel Hadj Tahar, T. Ban, Y. Ohya, Y. Takahashi, *J. Appl. Phys.*, **82** 865 (1997)

41. K. L. Chopra, S. R. Das, *Thin Film Solar Cells,* Plenum, (1983)

42. B. E. Yoldas, *J. Mat. Sci.*, **10** 1856 (1975)

43. T. Hayashi, H. Saito, *J. Mat. Sci.*, **15** 1971 (1980)

44. A. Chatterjee, D. Chakrovorty, *J. Mat. Sci.*, **27** 4115 (1992)

45. A. K. Bhattacharya, A. Hastridge, K. K. Mallick, J. L. Woodhead, *J. Mat. Sci.* **29** 6076 (1994)

46. P. F. James, *J. Non-Cryst. Solids,* **100** 93 (1988)

47. K. Dahmouche, C. Bovier, J. Dumas, J. Serughetti, *J. Mat. Sci.*, **30** 4149 (1995)

48. L. T. Canham, A. G. Cullis, C. Pickering, O. D. Dosser, T. I. Cox, T. P. Lynch, *Nature,* **368** 133 (1994)

49. H. Boegel, *A Collectors Guide to Minerals and Gemstones,* Thames and Hudson Ltd., London (1971)

50. W. Kleber, *An Introduction to Crystallography,* VEB Verlag Technik, Berlin (1970)

51. D. J. Goyal, C. Agashe, B. R. Marathe, M. G. Takwale, V. G. Bhide, *J. Appl. Phys.*, **73** 7520 (1993)

52. N. Mizutani, M. Kato, *J. Mat. Sci.*, **22** 915 (1987)

53. H. Kaneko, K. Miyake, *J. Appl. Phys.*, **53** 3629 (1992)

54. K. H. Kim, S. W. Lee, *J. Am. Ceram. Soc.*, 77 915 (1994)

55. R. R. Heikes, W. D. Johnston, *J. Chem. Phys.*, **26** 582 (1957)

56. P. J. S. Foot, B. A. Nevett, *Phys. Stat. Sol.*, **93** 283 (1986)

57. W-F. Wu, B-S. Chiou, *Thin Solid Films,* **293** 244 (1997)

58. J. P. Coleman, A. T. Lynch, P. Madhukar, J. H. Wagenknecht, *Solar Energy Materials and Solar Cells,* **56** 375 (1999)

59. R. Mulyadi, D. S. Campbell, *Solar Energy Materials,* **19** 187 (1989)

60. D. J. Goyal, C. Agashe, B. R. Marathe, M. G. Takwale, V. G. Bhide, *J. App. Phys.*, **73** 7520 (1993)

2.1 Introduction

This chapter describes the two sol-gel methods used in this project for the synthesis of tin oxide and the characterisation of the sol to gel processes. One method used $SnCl_4$ as its main precursor and partly followed procedures from the literature. ($SnCl_4$ is the most common starting material for sol-gel tin oxides[1-6].) The second method used tin bis-(acetylacetonate) dichloride, which is a novel precursor in the production of tin oxide by a sol-gel method. The reasons for choosing this precursor were outlined in Chapter 1.

It was found that the second method of producing tin oxide was superior to the more usual method of starting with tin tetrachloride. As a result, the $SnCl_4$ route was phased out in favour of the novel route starting with $Sn(acac)_2Cl_2$. Many variations were made to the process in order to optimize it for producing tin oxide coatings, and n-type and p-type dopant impurity ions were introduced to improve their conductivity. The following sections describe both methods of preparing doped and undoped tin oxide, the results of the different variations used on the processes and the characterisation work performed on the resulting sols and gels.

2.2 Experimental

2.2.1 Tin oxide produced from Tin (IV) Tetrachloride (Method 1)

The following reaction scheme (figure 2.1) outlines the general procedure used to produce tin oxide, which did not replicate exactly any process from the literature but used features from different published procedures[1-3]. It differed from references 1 and 3 by including a centrifugation step and from reference 2 by using dialysis as the main method of removing excess chloride ions. The $SnCl_4$ used was a 1M solution in dichloromethane and was obtained from Aldrich.

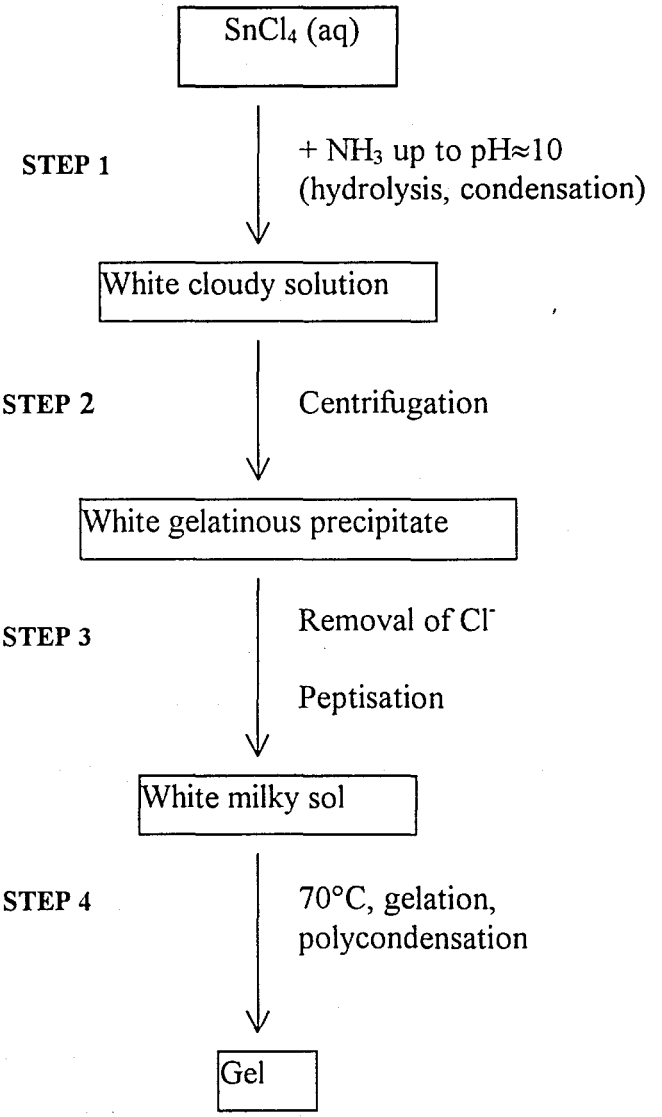

Figure 2.1: Preparation of Tin Oxide from $SnCl_4$

Variations were made to the above scheme as outlined below:

(i) The concentration of ammonium hydroxide in step 1 was varied over the range 0.6 to 10 mol dm^{-3}.

(ii) The concentrations of tin (IV) tetrachloride used in step 1 were 0.5 mol dm^{-3} and 1 mol dm^{-3}.

(iii) Two methods of removing the excess chloride ions were used in step 3, namely filtration (together with washing the precipitate with dilute ammonium nitrate) and dialysis. For the latter, the aqueous suspensions were placed in a sealed tube of Visking cellulose membrane, supported in a large beaker of distilled water (stirred). Several successive portions of water were used, until chloride ions were undetectable in the water. The loss of the chloride ions was monitored by a Corning specific ion electrode for chloride in conjunction with an Orion Research double junction reference electrode.

The details of the above experiments are contained in tables 1 to 3 (appendix 1), showing the amounts of reagents used and the conditions for each set of experiments.

2.2.2 $Sn(acac)_2Cl_2$ Route to Tin Oxide Gels (Method 2)

Acetone was chosen as a solvent for dissolving the tin bis (acetylacetonate) dichloride after some initial experiments investigating its solubility and reactivity in various common solvents.

The following scheme (figure 2.2) outlines the production of tin oxide using tin (IV) bis (acetylacetonate) dichloride as the starting material. Tables 4 to 16 in appendix 1 give specific details of the amounts of reagents used and the conditions for the experiments. 98% pure $Sn(acac)_2Cl_2$, 99% $InBr_3$ and 99% $SbBr_3$ were obtained from Aldrich. Acetone was obtained from Aldrich as a laboratory grade solvent and was dried over 3Å molecular sieve.

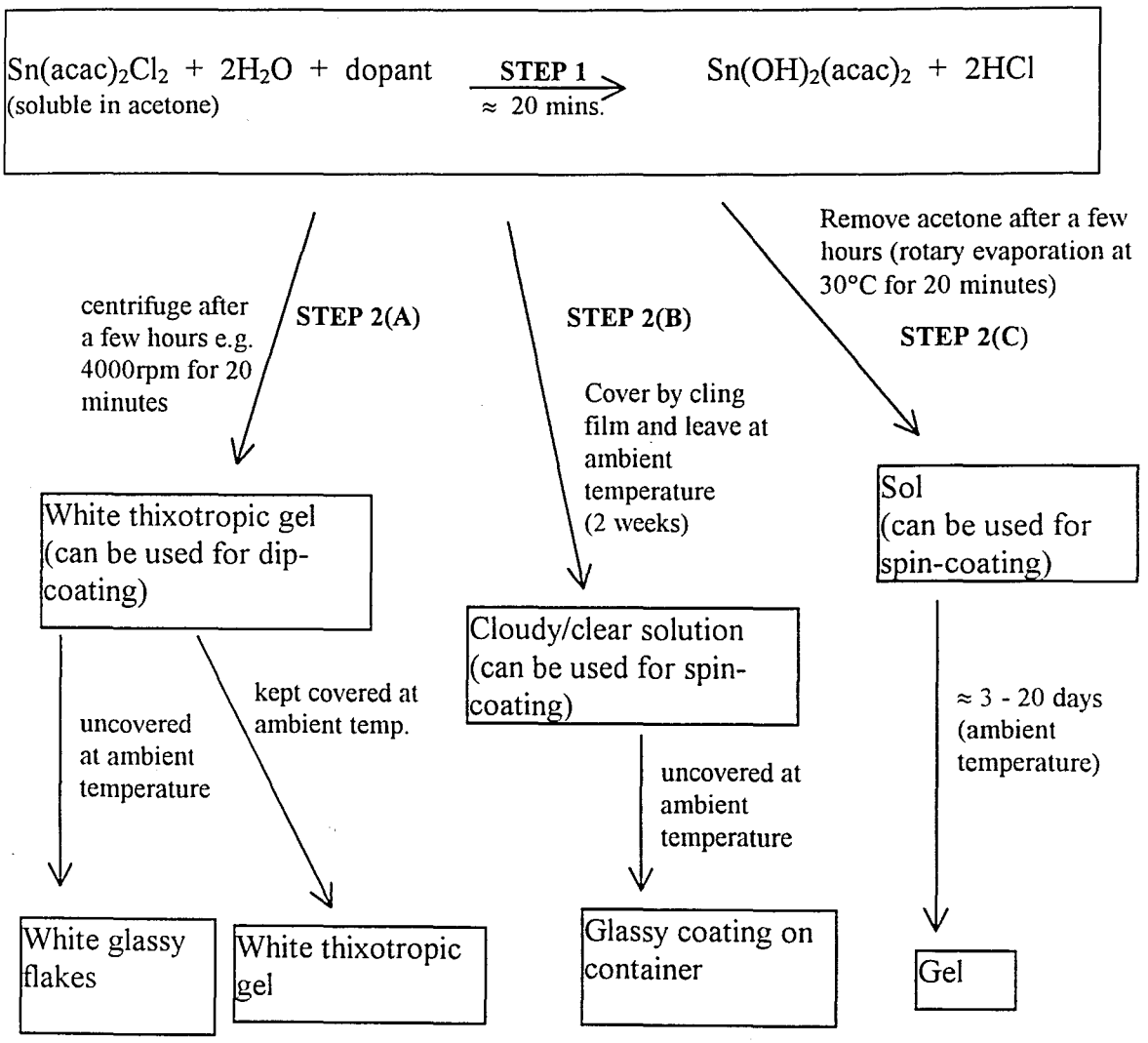

Figure 2.2: Preparation of Tin Oxide from $Sn(acac)_2Cl_2$

The following variations were made within the above reaction scheme:

(i) In step 1, the amounts of $Sn(acac)_2Cl_2$, acetone and water were kept roughly in the ratio 0.25g $Sn(acac)_2Cl_2$:10ml acetone:6ml H_2O for the experiments shown in tables 4 to 10. The ratio of starting materials was changed for tables 13 to 16, where less acetone and water was added per gram of $Sn(acac)_2Cl_2$.

(ii) 10ml of ethanol was added in step 1.

(iii) 60ml of dilute NH_4OH was added to some samples in step 1.

(iv) During step 1, a p-type dopant, $InBr_3(s)$ was added as a solid (0.01 to 0.25g) to achieve dopant concentrations of 2 to 20 atom % by cation substitution.

(v) Indium (III) bromide solution (1% w/v in water) was added in step 1 to achieve dopant concentrations from 1 to 7 atom % by cation substitution.

(vi) Step 2(a) was varied by changing the length of time between mixing the starting materials and centrifugation.

(vii) Antimony (III) bromide solution (1% $SbBr_3$ in acetone) was added as an n-type impurity in step 1, to give 1 to 13% cation substitution.

2.2.3 Analytical Techniques

Many analytical techniques were used to monitor different aspects of the sol-gel processes and to characterise the products of the processes. The average size of the colloidal particles produced by the $SnCl_4$ method were measured using an Industrial D Coulter Counter and a JEOL JSM-T300 Scanning Electron Microscope. The electrolyte used for the Coulter Counter experiments was 3% trisodium phosphate; 3% sodium pyrophosphate. The loss of chloride ions during method 1 (step 3, figure 2.1) was monitored by a Corning specific ion electrode for chloride in conjunction with an Orion Research double junction reference electrode.

The kinetics of hydrolysis in step 1 (figure 2.2) were initially studied by following the pH changes in a "standard" solution of 1g $Sn(acac)_2Cl_2$ in 10ml acetone, to which 6ml of water were added (at 25°C). These were carried out using a Jenway 3010 pH meter. A Phillips PW 1730/10 powder X-Ray Diffractometer was mainly used as a characterisation technique for confirming the identification of the materials but it also gave particle size information. Thermogravimetric analyses were performed on a Perkin Elmer TGA 7 Thermogravimetric Analyser, typically over the temperature range 40°C to 900°C at a heating rate of 20°C $minute^{-1}$.

2.3 Results and Discussion

2.3.1 $SnCl_4$ Preparations

This section describes the results of tin oxide preparations using tin tetrachloride as the main precursor. Three sets of experiments were carried out using this sol-gel route and various characterisation work was performed on the gels and sols. Variations were made in the reaction scheme shown in figure 2.1 and the specific details of the experiments, in terms of the amounts of reagents used and the conditions are given in tables 1, 2 and 3 in appendix 1. Also included is an indication of the general outcome of the experiments and whether there was any detectable conductivity response from the coating or solid product, when checked with a two-probe multimeter.

2.3.2 Particle Size Estimates

Coulter counter experiments were performed on samples which differed only in the concentration of ammonium hydroxide used in step 1 (see figure 2.1) of their preparation. The Coulter Counter is used for estimating the particle size distribution of a sample suspended in a suitable electrolyte. The two concentrations of ammonium hydroxide used were 0.5 mol dm^{-3} and 5 mol dm^{-3}. After centrifuging the samples, a few milligrams of the precipitates were used for the experiments. The sample with the higher ammonium hydroxide concentration had an average particle size of approximately 0.43 microns while the other had an average particle size of 4 microns. From these results it can be concluded that the more concentrated ammonium hydroxide produces smaller particles, probably due to rapid hydrolysis, and faster nucleation. A more detailed investigation was not carried out, because it was decided to concentrate on the other precursor system.

2.3.3 Removal of Chloride Ions

Step 1 of method 1 (see figure 2.1, page 23) involved the hydrolysis of tin tetrachloride using ammonium hydroxide and it resulted in a white flocculent precipitate in solution. To isolate the precipitate, centrifugation was used in step 2. Step 3 of the process involved the removal of chloride ions from the sols, since it is well known in inorganic colloid

chemistry that the electrolytic concentration in sols plays an important role in deciding whether or not the sol will gel, aggregate or even reprecipitate[7].

In this case, the sol system present was lyophilic. As discussed in the introduction, lyophilic sols cannot be destabilized by small quantities of electrolytes in the same manner as lyophobic sols. When electrolytes destabilize a lyophilic sol, they do so by a "salting out" effect which causes the formation of a floc. The electrolyte dehydrates the colloid by competing for its waters of hydration, therefore the salting out power of electrolytes increases with the tendency for them to become hydrated. Once the waters are removed from around the colloid particles, they are more likely to aggregate with other particles and form a floc. The electrolytes present in this system were chloride, nitrate and ammonium. It was only necessary to ensure the removal of the chloride ions since the charge density of chloride ions is much greater than ammonium or nitrate, and at high concentrations the chloride ions will compete with the colloid particles for the solvation layer. Also, according to the Hoffmeister series (or lyotropic series), chloride is more effective at destabilizing colloid systems than nitrate or ammonium ions[8-10].

For tin oxide sols, there is agreement in the literature that for successful gelling to occur, the optimum concentration of chloride is between 0.9 and 20mM[1-3]. Above 20mM Cl^- aggregation of the particles occurs and hence turbidity of the gels and below 0.9mM the colloidal suspensions are not stable[3]. It was decided to try to maintain the chloride ion concentration within these limits. Two methods were used to remove the chloride ions. The first involved washing the freshly precipitated tin dioxide with dilute NH_4NO_3 and checking the washings for turbidity with aqueous $AgNO_3$ (i.e. production of silver chloride). It was a messy procedure as the precipitate was highly gelatinous and not easy to filter.

Dialysis was the second method used, and the wash water of the various samples was again checked at intervals for turbidity with $AgNO_3$. After a few days the wash water no longer turned silver nitrate turbid which showed that the concentration of chloride

remaining was extremely small. At this stage a chloride ion-selective electrode was used to determine the chloride concentration of the wash water but the values were lower than that for distilled water (less than 5×10^{-4} mol dm^{-3}) and in some cases below the recommended range for optimum gelling conditions.

Dialysis was the most time-consuming stage of the preparation of tin oxide gels from $SnCl_4$. During the early stages of dialysis the sol has been reported to become as transparent as water[1], but in practice only one of the sols became transparent.. Most of the samples did not change appearance and remained white milky liquids even the chloride concentration for some samples was less than 0.6mM. Heating the dialysis vessels at 30°C was tried in order to speed up the dialysis of the sample but there was no improvement.

2.3.4 Electron Microscopy Observations

A sample which had been dialysing for one week was examined using the scanning electron microscope. The white milky sol was diluted one part in thirty in water and used to coat a cover slip by solvent evaporation. The coating was dried at ambient temperature for 3 hours and then gold coated. The sol appeared to be composed of fragmented aggregates of relatively monodisperse particles which had an approximate diameter of 150nm (see figures 2.3 for a photograph). There were some cracks evident which almost certainly resulted from too-rapid drying of the sol on the cover slip.

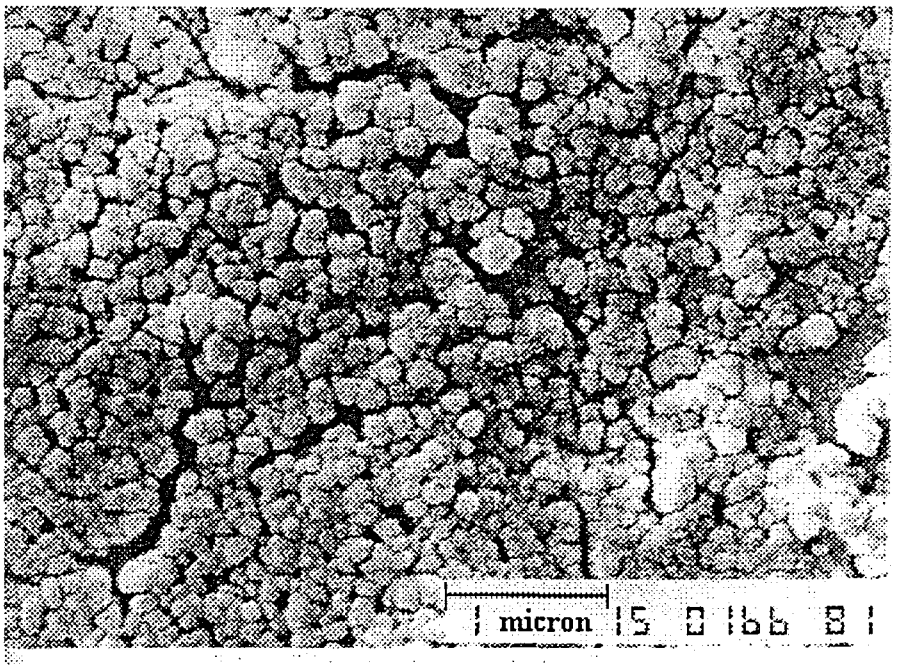

Figure 2.3: SEM of Tin Oxide

2.3.5 Thermogravimetric Analysis

Figure 2.4 shows a typical thermogram of a sample prepared by the $SnCl_4$ route. The thermogram has simply one weight loss due to the loss of water from the gel. The percentage of tin oxide remaining at 900°C is approximately 10%. Even though the eventual aim for the tin oxide coatings was to apply them to polymer substrates, it was still hoped to be able to heat the polymer substrates to at least 250°C to allow some annealing. Since the gels are almost 90% water this could lead to major incompatibility with the organic substrates and extensive cracking as the water is lost. As discussed later, special precautions are necessary to minimise the cracking during drying.

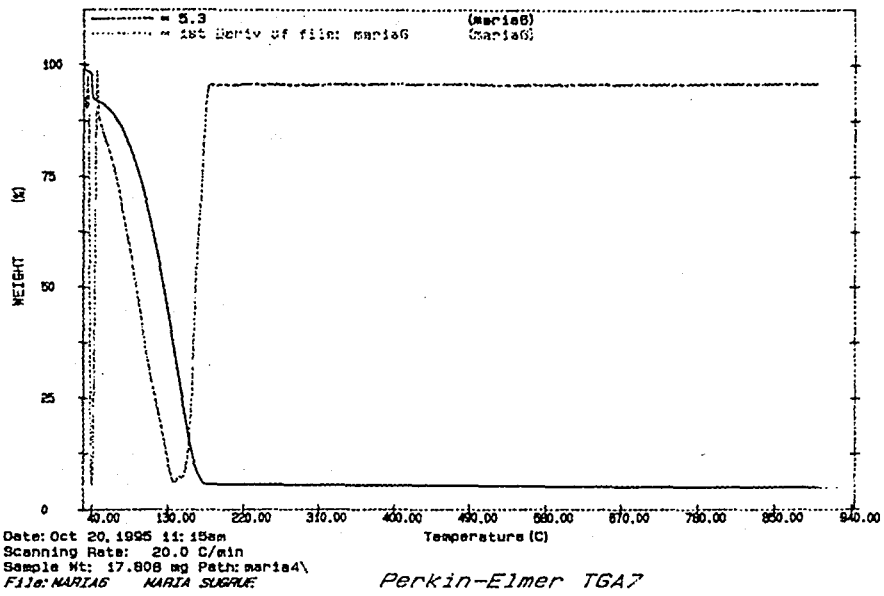

Figure 2.4: TG of SnO_2 Prepared from $SnCl_4$

2.3.6 XRD Studies

Figure 2.5 shows a typical diffractogram of an air-dried gel produced from the method shown in figure 2.1. By comparison with powder diffraction file standards[11], it showed that the three main characteristic peaks for cassiterite tin oxide were present (d = 3.34, 2.66, 1.76Å). The peak at 1.44 Å is also due to SnO_2.

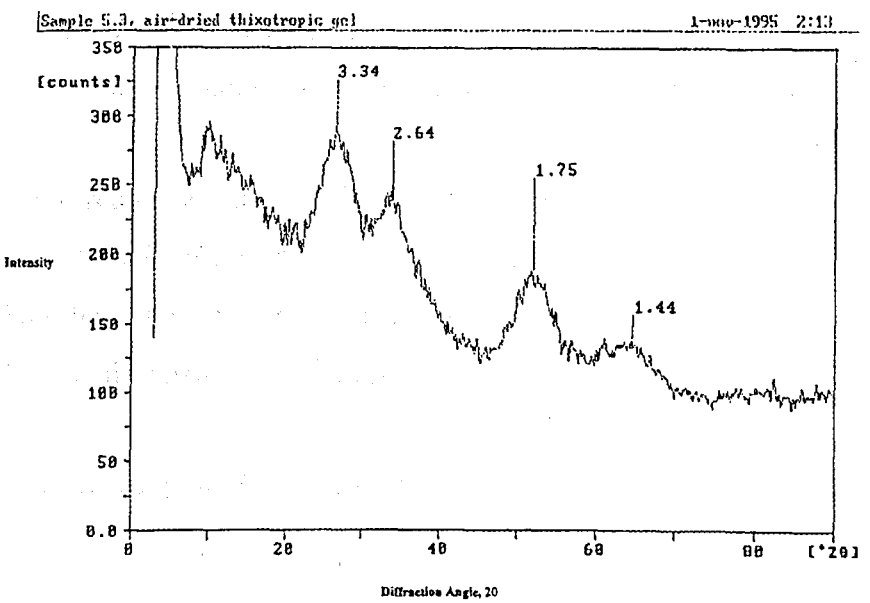

Figure 2.5: XRD of SnO_2 Prepared from $SnCl_4$

2.3.7 Shortcomings of $SnCl_4$ Method to Tin Oxide

Although this sol-gel process produced tin oxide, it took an extremely long time (because of the dialysis). Also the tin oxide produced was white/cloudy in appearance and did not adhere very well to glass. In tandem with this work, some preliminary work had begun using $Sn(acac)_2Cl_2$ as a precursor to tin oxide. Considerably more success was being obtained from the $Sn(acac)_2Cl_2$ process, and it was therefore decided to concentrate all efforts on that route.

2.3.8 Results of $Sn(acac)_2Cl_2$ Preparations

Initially, solubility tests performed on tin (IV) dichloro bis (acetylacetone) showed that acetone was the most suitable common solvent. Several series of experiments were performed, varying different experimental factors until a reproducible reaction scheme, which gave doped tin oxide, was derived. The remainder of this section 2.3 describes the characterisation of the sol to gel process and the results of the analytical tests carried out on the sols and gels.

2.3.9 Results of Different Preparations using Method 2 (Figure 2.2)

Tables 4 to 16 in appendix 1 show the samples prepared using the novel sol-gel process shown in figure 2.2. For step 1, it was found that using 10ml of acetone and 6 ml of water for 1g of $Sn(acac)_2Cl_2$ resulted in sol formation. The amounts of acetone, water and $Sn(acac)_2Cl_2$ used throughout all the experiments stayed roughly in that ratio.

The pH was measured during step 1, after addition of water. Figure 2.6 shows the change in pH with time at 25°C, from which a rate constant (quasi first order) of 0.034 s^{-1} was calculated. This first step of hydrolysis (according to the reaction below) is effectively complete within the first half-hour of mixing.

Proposed hydrolysis reaction: $Sn(acac)_2Cl_2 + 2H_2O \rightarrow 2HCl + Sn(acac)_2(OH)_2$

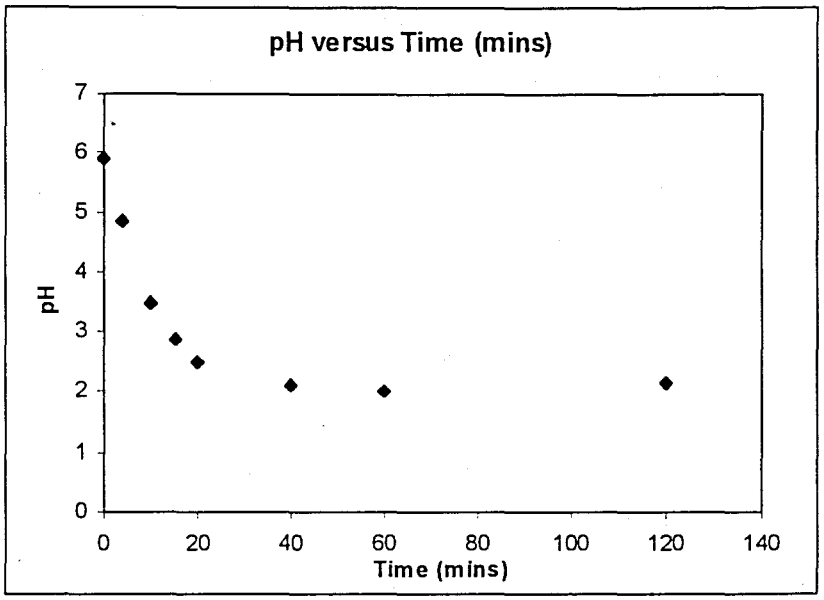

Figure 2.6: Kinetics of Hydrolysis

During step 1 of figure 2.2 (at the beginning of the study), ethanol was sometimes added as it had been previously reported that it prevented the resulting gels from becoming turbid i.e. that it inhibits aggregation[2]. In the case of this work, the addition of ethanol during step 1 caused the formation of precipitates and prevented gelation. Dilute ammonium hydroxide was also added in step 1 of the reaction scheme since Henry *et al.* state that complete hydrolysis of group IV metal cations occurs over the pH range 4-11[12]. Again there was no apparent beneficial change. After the method of producing tin oxide was established, dopant impurities were routinely added during step 1 to increase the conductivities of the tin oxide coatings.

Steps 2(A), 2(B) and 2(C) of Figure 2.2

In step 2(A) of the reaction scheme, the samples were centrifuged shortly after mixing. Varying the time between preparation of the sols and centrifuging did not affect the production of thixotropic gels. All the gels subsequently dried to give clear glassy residues.

Rotary evaporation of the sols soon after mixing (step 2(C)) served to remove the residual acetone. The resulting thin gels could be used for spin-coating. It was quite difficult to reproduce identical conditions for rotary evaporation (vacuum and temperature were difficult to control) but the separation of solvents was shown to be quite effective because of the very different boiling points ($(CH_3)_2CO$ = 56°C, H_2O = 100°C, H.acac = 140°C).

For step 2(B), the beakers containing the starting materials from step 1 were covered with cling film and left at ~25°C in a waterbath. After 10-14 days, the original volume of the solutions had decreased by about two-thirds and the beakers contained clear/slightly cloudy solutions which were suitable for coating purposes. If the cling film was removed at this stage and the beakers left at ambient temperature, the remaining solutions evaporated to leave a glassy conductive coating on the inside of the beakers. The route following step 2(B) from figure 2.2 became the usual route to use as it reproducibly produced tin oxide solutions which were suitable for coating purposes after approximately 10 days. It can be assumed from this section onwards, that the tin oxide solutions discussed were produced from the route which followed step 2(B).

2.3.10 Viscosity of the Sol-Gel Reaction Mixture

The viscosities of some samples were measured throughout the sol-gel reaction. A large amount of sample (~ 160ml) was needed for these measurements and hence large scale-ups of the normal samples were made.

The viscosity of the samples was found to increase dramatically in the first few days after preparation (see figure 2.7). This is expected as the colloid passes through the sol to gel transition. Surprisingly though, it was found that after about a week the viscosity of the sample decreased again, until it reached a steady value after three weeks. It was unexpected that the viscosity would decrease while the amount of liquid in the sample was decreasing, which would normally lead to higher viscosity. The same general phenomenon, sol to gel to sol occurred in all samples regardless of dopant concentration. A likely explanation is as follows: after approximately six days, the unbound water is lost more freely than the remaining acetylacetone due to the higher boiling point of the latter.

The acetylacetone does not form hydrogen bonds as freely with the forming tin oxide therefore the overall viscosity of the reaction solution decreases.

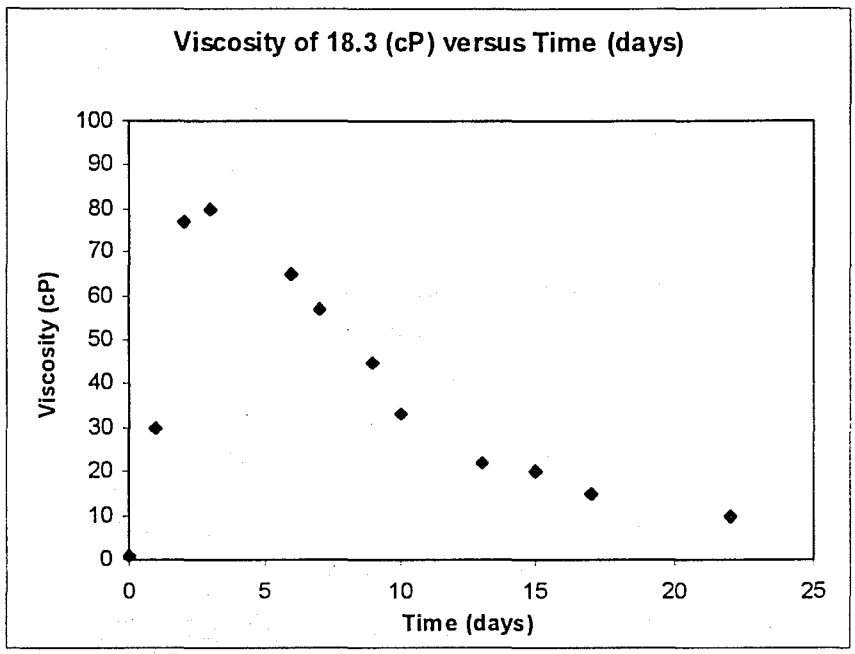

Figure 2.7: Viscosity of Sol-Gel Reaction

Spin coating is possible at either end of the time-scale when the liquid is not very viscous. Dip-coating can best be carried out when the tin oxide gels are at their most viscous at the peak of the graphs.

2.3.11 Particle Size Studies using Coulter Counter Measurements

A Coulter Counter Industrial D Model was used to obtain particle size distributions for tin oxide colloids which were doped 2, 3 and 4 mole % with antimony (samples 23.2 to 23.4 respectively). The samples were prepared in duplicate as described in table 16 (appendix 1). It was observed in previous series of samples with close doping concentrations that some sols changed more quickly to gels than others, although they had been prepared under apparently identical conditions. It was proposed that this could be due to a particle size effect caused by the dopant concentration. Particle size is a crucial parameter in the

production of thin films, for example if the particles are too large, this may lead to a decrease in the uniformity of thin coatings and their transparency.

It was found that for each specimen, the most common particle size occurred at approximately 5μm. Figure 2.8 below shows an example of the type of particle size distribution obtained for these samples.

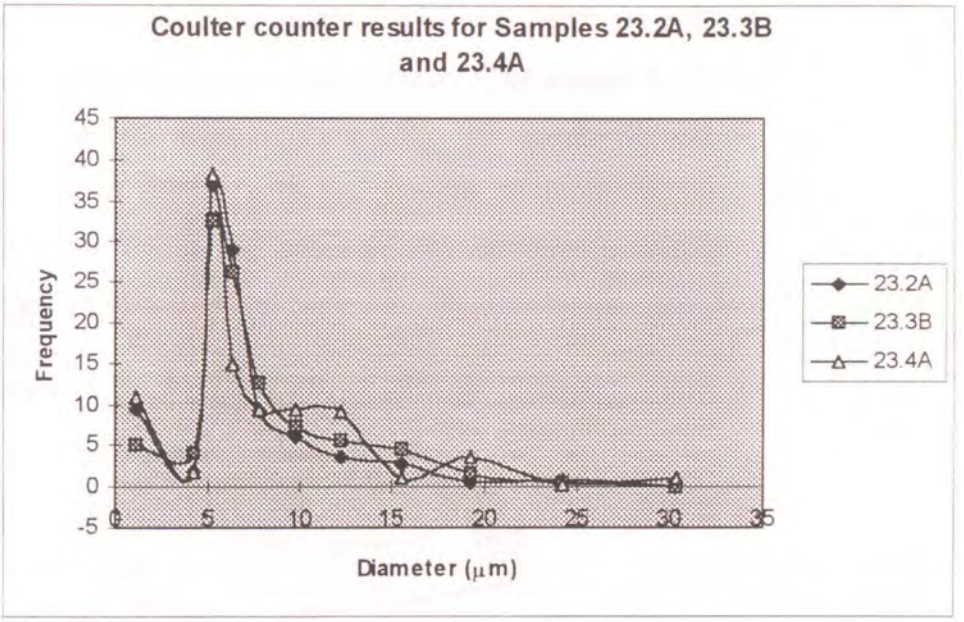

Figure 2.8: Particle size distribution for samples doped 2, 3 and 4% with antimony

From the above diagram, it is clear that all the samples give a similar frequency versus particle diameter relationship, with a substantial number of monodispersed particles around 5-6μm. Therefore the dopant concentration is not a crucial factor in the production of samples with similar particle sizes.

2.3.12 Thermogravimetric Studies

Figures 2.9 and 2.10 below show typical thermograms of gels produced from $Sn(acac)_2Cl_2$. The thermograms are very similar and from the derivative curve, it can be seen that two weight losses occur at ~120°C and ~140°C. The weight losses are believed

to be due to the loss of water and acetylacetone respectively, since acetylacetone has the higher boiling point. However, the first derivative on figure 2.9 shows two small dips; the first of these features is presumed to be due to the loss of any remaining acetone. Figure 2.10 does not show two dips on its first derivative. A likely reason for this is that the sample used for figure 2.9 was prepared 3 weeks before the analysis, whereas the sample used for figure 2.10 was prepared 7 weeks before the TG analysis, and had already lost its acetone through evaporation.

Further weight lost from the samples between 140°C and 400°C is probably due to evolution of remaining bound acetylacetone. The overall percentage weight lost due to the acetylacetone was approximately 30%. By comparison of the number of moles of SnO_2 remaining at 900°C with the number of moles of acetylacetone lost, it was estimated that half of the acetylacetone that was present initially had already been lost through evaporation before the analyses. On average the percentage mass remaining at 900°C was 55%.

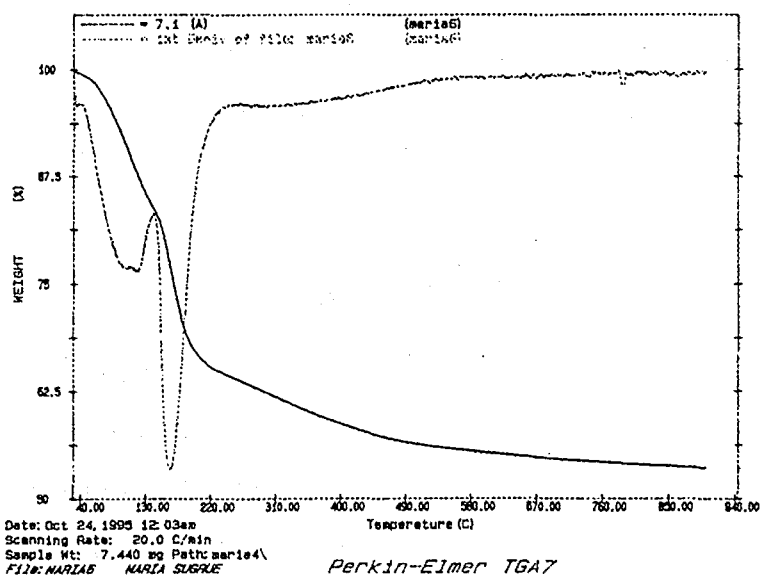

Figure 2.9: TG of Tin Oxide Prepared from $Sn(acac)_2Cl_2$

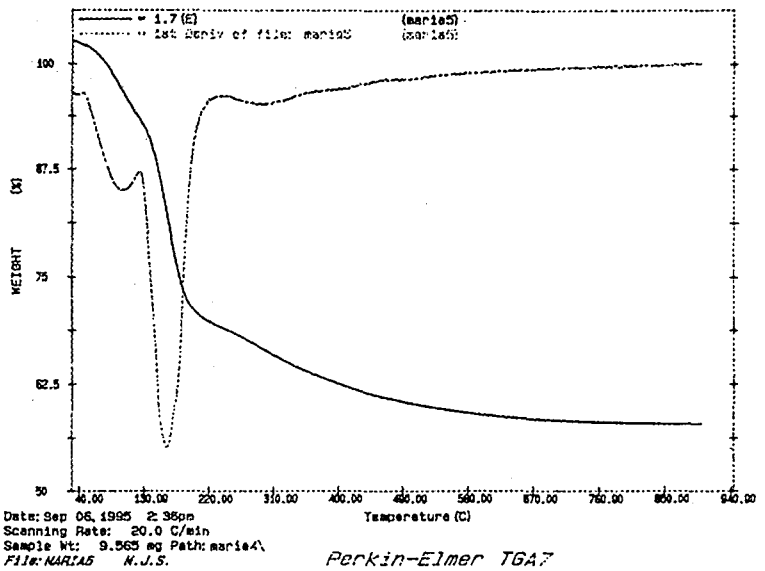

Figure 2.10: TG of Tin Oxide Prepared from $Sn(acac)_2Cl_2$

2.3.13 XRD Results for Tin Oxide Produced from $Sn(acac)_2Cl_2$

Some tin oxide gels were analysed using X-ray Diffraction (XRD). In all cases the major characteristic peaks for tin oxide (cassiterite) were present (d= 3.34, 2.66, 1.76Å)[11]. Particle sizes less than 200nm cause peak broadening of x-ray diffractograms, and it is possible to estimate the average particle size using the Scherrer formula, as follows:

$$d = \frac{D\lambda}{\Delta(2\theta)\cos(\frac{\theta_B}{2})}$$

where D = Scherrer constant (0.9)

d = average particle size

λ = x-ray wavelength (0.154nm)

$\Delta(2\theta)$ = FWHM Linewidth (radians)

θ_B = Bragg angle (degrees)

The first diffractogram below (figure 2.11) shows a sample which had no annealing treatment and was simply an air-dried gel, exhibiting the extremely broad peaks. The

sample used for the second diffractogram (figure 2.12) had been annealed at 400°C for two hours and had become more crystalline. Therefore the peaks are much sharper. Table 2.1 shows the hkl assignments for the peaks

Table 2.1

d (Å)	hkl
3.34	110
2.66	101
2.37	200
1.75	211
1.42	112
1.68	220
1.41	301
1.32	202
1.22	321

} Extra peaks due to annealing

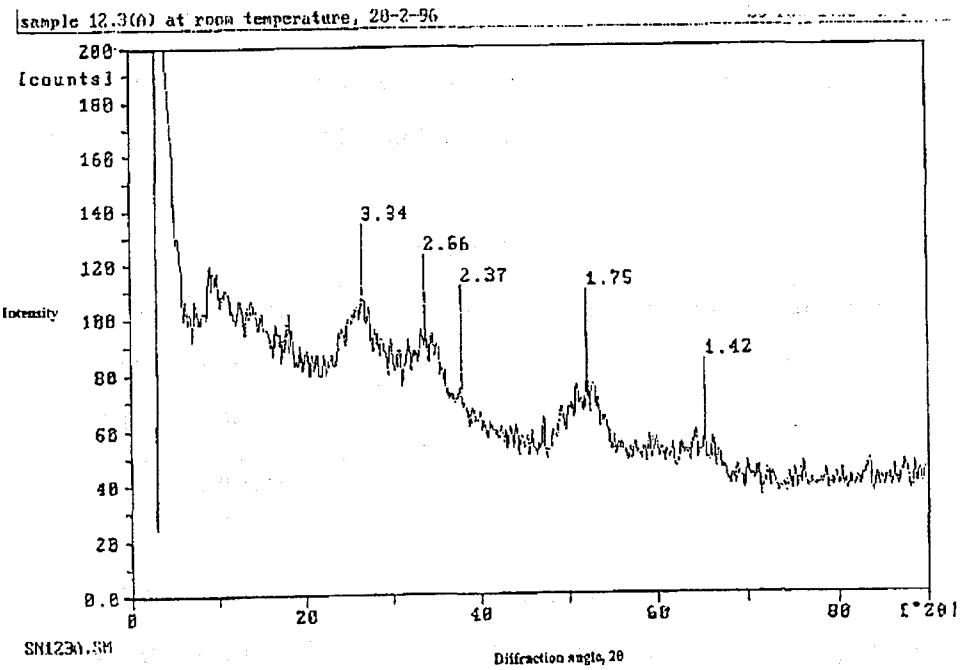

Figure 2.11: XRD of Unannealed Tin Oxide

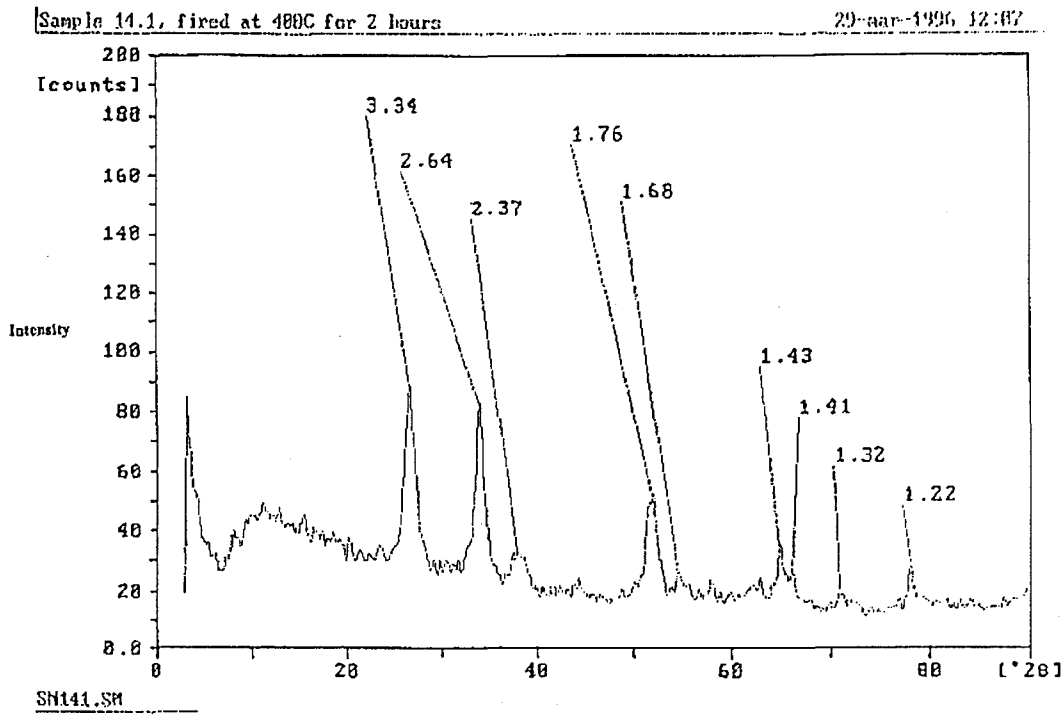

Figure 2.12: XRD of Annealed Tin Oxide

The following table shows the results of the Scherrer calculation for some samples and their annealing treatments. The [110] hkl line was used for the calculations.

Table 2.2

Annealing Conditions	Average Particle Size (nm)
No treatment	1.96
250°C for 1 hour	2.05
400°C for 2 hours	5.28

As the annealing temperature is increased, it causes an increase in average particle size. Annealing causes the material to become more crystalline and the particles to fuse together. This is clearly important for the development of high conductivity in SnO_2 coatings.

2.4 Conclusion

This chapter described the synthesis of tin oxide from two different sol-gel routes. The first method used tin tetrachloride as its main precursor and partly followed procedures from the literature. Thermogravimetric analyses showed that the resultant gels were 90% water and XRD analyses confirmed that the products were cassiterite SnO_2. However, the procedure was very time consuming due to the dialysis step to remove excess chloride ions. Also, the tin oxide produced was opaque and did not stick well to glass.

The second sol-gel route used $Sn(acac)_2Cl_2$ as its main precursor. From viscosity measurements taken, it was observed that the viscosity of the sol-gel reaction mixture increased rapidly in the first few days after mixing and then loses viscosity over the next 14 days to become a colourless solution, which was suitable for coating purposes. From thermogravimetric analyses, it was clear that two weight losses occurred at approximately 120°C and 138°C, due to the loss of water and acetylacetonate. It was observed from XRD analyses that the products were cassiterite tin oxide.

Both sol-gel methods discussed in this chapter produce tin oxide, but the second method was more favourable because of the ease of preparation, its novelty and its usefulness in applying the tin oxide to various substrates.

References

1. R. S. Hiratsuka, C. V. Santilli, D. V. Silva, S. H. Pulcinelli, *J. Non-Cryst. Solids,* **147** 67 (1992)
2. W. Lada, A. Deptula, T. Olczak, W. Torbicz, D. Pijanowsda, A. Di Bartolomeo, *J. Sol-Gel Sci. and Tech.,* **2** 551 (1994)
3. G. E. de Souzo Brito, S. H. Pulcinelli, C. V. Santilli, *J. Sol-Gel Sci. and Tech.*, **2** 575 (1994)
4. B. Orel, U. Lavrancic-Stangar, Z. Crnjak-Orel, P. Bukovec, M. Kosec, *J. Non-Cryst. Solids,* **167** 272 (1994)
5. W. Dazhi, W. Shulin, C. Jun, Z. Suyuan, L. Fangqing, *Phy. Rev. B,* **49** 14282 (1994)

6. Y. Lin, C. Wu, *Surface and Coatings Tech.* **88** 239 (1996)

7. D. H. Everett, *Basic Principles of Colloid Science*, Royal Society of Chemistry (1988)

8. C. J. Brinker, G. W. Scherer, *The Physics and Chemistry of Sol-Gel Processing,* Academic Press Limited, London (1990)

9. W. J. Poppiel, *Introduction to Colloid Science,* Exposition Press, Inc., New York (1978)

10. H. R. Hruyt, *Colloid Science I: Reversible Systems, Macromolecular and Association Colloids,* Elsevier Publishing Company, Inc., London (1949)

11. *Powder Diffraction Files-Inorganic Compounds,* JCPDS International Centre for Diffraction Data, Philadelphia (1984)

12. M. Henry, J. Jolivet, J. Livage, *Structure and Bonding,* 77 153 (1992)

3.1 Introduction

This chapter discusses a study of the application of sol-gel tin oxide coatings to glass substrates, and the electrical and optical properties of the coatings. Tin oxide adheres well to glass, and this is the most commonly used substrate. For our purposes, tin oxide was applied to inorganic glass substrates in order that they could be heated to high temperatures (~600°C), thus allowing the tin oxide coatings to anneal and become more conductive.

Pre-cleaned silica and borosilicate substrates were used for the experiments described below. The tin oxide coatings were applied to the substrates using dip-coating and solvent casting techniques. It was found that some of the coatings produced were very thin (sub-micron), a fact which caused difficulties in directly measuring their thicknesses. Several techniques were used in the determination of the thin film thicknesses. Optical microscopy was used to examine the quality of the tin oxide thin films and scanning electron microscopy backscattering analysis was used to investigate whether the n-type dopants were evenly distributed in the tin oxide films. The contribution made from polarons to the p-type conductivity was investigated using near-infrared spectroscopic analysis.

3.2 Experimental

3.2.1 Pre-cleaning of Glass Substrates

Pre-cleaning of the substrates is essential for optimum adherence of the coating on the substrates. The glass substrates used were borosilicate slides (BDH) and 1mm thick silica substrates (Moores EVIC glassworks, Walton-on-Thames, Surrey).

Precleaning of Borosilicate and Silica Substrates

Following a previously-published procedure, substrates were prepared as follows[1]:

(i) Ultrasonically cleaned in 10% aqueous Teepol detergent

(ii) Ultrasonically cleaned in acetone for 5 minutes

(iii) Ultrasonically cleaned in isopropanol for 5 minutes

(iv) Rinsed in distilled water and dried in air

(v) Stored in dry, clean boxes

3.2.2 Coating Methods

Solvent Casting

This simply involved applying the liquid coating solution to the horizontal substrate surface with a Pasteur pipette and spreading it across the surface. The coated substrate was left to dry at ambient temperature. After 1 hour, it was dry and ready for heat treatments or subsequent coatings.

Dip-coating

Dip-coating is the most popular method of applying metal oxide coatings which are produced by sol-gel processes and it is used extensively in the application of tin oxide coatings to glass[2-9]. For the purposes of this work, the dip-coating process consisted of dipping the substrate into the coating solution for 10 seconds, and withdrawing it at a steady speed. One side of the substrate was then wiped clean. The coatings were allowed to dry for about 30 minutes at ambient temperature before subsequent coatings or heat treatment.

3.2.3 Annealing Conditions

Annealing of the tin oxide coatings was carried out in air in a Carbolite Eurotherm type 11/7 Muffle furnace. The conditions for the p-type doped tin oxide coatings and n-type doped SnO_2 coatings were 2 hours heating at 400°C. After heating, the power was switched off, the furnace door was left ajar and the coatings had cooled to room temperature in about 3 hours.

Some of the n-type doped samples were coated and heated according to a method in reference 1. The procedure consisted of dip-coating and air-drying, followed by annealing under the following conditions:

(i) 110°C for 1 hour

(ii) 400°C for 10 minutes

The discs were dip-coated again at this stage followed by:

(iii) 400°C for 10 minutes

(iv) 600°C for 1 hour

The coatings were left in the furnace to cool gradually to room temperature.

3.2.4 Methods for Measuring Thicknesses of SnO_2 Coatings

The accurate measurement of the thicknesses of the coatings is a crucial factor in the correct determination of the conductivities of the SnO_2 thin films. Some of the coatings produced were of the order of 10-50 microns and these coatings could be measured directly with a micrometer. However, for the coatings which were sub-micron in depth, the techniques below were used to measure their thicknesses.

Surface Profiling

SnO_2 coated substrates were measured using a "Tencor" Alpha-Step 500 Surface Profiler. Since anomalous edge-effects caused peaks or corrugations at the sides of the samples, the thicknesses used for calculations were the average of values measured on the plateaux surfaces. It was also essential to have coatings on flat substrates, as this technique relied on the sample being perfectly level on the instrument platform. See appendix 2 for examples of two surface profile images.

Interference Patterns

Some UV/visible and FTIR spectra display interference patterns, which occur when an extremely thin parallel-sided transparent film is on top of a thicker transparent layer (microscope slide). Total internal reflection occurs and it causes interference patterns, which can be used to calculate the thickness of the layers causing the interference. In this case, UV/visible spectra of tin oxide coated borosilicate substrates were recorded on a Perkin-Elmer Lambda 2 UV/visible spectrophotometer using an uncoated borosilicate microscope slide as the reference. The resulting interference patterns were used to determine the thickness of the SnO_2 films. More details and a representative spectrum are shown in appendix 2.

Indirect Thickness Measurements by ICP Analysis

Another method used to try and determine film thicknesses was by indirect measurement using inductively coupled plasma analysis.

Pieces of the coated substrates (approximately $0.5cm^2$) were carefully cut from the samples to be measured. The dimensions of each sample were measured accurately with Vernier calipers, the samples were then put into separate sample bottles containing 16ml Aqua Regia (1 part concentrated HNO_3:3 parts concentrated HCl). After 14 hours, they were ultrasonically agitated for 10 minutes before diluting the acid solution to 10%. The tin contents were measured using a Jobin Yvon JY70 Plus ICP. Appendix 2 gives more details and includes a specimen calculation of the thickness using this method.

Thickness Measurements from SEM Analysis

Tin oxide coated silica substrates were prepared by cutting pieces of the glass substrates with a diamond knife and mounting them upright on a stub. They were then gold coated and the edges observed using a JEOL JSM-T300 scanning electron microscope. Little success was had with this method as it was very difficult to differentiate between the edge of the substrate and the tin oxide layer.

3.2.5 DC Conductivity Measurements

DC conductivity measurements were taken on the SnO_2 coatings using the van der Pauw four-probe method[10]. The diagram below shows the arrangement of wires for the van der Pauw measurements. One set of wires is connected to a digital voltmeter to measure the voltage obtained, and the other to a current source. The technique assumes that the sample is of uniform thickness. Three readings were taken using the set-up shown below, the sample was then turned 90 degrees and three more readings taken in the other direction. An average of the six readings was used in the formula below to calculate the DC conductivity.

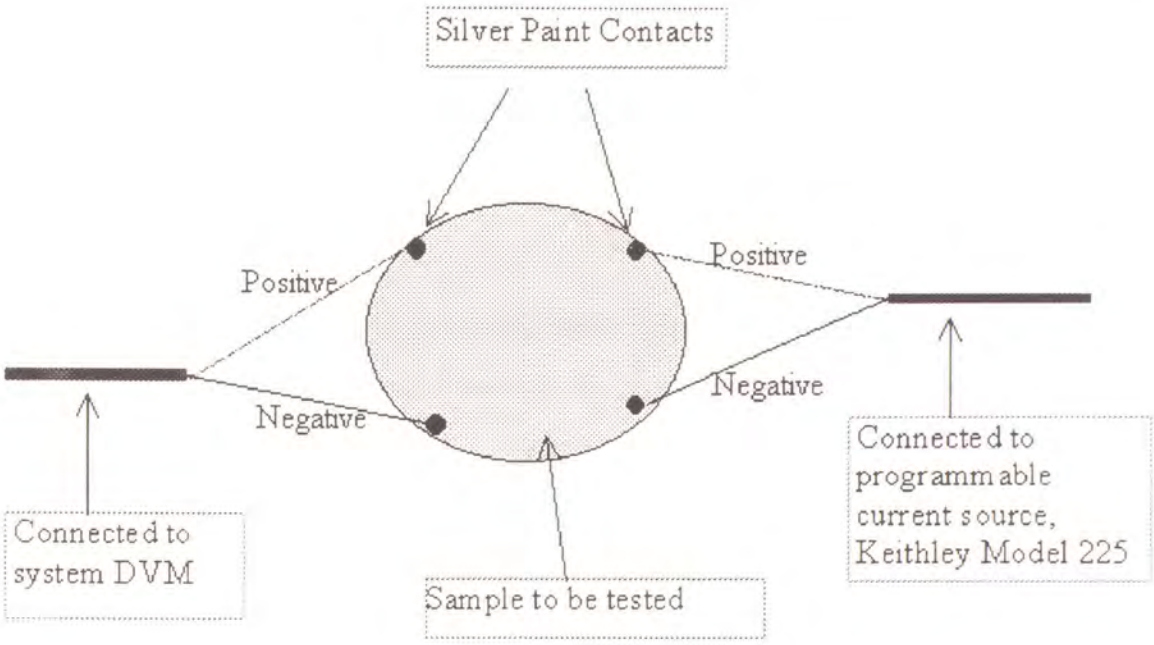

Figure 3.1: Set-up for van der Pauw Four Probe Measurements

This method gives a resistance (dV/dI) which can be converted to conductivity by the following equation:

$$\sigma = \frac{\ln 2}{\pi d R}$$

where σ = conductivity (Sm^{-1})

d = thickness of thin film (m)

R = average resistance reading of two different contact configurations (Ω)

3.2.6 Infrared Spectroscopy

Tin oxide coatings were applied to silica cover slips (1mm thick) by solvent evaporation and measured on a Perkin Elmer Paragon 1000 FTIR spectrometer over the range $7600cm^{-1}$ to $4000cm^{-1}$. The samples were not annealed. The absorbance values quoted (see section 3.3.3) were corrected for a reference (uncoated borosilicate coverslip). The absorption coefficients for the peak at $7600cm^{-1}$ were calculated using the following formula:

$$\alpha = \frac{2.303A}{t}$$

where α = absorption coefficient

A = absorbance of peak

t = thickness of thin film (calculated from interference patterns)

3.2.7 Preparation of SnO_2 Coatings on Silicon Substrates

Silicon wafer substrates with contact areas of 10 micron square were coated with tin oxide solutions by solvent casting. The tin oxide solution used was doped with indium (~ 4%). 5μL of the solutions were applied to the silicon substrates and they were dried at ambient temperature overnight. A 1 in 30 dilution was made of the coating solution and it was analysed using ICP-AES to determine the exact tin and indium concentrations. Since the volume of coating solution put on the substrate was known and the concentrations of tin and indium, it was possible to calculate the thickness of the tin oxide coating. Conductivity measurements were carried out according to the method described in section 5.2.5.

3.2.8 Electron Backscattering Analysis

A silica substrate, which had been dip-coated with an antimony doped (12% by cation substitution) tin oxide solution was carbon coated for back scattering experiments. It was analysed using a JEOL JSM-T300 scanning electron microscope.

3.2.9 Photomicroscopy

Photographs were taken of tin oxide thin films on silica substrates using a Leitz Orthoplan optical microscope with automatic camera attachment. The objective magnifications used for the photos were 2.5, 6.3, 10, 16 and 25. Photographs were taken of graticules at each magnification in order to measure the features on the tin oxide coatings.

3.2.10 Optical Transparency Measurements

The percentage transparencies of the coatings were measured using a Perkin-Elmer Lambda 2 UV/visible spectrometer over the range 350 to 900 nm. A pre-cleaned uncoated glass substrate was used as a reference.

3.3 Results and Discussion

3.3.1 Conductivity Results for P-type Doped Tin Oxide

In order to investigate the conductivity of the doped tin oxide coatings, a p-type dopant impurity (indium) was introduced into the tin oxide coating solutions, as described in chapter 2. Samples with dopant concentrations between 1 and 7 % by cation substituion were prepared and the coatings were applied to borosilicate substrates by solvent casting, and dried at room temperature for 5 hours. The thicknesses of the thin films were measured using a micrometer. It was found that there was an increase in the conductivity results as a function of dopant concentration. The bulk conductivity values for the unannealed thin films were between 4×10^{-4} Sm^{-1} and $3 \times 10^{-1} Sm^{-1}$ which is within the range for semiconductors.

Annealing of the substrates (as described in section 3.2.3) caused an increase in the conductivity by about 3 orders of magnitude to give results in the range 1 Sm^{-1} to 1×10^{2} Sm^{-1}. Disappointingly, there was no apparent trend between the conductivities and the dopant concentration. The coatings were examined using optical microscopy and it was evident that a lot of cracking had occurred. In order to try and lessen the effects of cracking on the conductivity results, special oxidised silicon substrates were used which had a 10 micron square contact area for the tin oxide coating (see section 3.2.7 for the preparation of the coatings). The conductivity values obtained for the coatings on the smaller substrates were a good deal higher, and gave ~ 400 Sm^{-1} for even unannealed p-type SnO_2. The indium dopant concentration was 3.4 at%. This confirmed what was suspected; that the cracking effect over greater sample area was masking the true conductivity results since unannealed samples on the silicon substrates achieved higher results than annealed coatings on glass substrates. It was possible that cracking still

occurred on the much smaller silicon substrates but the effect was not so great over the smaller area. Gentle annealing was carried out on the coated substrates using an infrared furnace. However, the substrates were mounted on epoxy resin composites and these were damaged in the furnace, even after the shortest possible exposure time.

Further spectroscopic studies were performed on the p-type doped material to investigate the nature of the electronic effects of doping. Those results are discussed in section 3.3.3.

3.3.2 DC Conductivity Results for N-type Doped Samples

Several sets of samples with different antimony doping concentrations were measured for this section in order to study the relationship between the conductivity results and the antimony doping concentration. Initially, DC conductivity measurements were made on unannealed samples. The following table shows the results of such a typical set of samples.

Table 3.1

Dopant conc. (Atomic %)	Bulk Conductivity (Sm^{-1})
0	1.54×10^{-4}
1	1.1×10^{-3}
2	4.7×10^{-3}
3	7.9×10^{-3}
4	8.7×10^{-3}
5	1.5×10^{-2}
6	3.4×10^{-2}
7	4.3×10^{-2}
8	1.1×10^{-1}

Figure 3.2 below shows the conductivity-concentration relationship for the data in Table 3.1. The set of samples had a fairly progressive increase in conductivity as the dopant concentration increased, the highest conductivity being the sample doped 8%.

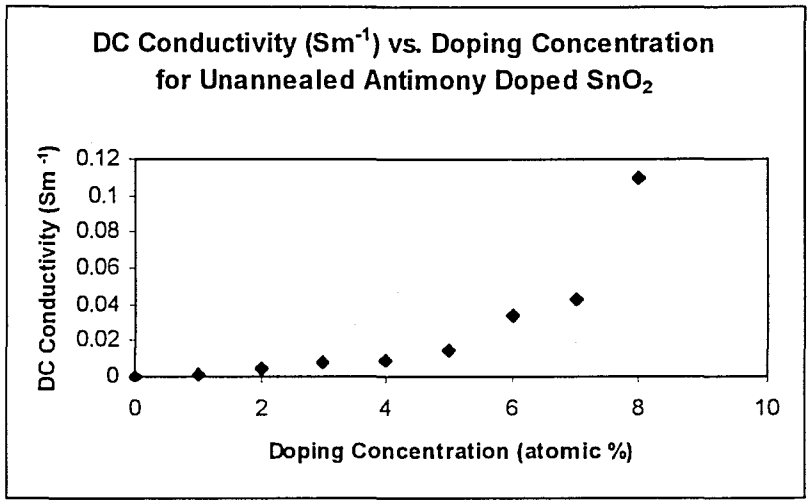

Figure 3.2: DC Conductivity Values for Unannealed n-type Doped SnO_2

From chapter two, it was seen from the thermogravimetric studies that in some cases acetone remains in the tin oxide samples. It was not known whether the residual acetone in the coating solutions was having an effect on the sol-gel process, in terms of the resulting conductivities of the tin oxide coatings. It was decided to remove the acetone (by rotary evaporation) from a set of antimony doped samples, use the solutions to coat glass substrates, measure the conductivities and compare the results with those obtained above. However, it was found that there was no obvious correlation between the conductivity values and the dopant concentration. The values obtained were scattered in a random fashion within the range 1×10^{-2} Sm^{-1} to 7×10^{-3} Sm^{-1}, which is slightly lower than the typical values obtained for the samples still containing acetone. (It appeared that the reason for the erratic results was due to morphological variations.) Therefore, the presence of residual amounts of acetone in the coating solutions did not have an appreciable effect on the conductivities of the tin oxide coatings.

Experiments were then carried out to investigate the effects of the antimony doped tin oxide samples on the DC conductivities of the coatings. The annealing conditions were

described in section 3.2.3. A typical set of results is shown in table 3.2 below for the annealed antimony doped samples. Unfortunately, in all cases a trend did not appear between the conductivity values and the dopant concentration. It was evident though, that in general the n-type doping effect led to higher conductivities than those achieved through p-type doping with indium.

Table 3.2

Doping conc. (Atomic %)	Surface Resistance (kOhms)	Bulk Conductivity(Sm^{-1})
0	79.3	13.0
3	1.8	551.0
7	8.1	123.0
9	1.2	813.0
10	6.8	148.0
11	1.0	979.0
12	12.4	80.0
13	2.4	416.0

From the literature, the optimum level of antimony dopant found for maximising bulk conductivity results was within the range 2 to 10 mol %[11-16]. In general, it was reported that antimony doped tin oxide prepared by the spray pyrolysis method[12,14,15] gave higher conductivities than those prepared by sol-gel methods[11,13,16]. Literature values vary widely, but the best previously reported conductivity result obtained for antimony doped tin oxide prepared by a sol-gel process was ~ 4 x 10^5 Sm^{-1} for an antimony doping concentration of 10 mol %[16]. As can be clearly seen from table 3.2, the best DC conductivity result obtained for antimony doped tin oxide in this work was about three orders of magnitude lower than that. The proposed reason for this was the cracking problem, which also occurred with the p-type coatings.

Photomicroscopy carried out on some coated silica substrates showed the extent of the cracking problem (see figures 3.3 and 3.4).

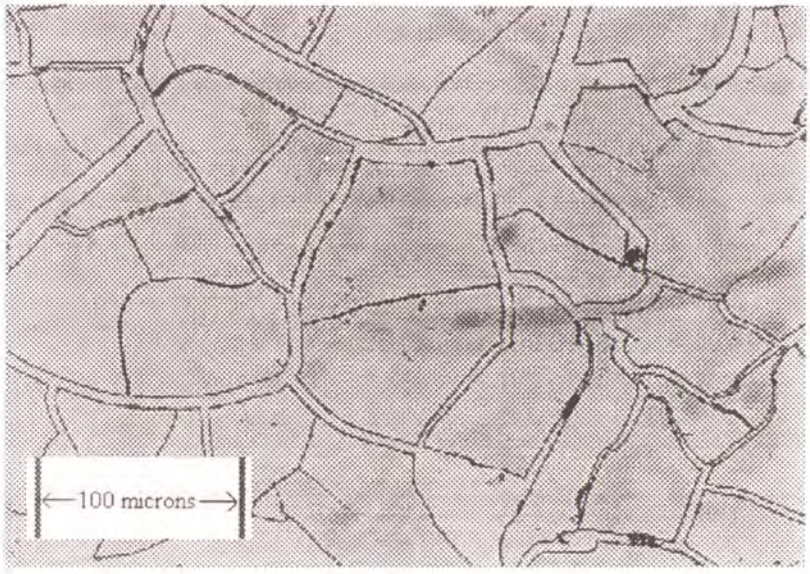

Figure 3.3: Annealed antimony Doped SnO_2 Coating on Silica (magnification x 25)

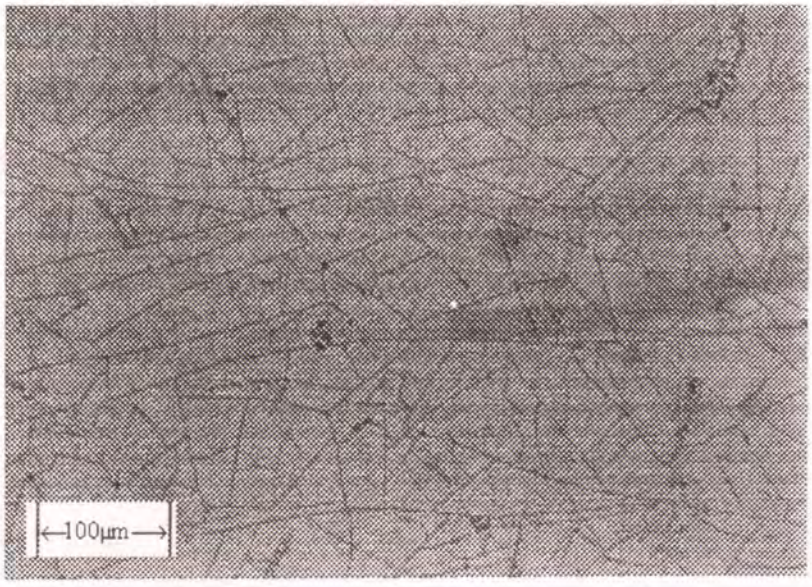

Figure 3.4: Annealed antimony Doped SnO_2 Coating on Silica (magnification x 16)

Since the overall aim of the project was to apply tin oxide coatings to polymer substrates, the cracking problem on glass substrates was not investigated further. However, a possible reason for the cracking is the high water and acetylacetone contents in the tin

oxide, as shown from thermogravimetric analysis. A possible solution would be to dry the coatings using supercritical conditions, which allow the escape of any residual water or solvents from the coatings without causing cracks.

For the work described in this section, several different coating techniques were used and it was found that measuring the thicknesses of the thin films with a micrometer or by surface profilometry were the most reliable methods.

As mentioned in section 3.2.4, the SEM technique of measuring was not unsuccessful. Also, the ICP analysis method gave very unrealistic and unreliable results. It seemed that the tin oxide did not fully dissolve and also it tended to reprecipitate subsequently, since repeat measurements made three days after the first ones showed a much lower tin content than initially.

3.3.3 Spectroscopic Studies on P-type Tin Oxide

Near-infrared spectra of tin oxide samples doped 0 to 7 mol% with indium were recorded over the range 4000 $\rightarrow$ 7800cm^{-1}. The coatings were applied by solvent evaporation and were unannealed. In all samples the films were of sufficient quality to show an interference pattern, and so it was easy to determine the film thicknesses from its periodicity. In some cases there was a second wave running through the spectrum due to step formation, but this was not a serious problem (see figure 3.5 for a representative FTIR spectrum).

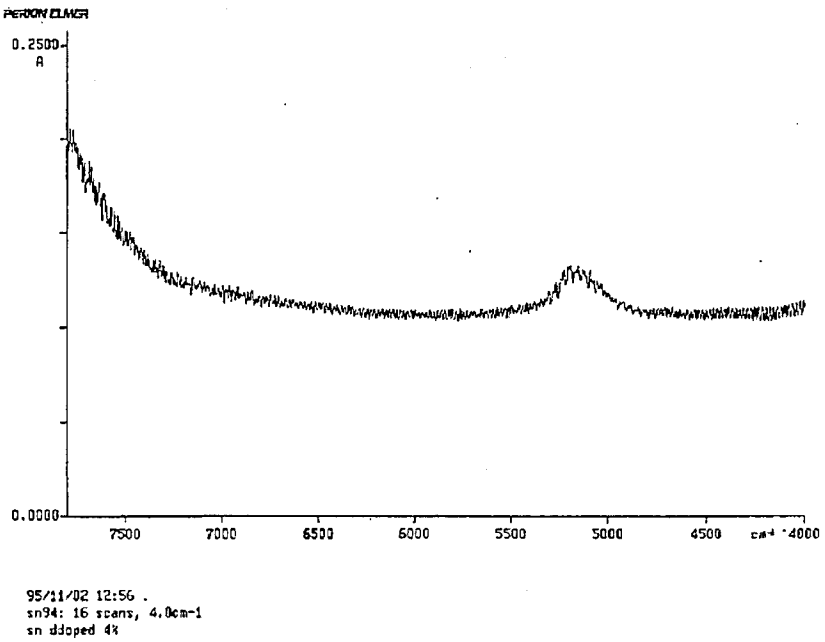

Figure 3.5: Near infrared spectrum of a p-type doped SnO_2 sample

Each spectrum contained a peak at approximately 5200cm^{-1}, and in all samples there was a new, intense peak extending beyond the range of the instrument (at approximately 7600cm^{-1}). Table 3.3 lists the absorbances of the peaks at 5200cm^{-1} and the absorption coefficients of the peaks at 7600cm^{-1}.

Table 3.3

Doping conc.(mol%)	Absorbance of peak at 5200cm^{-1}	Absorption coefficient of peak 7600cm^{-1} (m^{-1})
0	0.025	2.51×10^5
1	0.030	5.02×10^5
2	0.026	9.50×10^5
3	0.018	1.13×10^6
4	0.029	1.05×10^6
5	0.036	1.08×10^6
6	0.014	5.75×10^5
7	0.028	6.10×10^5

The peak at 5200cm^{-1} is attributable to the presence of a small polaron which is a bound carrier of low mobility, caused by the cationic defects in the amorphous tin oxide[17,18]. As discussed in section 1.6, polarons can exhibit an absorption in the mid-infrared region due to the resonance of the polaron hopping process caused by the application of the infrared frequency.

The stronger, broader peak at around 7600cm^{-1} is typical of the kind caused by free carriers (large polarons) and its intensity was also expected to be an indication of the amount of dopant needed to achieve maximum conductivity after annealing. (In effect, it is an indication of the "local" a.c. conductivity of the material.) From the graph of absorption coefficients at 7600cm^{-1} versus doping concentration (see figure 3.6) the maximum of the peak occurs at approximately 3.5% doping level. The optimum amount of dopant was therefore expected to be 3.5%. As shown in section 3.3.1, the optimum level of dopant required for maximising the bulk conductivity was not established by experimentation.

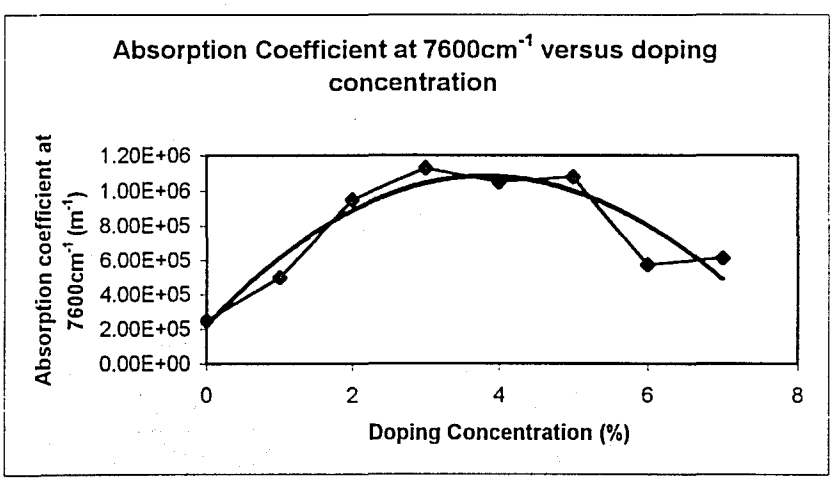

Figure 3.6: Absorption Coefficient at 7600cm^{-1} as Dopant Concentration Varies

To further investigate if the peaks were due to the presence of polarons in the p-type tin oxide coatings, the mobility of carriers in an unannealed indium doped tin oxide sample (see section 3.2.7 for its preparation) was calculated as 2.4 x 10^{-2} $cm^2V^{-1}s^{-1}$ using the following equation:

$$\sigma = n\, e\, \mu$$

where σ = conductivity (measured)

n = density of free carriers (calculated from the measured concentration of dopant)

e = charge of free carriers (1.602×10^{-19} C)

μ = mobility

This value calculated for the mobility of the carriers is at the higher end of the range of mobilities for polaronic charge carriers (see section 1.6) and is further evidence for the presence of large polarons.

In SnO_2, n-type conduction seems to be band-like while p-type SnO_2 mobility is significantly less, and involves polarons. We could propose an energy band diagram for SnO_2, typical of post-transition metal oxides, and bearing in mind that Sn is 4^+.

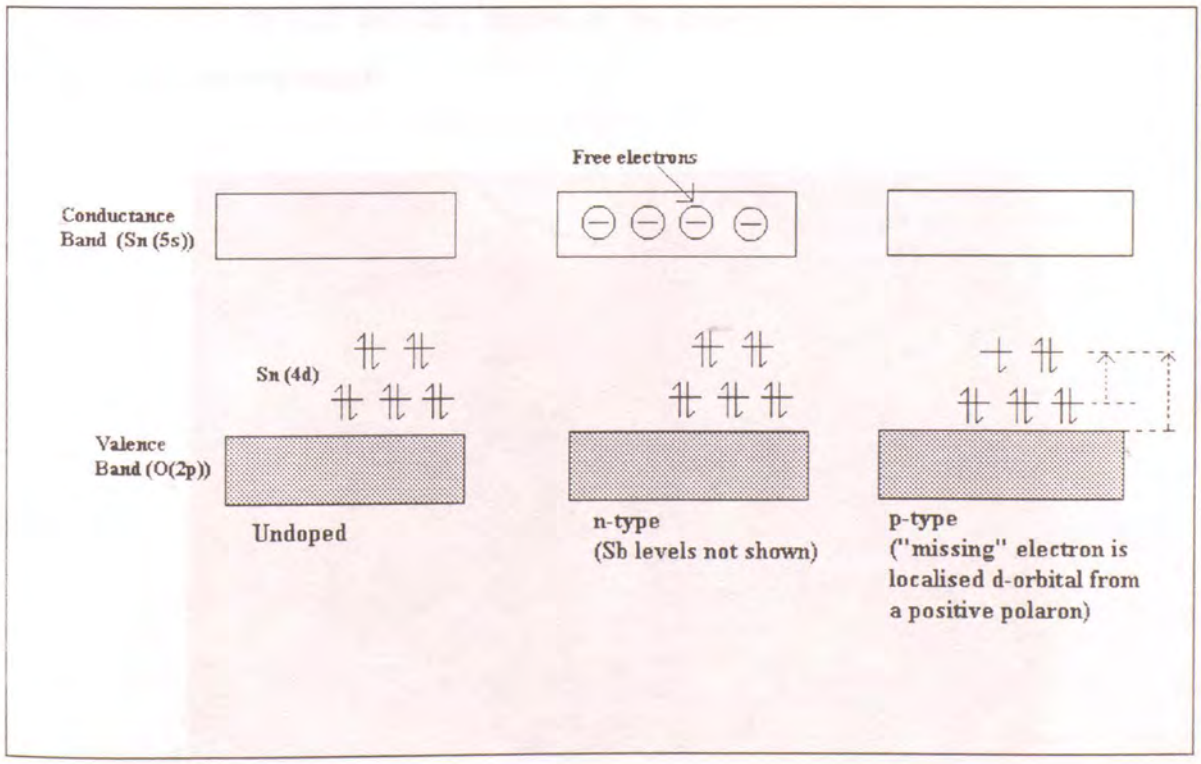

Figure 3.7 Energy Band Diagram for SnO_2

From the FTIR spectra, it is possible to estimate both the transition energies (shown in dashed arrows above) and the activation energy for polaron motion, ΔE_{act}.

3.3.4 Backscattering Evidence for Uniform Coatings

It was decided to look at a highly doped tin oxide coating using scanning electron microscopy to see whether the antimony would be detectable by x-ray elemental analysis, and if so to examine whether the antimony was evenly distributed throughout the thin film. It was not found possible to obtain separate x-ray elemental maps for tin and antimony they are only one atomic number apart and their x-ray emission patterns are very similar. In the coating examined, tin had such a high concentration in relation to antimony that the small peaks for antimony got overshadowed by the peaks for tin.

However, it was possible using back scattering electron images to establish the areas which were tin or antimony rich. Back scattering electron techniques show up areas of higher atomic number as lighter areas. The relative percentages of tin and antimony were calculated from the light and dark regions of the image (see figure 3.8 for a small section of the backscattered image).

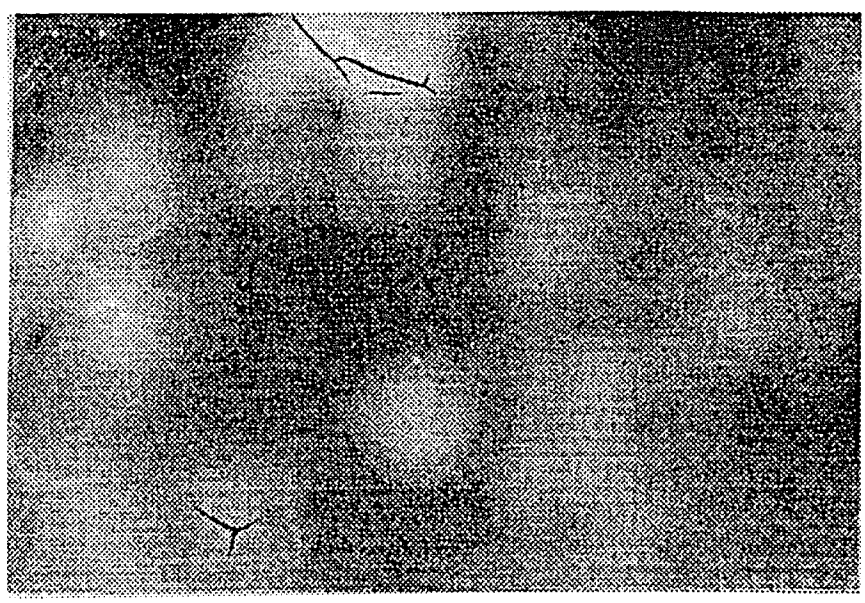

Figure 3.8: Backscattering Image of Antimony Doped SnO_2

The lighter areas gave a relative percentage of 17% antimony in relation to tin, while in the darker areas the relative percentage of antimony was 14%. The percentages were calculated using the software on the SEM. The original dopant concentration in the sol-gel mixture was 12 atom %. This indicates slight fluctuations of antimony concentration at high dopant loadings, but not a disproportionation into segregated phases of metallic and insulating material.

3.3.5 Percentage Transparency Results

Borosilicate and silica substrates were coated with tin oxide of various concentration of dopant. UV/visible spectra of these substrates were recorded over the range 400 to 1100nm. The transmittance of the coatings was calculated from the the absorbance of the coatings using the equation below. Multiplying the transmittance by 100 gave the percentage transparency of the tin oxide films.

$$A = \log_{10} \frac{1}{T}$$

where A = absorbance and T = transmittance.

They had an average percentage transparency of 85%. After annealing, the average percentage transparency value for these substrates was approximately 45%. Figure 3.9 and 3.10 shows two of the UV/Visible spectra.

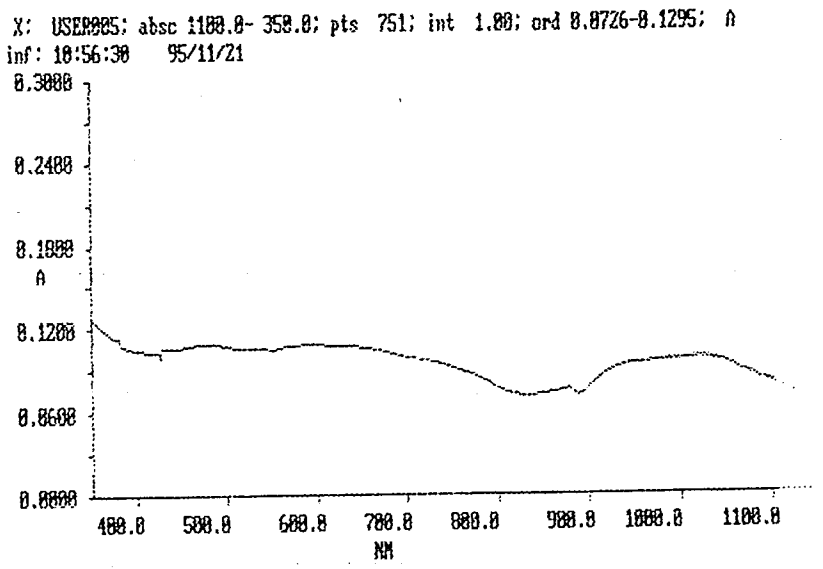

Figure 3.9: UV/visible Spectrum of Unannealed SnO_2

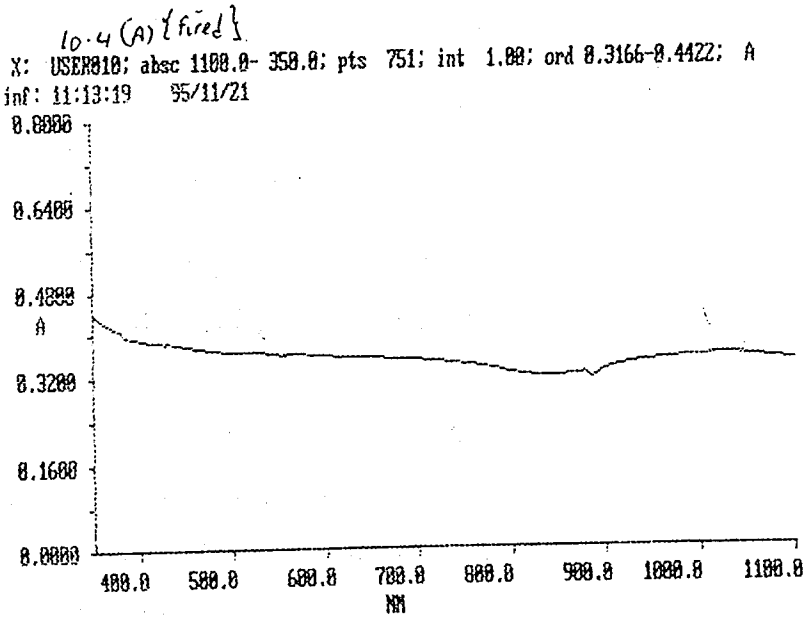

Figure 3.10: UV/visible Spectrum of Annealed SnO_2

The loss of transparency was substantially due to micro-cracking of the ITO films. There was no significant difference between the transparencies of p-type and n-type doped SnO_2.

3.4 Conclusions

Pre-cleaned borosilicate and silica substrates were coated with indium and antimony doped tin oxide coating solutions by dip-coating and solvent casting. Some of the samples were annealed and the DC conductivities of all the samples were measured using the van der Pauw four probe method. Completely reproducible relationships were not established between the conductivities and dopant concentrations, however it was clear that superior results were obtained from the antimony doped samples (see table 3.4 below for a summary).

Table 3.4

Sample	DC Conductivity Results Range (Sm^{-1})
Unannealed p-type SnO_2	4×10^{-4} to 3×10^{-1}
Annealed p-type SnO_2	1 to 100
Unannealed n-type SnO_2	1×10^{-3} to 1×10^{-1}
Annealed n-type SnO_2	13 to 800

On the basis of these findings, it was decided to concentrate all efforts on applying antimony doped tin oxide coatings to the polymer substrates in order to maximise the resulting conductivities.

From near-infrared spectroscopic studies on the p-type samples, bands due to the presence of polarons were observed. The magnitude of the calculated carrier mobilities was typical of those due to large polarons.

Backscattering analysis on antimony doped samples using the SEM showed that the antimony dopant was quite evenly distributed throughout the coatings.

The percentage transparency for all unannealed coatings was high at approximately 80% over the visible range. After annealing, the percentage transparency was reduced to about 40%. The loss of transparency was not due to new optical absorptions caused during

annealing, as there were no extra peaks present in the UV/visible spectra. Also, it was not due to crystallization effects since the SnO_2 crystallite sizes after annealing (as shown in chapter 2) were not large enough to cause scattering effects. Therefore the loss in transparency was believed to be due to micro-cracking of the films on annealing.

References

1. S. Park, J. D. Mackenzie, *Thin Solid Films* **258** 268 (1995)
2. R. Puyane, I. Kato, *Proc. Soc. Photo-optical Instrumentation Eng.*, **401** 190 (1983)
3. D. Mattox, *Thin Solid Films,* **204** 25 (1991)
4. W. Lada, A. Deptula, T. Olczak, W. Torbicz, D. Pijanowska, A. Di Bartolomeo, *J. Sol-Gel Sci. and Tech.*, **2** 551 (1994)
5. A. Maddalena, R. Dal Maschio, S. Dire, A. Raccanelli, *J. Non-Cryst. Solids,* **121** 365 (1990)
6. C. Terrier, J. P. Chatelon, R. Berjoan, J. A. Roger, *Thin Solid Films,* **263** 37 (1995)
7. C. Terrier, J. P. Chatelon, J. A. Roger, *Thin Solid Films,* **295** 95 (1997)
8. R. Bel Hadj Tahar, T. Ban, Y. Ohya, Y. Takahashi, *J. Appl. Phys.*, **82** 865 (1997)
9. M. A. Aegeter, A. Reich, D. Ganz, G. Gasparro, J. Pütz, T. Krajoewski, *J. Non-Cryst. Solids,* **218** 123 (1997)
10. L. J. van der Pauw, *Philips Res. Reports,* **13** 1 (1958)
11. B. Orel, U. Lavrencic-Stangar, A. Crnjak-Ore, P. Bukovec, M. Kosec, *J. Non-Cryst. Solids,* **167** 272 (1994)
12. E. Shanthi, V. Dutta, A. Banerjee, K. L. Chopra, *J. Appl. Phys.*, **51** 6243 (1980)
13. S-S. Park, H. Zheng, J. D. Mackenzie, *Materials Letters,* **22** 175 (1995)
14. H. Kaneko, K. Miyake, *J. Appl. Phys.*, **53** 3629 (1992)
15. D. J. Goyal, C. Agashe, B. R. Marathe, M. G. Takwale, V. G. Bhide, *J. Appl. Phys.*, **73** 7520 (1993)
16. C. Terrier, J. P. Chatelon, J. A. Roger, *Thin Solid Films,* **295** 95 (1997)
17. H. G. Reik, D. Heese, *J. Phys. Chem. Solids,* **28** 581 (1967)

18. B. Fisher, D. S. Tannhauser, *J. Chem. Phys,* **44** 1663 (1966)

19. H. J. Pain, *The Physics and Vibrations of Waves,* 3rd Edition, John Wiley and Sons Limited, New York (1983)

4.1 Introduction

4.1.1 Overview of Chapter

This chapter concentrates on the surface pre-treatments given to the polymer substrates before they were coated with tin oxide. In order to determine the effects of the surface treatments, contact angle measurements were made, which could be used to calculate the surface energies of the polymers. An increase in surface energy reflects an increase in the wettability of the polymer surfaces. Fourier transform infrared diffuse reflectance methods also helped to characterise some of the structural changes happening on the surface of the polycarbonate substrates as a consequence of the surface treatments.

The polymers used in these studies were polycarbonate and poly (methyl methacrylate) (supplied by VT Plastics, Mitcham) and poly (ethylene terephthalate) (RS Components Ltd).

4.1.2 Surface Energy Measurements

The extent to which a solid is wetted by a liquid (and the extent to which the liquid spreads) are loosely described as the wettability of the solid. This was an important factor to consider in this work as the even coating of the doped tin oxide colloids depended on the compatibility of the polymer substrates.

The usual way of quantifying the wettability is through the measurement of the contact angles of a certain liquid (usually water) on the surface of the polymer and then using the measurements in the calculation of the surface energy of the substrates. The contact angle (θ) is defined as the angle between a solid surface and a tangent drawn to the profile of the droplet taken through the liquid where it meets the solid surface (see figure 4.1). The smaller the contact angle the more wettable the surface and the higher the surface energy of the substrate.

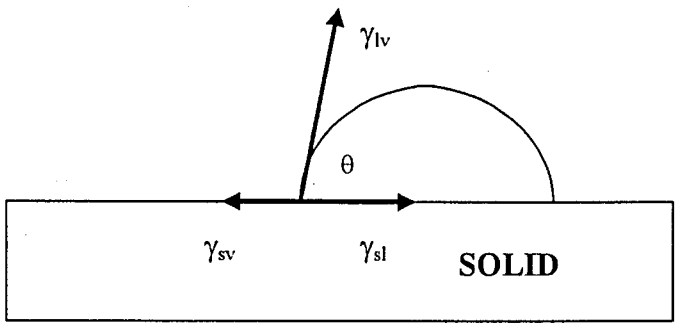

Figure 4.1: Contact angle (θ) of a liquid on a solid

The drop of liquid is in equilibrium when the three forces of interfacial tension acting upon it satisfy the following equation, which is known as Youngs equation[1,2].

$$\gamma_{sv} = \gamma_{sl} + \gamma_{lv} \cos \theta$$

Equation 4.1

θ = contact angle;

γ_{sv} = surface tension (free energy) at solid/vapour interface;

γ_{sl} = surface tension at solid/liquid interface;

γ_{lv} = surface tension at liquid/vapour interface.

The total free energy of a solid or liquid can be divided into the two components which arise from the different intermolecular forces present:

$$\gamma^{(total)} = \gamma^{d} + \gamma^{p}$$

Equation 4.2

γ^{d} = dispersive component of surface free energy;

γ^{p} = polar component of surface free energy.

Non-polar background forces in molecules e.g. van der Waals forces are characteristic of the dispersive component whereas the polar component is the result of any molecular dipoles which are present.

Fowke used the following equation to show that the interfacial tension of a solid and liquid (γ_{sl}) can be expressed in terms of the surface tensions of the two individual phases (γ_s and γ_l)[3-6]:

$$\gamma_{sl} = \gamma_s + \gamma_l - 2(\gamma_s^d \gamma_l^d)^{1/2} - I_p$$

Equation 4.3

where the superscript d is the dispersive force component from the two phases and I_p is the contribution from the polar component. If contact angle measurements are made using liquids with known dispersive and polar components, it is possible to calculate the polar and dispersive components of the solid.

The "two liquid" method of measuring contact angles was used in this work. It involves measuring the contact angle of a drop of water on a solid, while immersed in another liquid, usually an n-alkane (see figure 4.2).

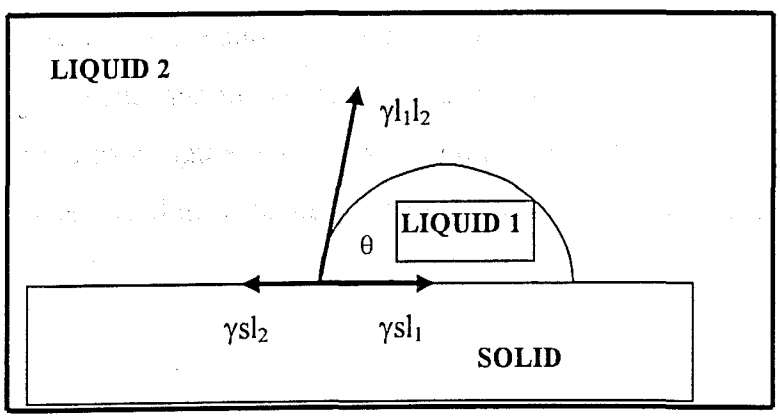

Figure 4.2: Two Liquid Method of Measuring Contact Angles

Using equation 4.3, the interfacial tensions can be expressed as that between the solid and liquid 1 (γsl_1) and that between the solid and liquid 2 (γsl_2), as shown below in equations 4.4 and 4.5.

$$\gamma sl_1 = \gamma s + \gamma l_1 - 2(\gamma s^d \gamma l_1^d)^{½} - I^p sl_1$$

Equation 4.4

$$\gamma sl_2 = \gamma s + \gamma l_2 - 2(\gamma s^d \gamma l_2^d)^{½} - I^p sl_2$$

Equation 4.5

By combining these equations and using Youngs equation (equation 4.1) to replace γsl_2-γsl_1 with $\gamma l_1 l_2 Cos\theta$ gives:

$$\gamma l_1 - \gamma l_2 + \gamma l_1 l_2 Cos\theta = 2(\gamma s^d)^{½} [(\gamma l_1^d)^{½} - (\gamma l_2^d)^{½}] + (I^p sl_1 I^p sl_2)$$

Equation 4.6

If liquid 1 (l_1) is water and liquid 2 (l_2) is an alkane e.g. hexane, the equation becomes:

$$\gamma_w - \gamma_h + \gamma_{wh} Cos\theta = 2(\gamma s^d)^{½} [(\gamma_w^d)^{½} - (\gamma_h^d)^{½}] + I^p sw$$

$$Y = M X + C$$

Equation 4.7

This can be expressed as the equation of a line (y = mx + c), as shown above. Using the contact angle measurements and the necessary constants for water and the second liquids, a graph can be plotted as in figure 4.3 below. On the graph C5, C7 and C12 are written beside the co-ordinates found for pentane, heptane and dodecane respectively.

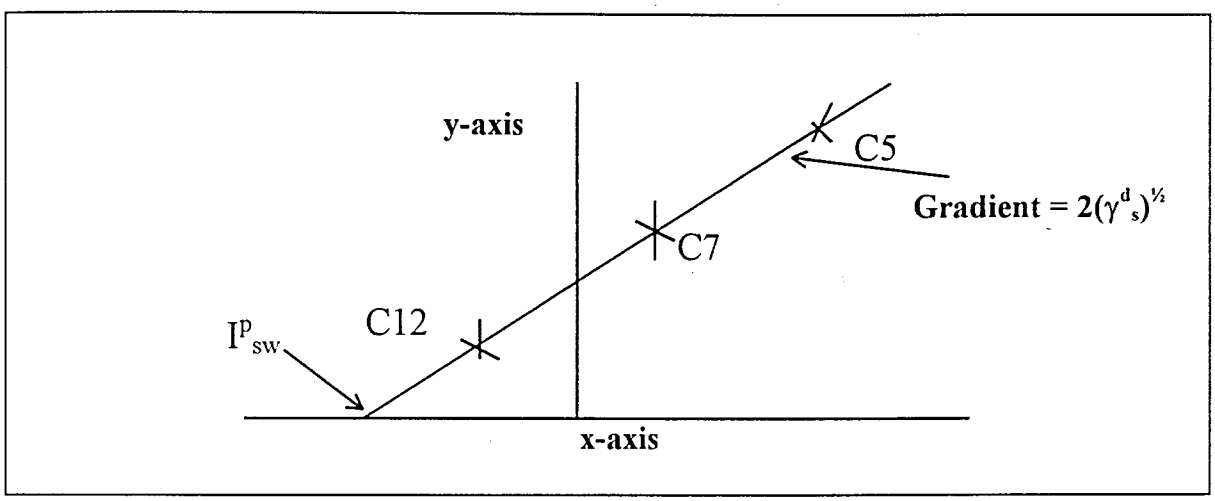

Figure 4.3: Calculation of Polar and Dispersive Components of Surface Energy

The gradient gives a value for the dispersive component of the solid surface by the relationship shown. The polar component of the surface energy is calculated from the intercept that the plot makes with the x-axis, where: $\gamma^p_s = (I^p_{sw})^2 / 4\gamma^p_w$. Sum of polar and dispersive components give the total surface energy of the solids in mJm^{-2}. For this work, the three alkanes selected as second liquids were pentane, heptane and dodecane.

4.1.3 Background to Polymer Pre-Treatments

The three polymers used in the studies were poly (methyl methacrylate), polycarbonate and poly (ethylene terephthalate), the structures of which are shown below[7].

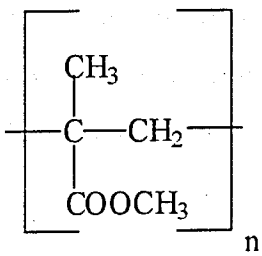

Figure 4.4: Poly (methyl methacrylate)

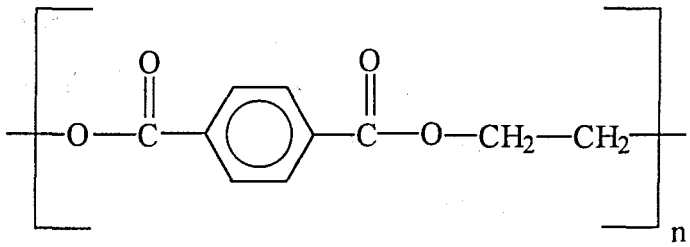

Figure 4.5: Poly (ethylene terephthalate)

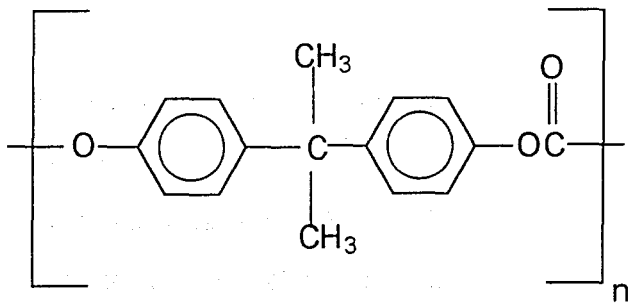

Figure 4.6: Polycarbonate

The polymers are hydrophobic in nature, with little affinity for wetting by aqueous based solutions. From a literature review of relevant papers[8-10] it was found that various methods have been used to increase the wettability of hydrophobic polymers. These include cold plasma treatment, treating the polymers with acid and UV/ozone treatment. The most promising results were reported by Pointer *et al.* with their pre-treatment of polycarbonate substrates using a combination of UV radiation and ozone[8]. Using the method devised by Vig[9], they increased the surface energy of polycarbonate by 60% in just two minutes. For this work, it was decided to construct a similar UV/ozone cleaning apparatus and examine its effect on the wettability of the polymer substrates.

4.2 Experimental

4.2.1 Pre-Cleaning of Polymers

A necessary part of the polymer preparation is the pre-cleaning of the polymers before actual surface treatment. This process removes any greasy or dusty residues on the polymer surfaces before treatments.

A Pre-cleaning of Polycarbonate Substrates

Following the recommendations of Vig, the following method was used to pre-clean the polycarbonate substrates[9]:

(i) While immersed in ethanol the substrate was wiped with a tissue.

(ii) Ultrasonic cleaning in IMS for 5 minutes.

(iii) The substrate was placed in boiling ethanol for 2 minutes.

(iv) Ultrasonic cleaning in ethanol for 5 minutes.

(v) The substrate was rinsed several times with distilled water and placed in a dust free environment for storage.

B Pre-Cleaning of PMMA

The method used in the pre-cleaning of PMMA substrates was as follows:

(i) Ultrasonic cleaning in detergent (10% Teepol) and water for 5 minutes

(ii) Rinsing with distilled water

(iii) Ultrasonic cleaning isopropanol for 5 minutes

(iv) Rinsing with distilled water

The substrates were stored separately in clean plastic boxes.

C Pre-cleaning of Poly (ethylene terephthalate)

The following pre-cleaning method was used on PET and PEN substrates prior to coating with tin oxide. Further surface treatments were not necessary for these substrates.

(i) Ultrasonic cleaning in detergent (10% Teepol) and water for 5 minutes

(ii) Rinsing with distilled water

(iii) Ultrasonic cleaning in isopropanol for 5 minutes

(iv) Rinsing with distilled water

The PET substrates were then stored separately in dry, clean polythene bags.

4.2.2 Surface Treatment with Sodium Hydroxide

Polycarbonate, poly (methyl methacrylate) and poly (terephthalate) substrates were treated by heating in 2M NaOH at 50°C for different periods of time. After treatment, they were rinsed with distilled water, dried and stored in clean dry boxes.

4.2.3 Surface Treatment using UV/ozone

The UV/ozone apparatus (see figure 4.7) was set up similarly to the apparatus described by Vig[9]. The UV source was a 200 Watt low pressure mercury lamp which emits radiation mainly over the range 180 – 300nm.

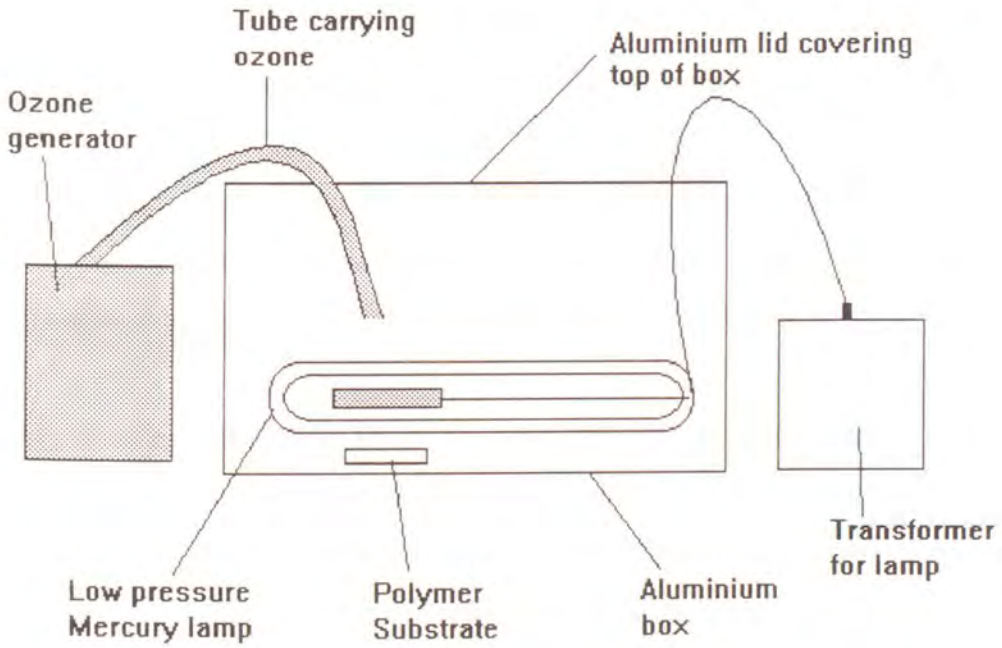

Figure 4.7: UV/ozone Apparatus

The polymer substrates were placed about 3 cm from the mercury lamp, making sure that the substrates were directly underneath the arc of the lamp. The ozone generator produced ozonized air at a rate of 600 cm^3 min^{-1} which meant that it took approximately ten minutes for the aluminium box to become saturated with ozone. The lamp was then turned on for the required length of time. After treatment, the polymer substrates were immediately put in clean, dry plastic boxes for storage.

4.2.4 Contact Angle Measurements

The "sessile drop" method was used to measure the contact angles of water on the polymer substrates[6]. This involved viewing the drops of water through a travelling microscope and using a goniometer eyepiece to directly measure the contact angles. The measurements were carried out in a darkened laboratory with a light reflecting off a white surface directly onto the samples to increase the contrast between the drops of water and the surrounding liquid.

In all cases, three drops of water were placed along the surface of the substrates using a microsyringe. The substrate was then lowered into a glass container filled with the appropriate n-alkane (pentane, heptane or dodecane) and the container was covered. The contact angles were measured on both sides of the drops of water and an average of the six results was used in the calculations. Between measurements with different alkanes, the polymer substrates were rinsed thoroughly with distilled water.

4.2.5 Fourier Transform IR Reflectance Spectral Measurements

Specular reflectance mid-infrared measurements were carried out on surface treated polycarbonate substrates using a Perkin Elmer System 2000 FTIR spectrometer. It was possible to vary the angle of incidence of the infrared beam, and the angles used were 20, 45 and 80 degrees. The number of scans used for each spectrum was 16. After scanning, the spectra were normalised and baseline corrected using a Sadtler Search infrared software package. (This work was carried out by the author in the laboratories of DERA, Farnborough.)

4.3 Results and Discussion

4.3.3 Results of Surface Treatments with Sodium Hydroxide

Polycarbonate and poly (methyl methacrylate) substrates were treated for 2 hours at 50°C in 2M NaOH. Contact angle measurements were recorded using the "two liquid" method as described earlier and their equivalent surface energies calculated. An example is shown below for the calculation of the surface energy for the PMMA sample which had received surface treatment. Table 4.1 shows the average contact angles measured in the three different alkanes and the calculation of the x-axis and y-axis coordinates (see section 4.1.2 for more details).

Table 4.1: Calculation of values for Treated PMMA Substrate

Alkane	Pentane	Heptane	Dodecane
Average θ	78.7° ± 0.5°	67.5° ± 0.5°	56.5° ± 0.5°
Cos θ	0.20	0.38	0.55
γ_w^d	21.6	21.6	21.6
γ_h^d	16.2	20.3	25.4
$x = [(\gamma_w^d)^{½} - (\gamma_h^d)^{½}]$	**0.63**	**0.15**	**-0.39**
γ_w	72.6	72.6	72.6
γ_h	16.2	20.3	25.4
γ_{wh}	51.4	51.0	51.1
$y = \gamma_w - \gamma_h + \gamma_{wh}\text{Cos}\theta$	**66.7**	**71.8**	**75.3**

By plotting the x and y co-ordinates, the following graph is obtained (figure 4.8). A line of best fit was plotted through the co-ordinates and the equation of the line is shown on the graph.

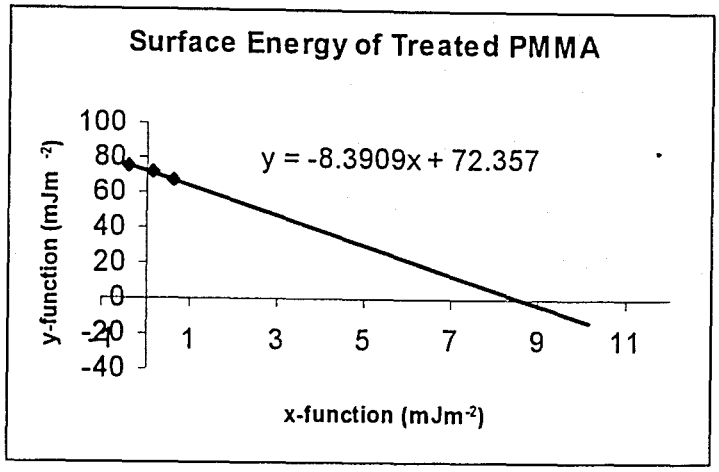

Figure 4.8: Calculation of the Surface Energy of a PMMA Sample

The dispersive and polar components of the surface energy were calculated from the slope of the graph and the interception it makes with the x-axis respectively, as described in section 4.1.2. A value of 17.60 ± 1.5 mJm^{-2} was obtained for the dispersive component and 0.37 ± 0.2 mJm^{-2} for the polar component of the surface energy.

Table 4.2 shows the polar, dispersive and total surface energies for all the samples.

Table 4.2 Average Surface Energy Results for PMMA and PC

	Untreated PMMA substrate	Treated PMMA substrate	Untreated PC substrate	Treated PC substrate
Polar component (mJm^{-2})	0.71	0.37	0.17	0.38
Dispersive component (mJm^{-2})	6.89	17.60	30.97	20.29
Total Surface energy (mJm^{-2})	7.60	19.97	31.14	20.67

From the table, it can be seen that the overall surface energy of the polycarbonate sample decreases as a result of the treatment with sodium hydroxide. The polar component of the surface energy showed a slight increase but there was a large decrease in the dispersive

component. Decreases in the dispersive component of surface energies represent a degradation of the polymer surface. This was visibly evident for the surface treated PC sample, as the polymer substrate had become cloudy in appearance as a result of the surface treatment. Since it was necessary for the polymers to remain transparent, a gentler method of treating the PC was obviously called for and this led to the introduction of UV/ozone treatment for the polycarbonate substrates.

For the PMMA sample, there was an increase in its total surface energy. It had a relatively large increase in the dispersive component and a slight decrease in the polar component. An increase in the dispersive component represents the formation of C=C bonds or free radicals on the surface of the polymer. Experiments on treating PMMA for different lengths of time in the sodium hydroxide solutions were carried out to further investigate the effect of surface treatment on the surface energies of the substrates. The results are shown in the graph in figure 4.9.

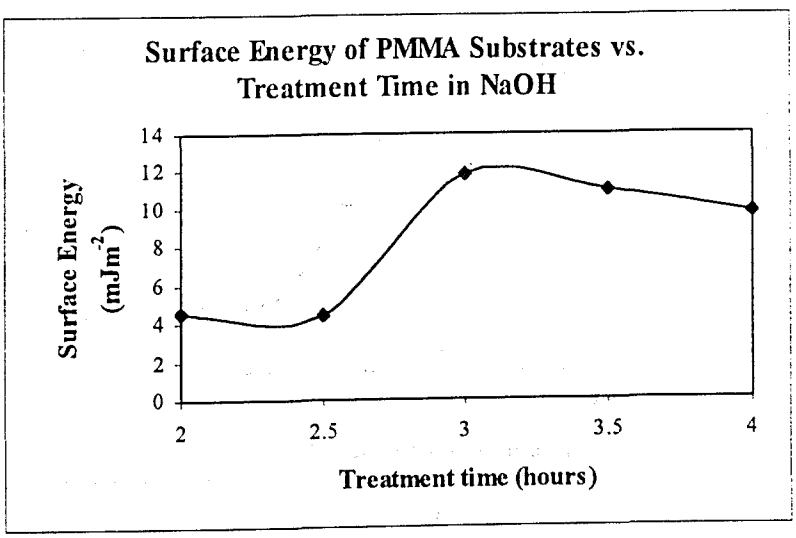

Figure 4.9: Change in Total Surface Energy as a Result of Treatment with NaOH

As can be seen from the graph, the surface energy is greatest for the samples treated for 3 hours. After 3 hours, the surface energy of the samples decreases again. It may be noticed by the reader that surface energies can vary for samples which have undergone the same

treatment e.g in table 4.2 the sample which had been treated for 2 hours had a value of 20.12 mJm^{-2} but for the sample shown in figure 4.9, its surface energy was ~4.5mJm^{-2}. These discrepancies in results are often found in the calculation of surface energies but it is usually the relative change which is more significant than the actual value[8]. However, the graph above clearly shows a trend that the samples treated for three hours had the biggest change in surface energy and that the surface energy decreases again after that amount of treatment time.

The graph (figure 4.10) showing the variation of the dispersive component with treatment time has roughly the same shape as the graph showing the total surface energy (figure 4.9). This is mainly due to the fact that the dispersive component makes a larger contribution to the overall surface energy than the polar component.

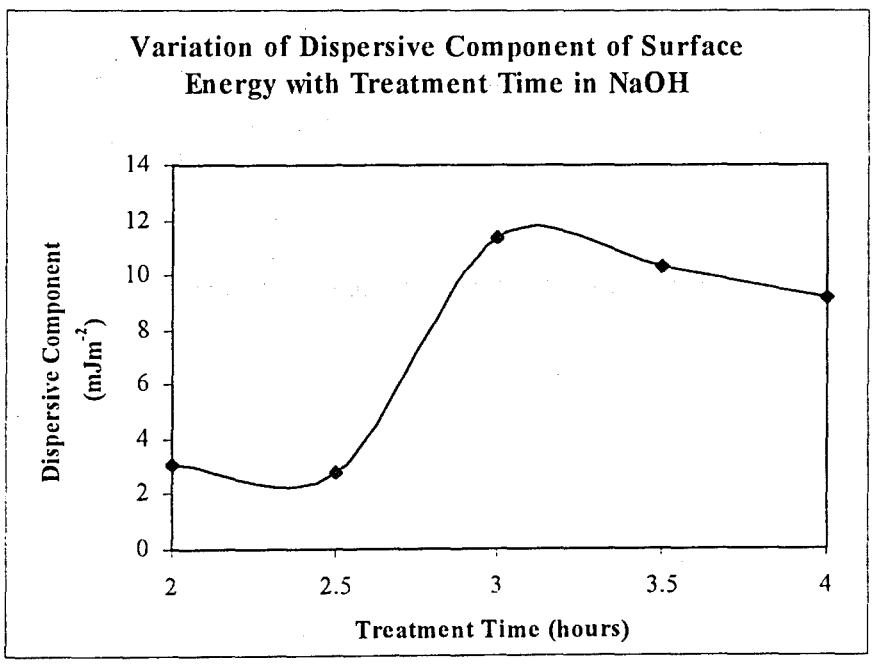

Figure 4.10: Dispersive Component of Surface Energy

The polar component of the surface energy (see figure 4.11) changes in the opposite direction to that of the dispersive component. A reasonable explanation for the initial

increase in polar component is that the polyester is hydrolysed to some extent at the surface.

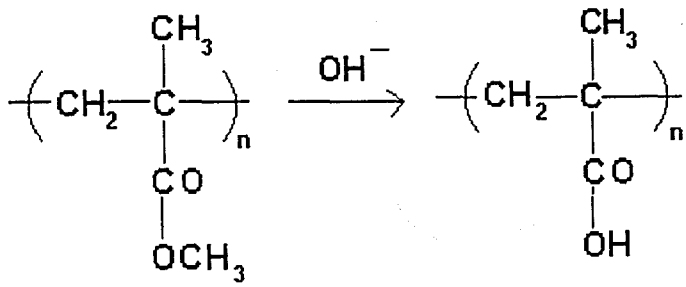

However after longer treatment times, there could be base-catalysed elimination to produce isolated double bonds in the polymer backbone:

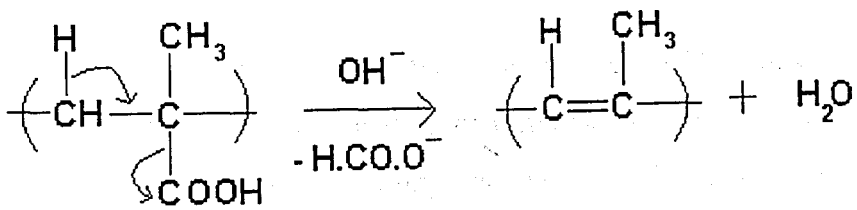

Hence and increase in the dispersive component and a decrease in the polar part.

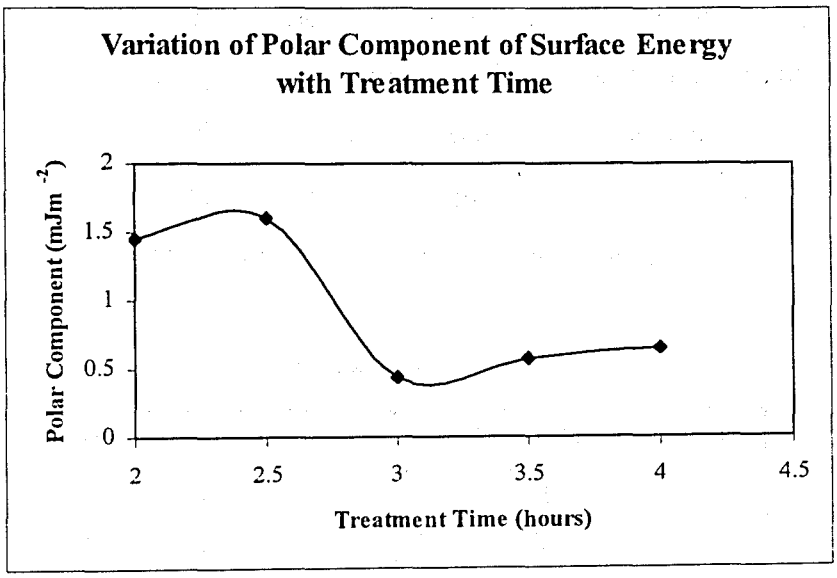

Figure 4.11: Polar Component of Surface Energy

It was not possible to measure contact angles on the treated PET substrates as the material was very flexible and this caused the drop of water to move around during measurements. Simple experiments involving observing the wetting of water on the surface of the substrates showed that the sodium hydroxide treatment increased the wetting power of the PET surfaces.

4.3.2 Results of UV/ozone Treatments

Pointer *et al.* investigated the effect of UV/ozone on the surface energy of PMMA, PC and PTFE[8]. They found that for PMMA, the UV/ozone treatment caused the formation of water soluble surface products which affected the contact angle measurements and for PTFE it caused etching of the surface and an increase in surface roughness. In the present work, a method had already been found to treat the PMMA substrates, and so the UV/ozone cleaning technique was only used for PC and PET. However, it was found that very short periods of exposure (10 minutes) caused the PET substrates to buckle and become opaque, therefore the method was restricted to PC substrates.

The first experiment involved giving pieces of pre-cleaned PC ten minute periods of irradiation using the UV/ozone apparatus. Table 4.3 shows the change in contact angle against exposure time. It was found in the last section that the reproducibility of the surface energy results can be unreliable for repeat experiments, therefore for these results, the change in wettability was monitored by the change in contact angle.

Table 4.3:

Exposure time (minutes)	Contact angle (degrees)
0	61 ± 2
10	57 ± 2
20	53 ± 2
30	53 ± 2
40	43 ± 2
50	50 ± 2
60	42 ± 2
70	38 ± 2
80	40 ± 2

Since there was only a reduction of about 20° in the contact angle, more series of experiments were performed, exposing the polycarbonate substrates for longer lengths of time to the UV/ozone radiation. Table 4.4 below shows the results of the experiments where each contact angle result shown is the average of 6 samples.

Table 4.4

Exposure Time (hours)	Contact Angle (degrees)
1	56 ± 2
2	28 ± 2
3	47 ± 2

It is clear from the results that longer exposure to the UV/ozone is more effective than shorter periods. However, in comparison to the work of Pointer, the cleaning action of this work took considerably longer than their results. This was due to variations in the set-up of the two UV/ozone cleaning boxes.

From the results, it was concluded that an exposure time of two hours gives the lowest contact angle results. Earlier in this section, we saw that the contact angle for untreated polycarbonate is about 60°, therefore two hours of exposure reduces the contact angle approximately by half. All subsequent polycarbonate substrates were treated for 2 hours in the UV/ozone apparatus before coating with the tin oxide solutions.

Figure 4.12 below gives a simplified view of the proposed method for the cleaning action of the UV/ozone technique.

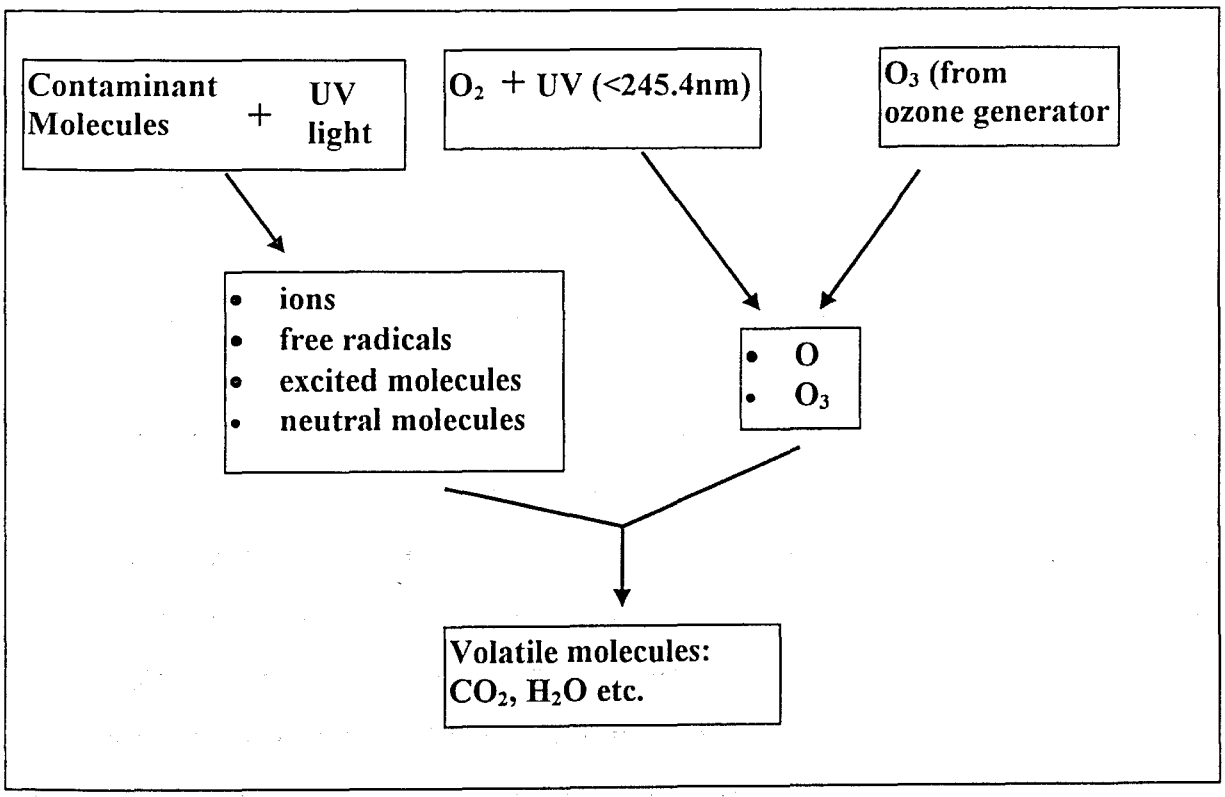

Figure 4.12: Proposed Cleaning Action of UV/ozone

4.3.3 FTIR Reflectance Spectral Measurements on Ozonised Polycarbonate Substrates

FTIR specular reflectance measurements were carried out on surface treated polycarbonate samples. The three sets of polycarbonate substrates measured had been exposed to UV/ozone for periods of 0.5, 1 and 2 hours. The reflectance attachment used allowed the possibility of varying the angle of incidence between 0° and 90°. It was found that an incidence angle of 70° from the normal gave the most detailed spectra. Figures 4.13 and 4.14 show one of the original spectra recorded plus a figure overlaying all three traces.

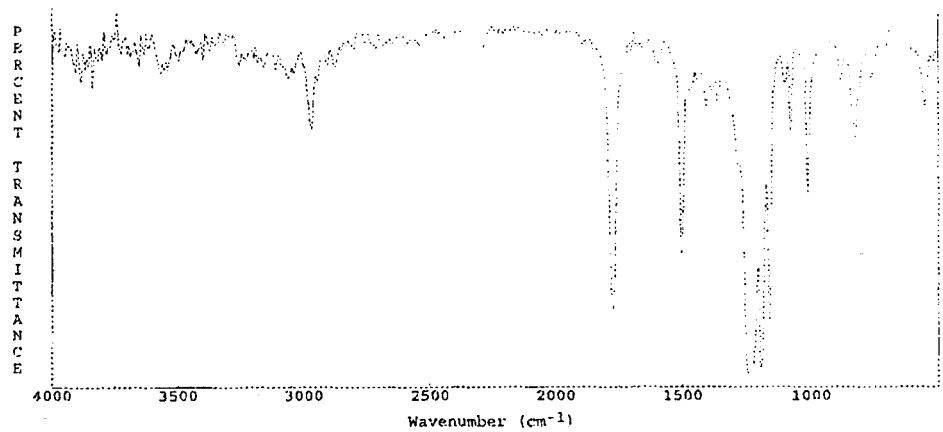

Figure 4.13: Specular Reflectance FTIR of Untreated Polycarbonate Surface

From figure 4.14, the subtle differences in the spectra can be seen. The PC substrate exposed for 0.5 hours (to UV/ozone) displays a spectrum typical of polycarbonate. For the substrates exposed for longer periods of time, their spectra exhibit apparent broadening of the carbonyl peak towards the higher wavenumber end. Also the signal due to aliphatic carbon hydrogen bonds (~2950cm^{-1}) has weakened considerably. To account for the loss of intensity of the aliphatic carbon hydrogen bond, it is reasonable to propose that the methyl groups (see figure 4.6) are oxidised to carboxylic acid groups. This correlates with the asymmetric broadening of the carbonyl peak, since a carbonyl peak due to carboxylic acids occurs at higher wavenumber than that due to esters therefore the apparent

broadening could actually be due to the formation of another carbonyl peak. Another feature on these spectra points towards the presence of carboxylic acid, namely the beginning of a broad peak at 3000 to 3500cm^{-1}. This peak is characteristic of hydrogen-bonded OH bond stretching for acids.

The formation of carboxylic acid groups on the surface of the polycarbonate substrates means that there are extra OH groups on the surface of the polymer which would help the adherence of the aqueous tin oxide colloids.

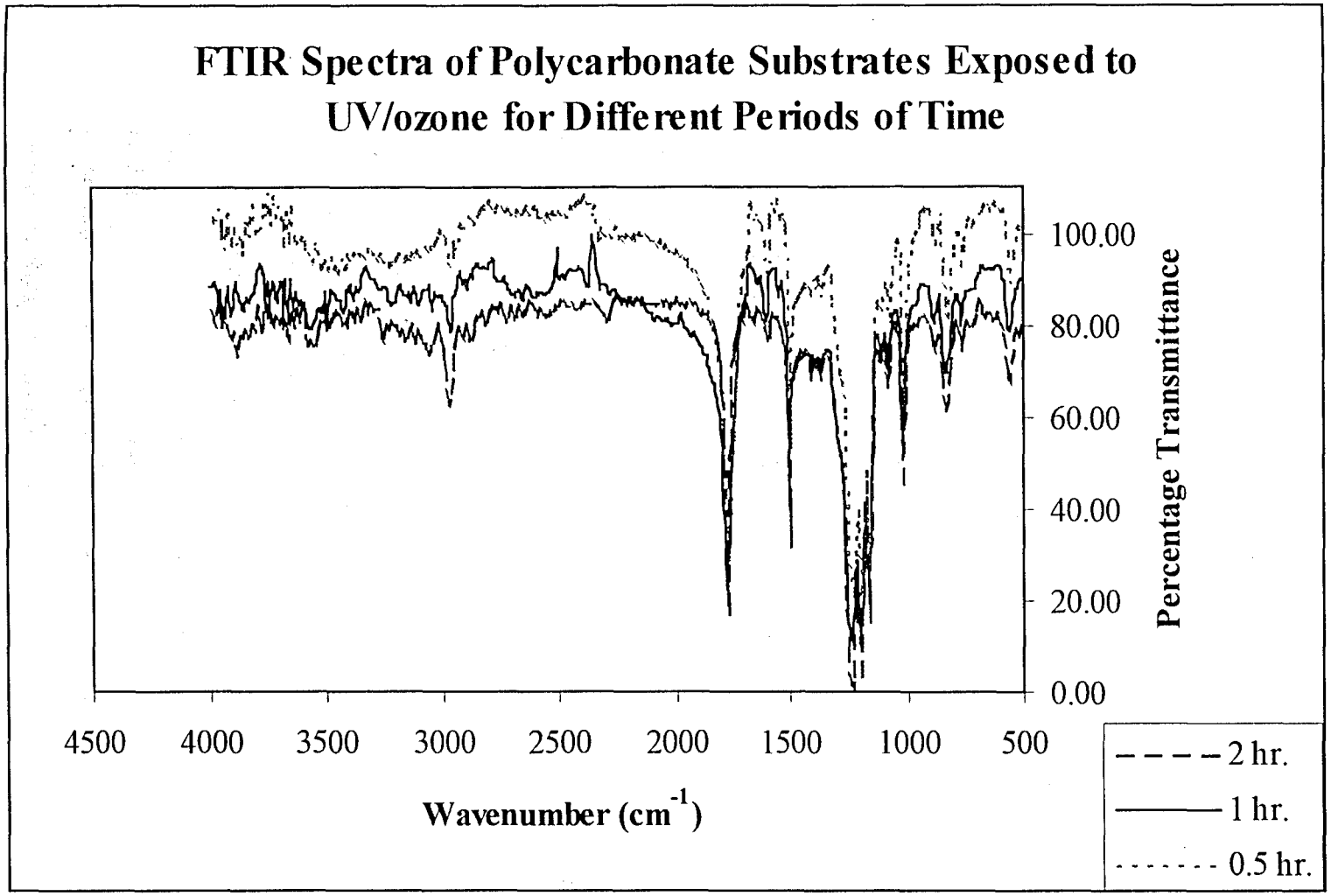

Figure 4.14: Overlay of Specular Reflectance FTIR

4.4 Conclusions

The surface treatments methods described in this chapter resulted in PC and PMMA surfaces which had higher wettabilities and therefore more affinity for coating with tin oxide solutions. By exposing polycarbonate substrates to a mixture of low wavelength ultra-violet light and ozone gas, it resulted in a decrease in the contact angle made with water from about 60° to 30°. Treating poly (methyl methacrylate) with 2M NaOH at 50°C for 3 hours resulted in favourable increases in the surface energy of the polymer surfaces. The PET substrates required 1 hour of treatment in sodium hydroxide to render their surfaces more wettable with water. Pre-cleaning of the polymers prior to the surface treatments was essential in getting the optimum result from the surface treatments.

FTIR diffuse reflectance studies performed on the ozonized polycarbonate substrates showed that the structural changes which occurred were due to the formation of extra carboxylic acid groups on the surface of the polymer.

References

1. S. J. Gregg, *The Surface Chemistry of Solids,* 2nd Edition, Chapman and Hall Ltd., London (1961)
2. A. W. Adamson, A. P. Gast, *Physical Chemistry of Surfaces,* 6th Edition, John Wiley and Sons, Inc., New York, (1997)
3. S. Wu, *J. Phys. Chem.,* **74** 632 (1970)
4. D. Briggs, D. G. Rance, B. J. Briscoe, Chapter 23, *Comprehensive Polymer Science: The Synthesis, Characterisation and Applications of Polymers,* **Volume 2**, G. Allen, J. C. Bevington, Pergammon Press, UK (1989)
5. S. Wu, *Polymer Handbook 2nd Edition,* John Wiley and Son Inc., Canada (1975)
6. K. Jonsen, PhD Thesis, Kingston University (1995)
7. O. H. Wyatt, D. Dew-Hughes, *Metals Ceramics and Polymers,* Cambridge University Press, London (1974)
8. A. B. Pointer, W. R. Jones Jr., R. H. Jansen, *Polymer Engineering and Science,* **34** 1233 (1994)

9. J. R. Vig, *J. Vac. Science and Tech.*, **A3** 1027 (1985)

10. P. Duchateland, G. Baud, J. P. Besse, M. Jacquet, *Thin Solid Films*, **250** 142 (1992)

5.1 Introduction

5.1.1 Group 14 Dioxide Films on Polymer Substrates

In chapters 2, 3 and 4 the preparation of tin oxide, the application of tin oxide to glass substrates and the surface preparation of the polymer substrates were discussed. This chapter uses the results of those three chapters to focus on the application of tin oxide to the polymer substrates.

The results of this chapter are discussed in terms of the conductivities, optical transmittance, adherence and morphology of the coatings on the polymers. The polymers used for the studies were polycarbonate, poly (methyl methacrylate), poly (ethylene terephthalate) and poly (ethylene naphthalate) (trade name Kaladex ®, from ICI).

Previous work on coating polymers with metal oxides has included the application of indium tin oxide to polymeric substrates. Minami *et al.* prepared thin films of ITO on PET at a deposition temperature of 60°C by DC magnetron sputtering[1]. After heat treatment at 150°C for up to 100 hours, they achieved resistivities of approximately 10^{-1} Ωm for the coatings. Chiou and co-workers deposited their ITO films on acrylic substrates using a radiofrequency magnetron sputtering technique[2]. The coatings had resistivities between 10 and 7 x 10^{-2}Ωm, depending on the film thickness, rf power and target to substrate distance. Reactive sputtering was again used by Mukherjee to put indium oxide thin films on glass, acrylic and polycarbonate substrates[3]. It was found that the best resistivity (6.8 x 10^{-6}Ωm) was obtained for indium oxide doped ~20 % with tin. Tin doping also improved the abrasion resistance of the acrylic and polycarbonate substrates and their resistance to environmental conditions. In a related study, conductive copper selenide films were applied to polyester sheets using an electroless chemical deposition technique[4]. The surface resistances of the coatings were in the range 50 to 500Ω/□.

Wu *et al.* applied silicon dioxide to glass, polycarbonate and silicon wafers by radiofrequency magnetron sputtering[5]. The films on polycarbonate formed cracks after storage for several hours in an atmospheric environment, the cracks were assumed to be

due to thermal expansion differences between the silicon oxide and the polycarbonate. A sol-gel process was used by Mizutani and co-workers to also prepare silicon oxide thin films on PMMA substrates[6]. After deposition of the coatings, they were heated at 80°C for 6 hours. This study was concerned with changes in the hardness of the polymers due to the coatings and they found that the apparent hardness had increased by 1.6 times in comparison to uncoated PMMA. This was the only paper found during the course of the present research that referred to using a sol-gel process for depositing a metal oxide coating on a polymeric substrate.

5.1.2 Methods to Improve Interfacial Adhesion and Wetting

In chapter 3, it was seen that a lot of cracking occurred in the tin oxide coatings on glass substrates. Even though the polymer substrates were pre-treated (as described in chapter 4) to make them more suitable for coating with an aqueous based coating, it was decided to try modifying the coating solutions with further treatments to improve the overall adhesion of the coatings on the substrates.

Due to the incompatibility of the ionic and polymer layers, it was decided to use surface treatment methods which would provide an intermediary link between the two layers. One method proposed was through the addition of a surfactant to the tin oxide coating solution. It was hoped that small additions of a surfactant would reduce the interfacial tension between the hydrophilic ionic tin oxide coating and the hydrophobic polymer substrate by forming an interface between them. It was decided to use a non-ionic surfactant which would not ionize in aqueous solutions and therefore would not destabilize the tin oxide colloidal solutions[7].

The other proposed method was to add a coupling agent to the coating solutions to act as a "chemical bridge" between the polymer and inorganic layers. Coupling agents are often used in polymer research to improve adhesion between different phases in composite materials[8]. Organic or halo-organic derivatives of silicon hydrides (organosilanes) are commonly used as coupling agents; they have organic groups replacing the hydrogens of a

silicon hydride. The organosilane coupling agents contain at least one group which is reactive towards the functional group of the polymer and at least one group which is reactive towards the inorganic layer. Figure 5.1 shows a simplified illustration of the way in which a simple coupling agent ($RSi(OCH_3)_3$ "bridges" the polymeric and inorganic layers. The coupling agent in the figure below is behaving in a similar fashion to the proposed bridging action of the surfactant, as described earlier.

Step 1

$$R\text{--}Si(OCH_3)_3 + 3H_2O \rightarrow 3CH_3OH + R\text{--}Si(OH)_3$$

Step 2

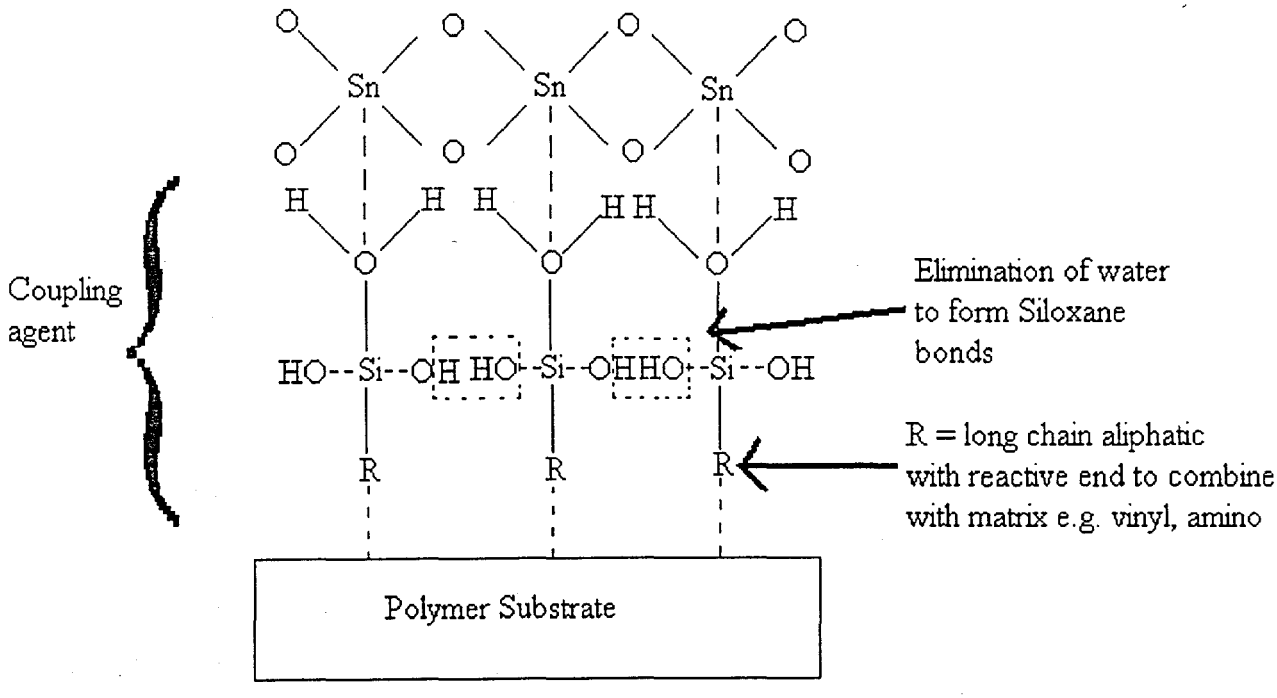

Figure 5.1: Proposed Action of Coupling Agent

5.1.3 Literature Search on Flash Annealing

To maximise the conductivities of the tin oxide coatings on the polymer substrates, a technique was required which would strongly heat the tin oxide coatings without unduly damaging the underlying polymer substrates. The polymers used in this work, were thermoplastics. Since bonding between the polymeric units in thermoplastics is due to van der Waals forces, and therefore weak, the addition of a relatively small amount of heat causes the molecules to become thermally agitated and free to move and the polymer softens and becomes ductile. The temperature at which the polymer softens (or glass transition temperature, T_g) varies from one polymer to another, depending on the degree of polymerisation (i.e. molecular mass). The polymer substrates used in this research had glass transition temperatures between 67°C and 149°C[9]. This obviously put a restriction on the type and amount of heating which could be applied to the tin oxide coated polymer substrates.

A literature survey was carried out to discover possible methods to anneal a material quickly at a high temperature for a very short period of time. There are various terms for this process: flash annealing, rapid thermal annealing and flash lamp annealing. The time-scales vary widely, although the duration of heating in all cases is much shorter than for most annealing processes.

Ganz *et al.* have very recently used a CO_2 laser to densify sol-gel derived antimony doped tin oxide coatings on silicon substrates[10,11]. The tin oxide coatings were applied by dip-coating or spin-coating and dried at 25°C before firing with the CO_2 laser. A comparison between the films fired by laser and films fired in a furnace at 550°C showed that the laser fired films had lower resisitivities and less cracked coatings. Neta and co-workers also used a CO_2 laser for the thermal treatment of low melting temperature materials[12]. The samples were heated at 450°C for 10 seconds. Auger Electron Spectroscopy depth profiling showed that only the uppermost 200Δ of the sample had been affected by the heating.

A rapid thermal annealing technique was used by Bashkov *et al.* to heat tin oxide coatings applied to silicon substrates by spray pyrolysis[13]. They heated the samples for 1 minute at 1000°C under vacuum. This resulted in coatings that were less cracked than those heated conventionally, but it was found that the sheet resistance of the coatings had increased in comparison to the SnO_2 coating heated for 90 minutes at 1000°C in oxygen. Prasad *et al.* used rapid thermal annealing on their n-WeS_2 single crystal photoelectrochemical solar cells[14]. The annealing caused an enhancement in the photovoltic potential of the solar cells.

Page reported the production of an infrared furnace which could heat a sample from ambient to 800°C in 60 seconds, keep it at 800°C for 40 seconds and cool down to 100°C in 20 seconds[15]. The method of heating was by infrared lamps (10 on each side) and it was used for steel samples. Similarly, Usami and co-workers used pulsed light irradiation from a Xe flash lamp system to activate ion-implanted silicon[16]. The apparatus consisted of nine xenon flash lamps, a reflection mirror and sample holder. The process was carried out under a nitrogen atmosphere and the estimated maximum temperatures reached for the silicon wafers were between 1070°C and 1420°C; the annealing times were about 20 minutes.

Flash annealing by means of applying a high current (~ 15 to 20A) to the sample for very short pulses (a few milliseconds) has been used to improve the magnetic and mechanical properties of metallic glasses and ferromagnetic materials [17-22]. The heating rate was about $500°s^{-1}$ to a final temperature of about 800°C. Generally, the samples used for these experiments were quite small and even so, the heating was not uniform across the surfaces.

After consideration of the methods revealed by the literature survey, it was decided to use the pulsed infrared heating method to heat the tin oxide coatings on the polymer substrates. A furnace was designed and produced (at Seven Furnaces Limited, Bristol) for the specific purposes of this project (see appendix 3). The results of the heating experiments in the infrared furnace are discussed in section 5.3.3 of this chapter.

5.2 Experimental

5.2.1 Preparation of Coating Solutions Containing Surfactants

The non-ionic surfactant chosen for the experiments was poly oxyethylene (23) lauryl ether ($C_{12}H_{25}(OCH_2CH_2)_4OH$), its common name being Brij-35. A 0.1mM stock solution of the surfactant was made, from which solutions in the concentration range of 1 x 10^{-6}M to 5 x 10^{-4}M were prepared. Surface tension measurements were made using a White Digital Balance, Model DB 2kS.

Small volumes of the surfactant solutions were added to antimony doped tin oxide sols. Surface tension measurements were again carried out on the surfactant-containing tin oxide solutions, and the results of the study are shown in section 5.3.1.

5.2.2 Preparation of SnO_2 Solutions Containing Coupling Agents

The coupling agents used were methyltrichlorosilane ($MeSiCl_3$), allyltrimethoxysilane ($H_2C{=}CHCH_2Si(OCH_3)_3$) and tin tetrachloride ($SnCl_4$). Different approaches were tried in the addition of the coupling agents to the tin oxide coating solutions. The tables below show the details of the different preparations and they also show the general outcome of each experiment. In all cases n-type doped tin oxide coating solutions were used for the experiments. (The doping concentrations of the solutions are shown in the tables). The first set of samples was prepared by adding the coupling agents directly to two antimony doped tin oxide solutions.

Table 5.1

Sample Name	Sample Contents	Observations
A	1% n-type doped SnO_2 solution (1ml) and $MeSiCl_3$ (80µl)	Gel formed throughout solution
B	4% n-type doped SnO_2 solution (1ml) and $MeSiCl_3$ (40µl)	Gel formed throughout solution

The second set of samples was prepared by dissolving small volumes of the coupling agents in common solvents.

Table 5.2

Sample Name	Sample Contents	Observations
C	IPA (5ml) and $SnCl_4$ (0.5ml)	Fuming occurred on addition of $SnCl_4$, settled to clear solution
D	THF (5ml) and $SnCl_4$(0.5ml)	Fumed wildly on addition of $SnCl_4$; resulted in formation of white precipitate
E	IPA (3ml) and $MeSiCl_3$ (80µl)	Resulted in clear colourless solution
F	Methanol (3ml) and $MeSiCl_3$ (180µl)	Clear colourless solution
G	IPA (3ml) and $Allyl(OMe)_3Si$ (80µl)	Clear colourless solution
H	Methanol (3ml) and $Allyl(OMe)_3Si$ (80µl)	Clear colourless solution

For the experiments summarised in table 5.3, the samples from table 5.2 were mixed with previously prepared tin oxide coating solutions.

Table 5.3

Sample Name	~ Dopant Conc. (mol %)	Sample Contents	Observations
I	2	Soln. E (80µl) and SnO_2 (2ml)	Clear yellow solution
J	5	Soln. G (0.5ml) and SnO_2 (3ml)	Clear yellow solution
K	3	Soln. E (180µl) and SnO_2 (4ml)	Clear yellow solution

Some of the above coupling agent containing tin oxide colloids were applied to polymer substrates and the results of these studies are given in section 5.3.4.

5.2.3 Coating Methods

A. Spray Coating

Two different spray coating methods were used. The first apparatus consisted of a compressed air pump attached to a nebuliser (from a flame photometer). An air output of approximately 1 bar resulted in an uptake of tin oxide solution of about 2.5ml/minute. The nebuliser was clamped vertically above the samples at distances between 10 and 25 cm. Polymer substrates were sprayed for 2 to 10 second periods.

More spray coating was done using a De Vilbiss "air brushing" spray pen. This contained a nebuliser working from a filtered air supply (5 psi from a diaphragm pump). The polymer substrates were sprayed horizontally between 4 and 20cm from the pen.

B. Spin-Coating

A Dynapert PRS 14E spin-coater was used to apply coatings to the polymer substrates. A drop of the coating solution was placed on the sample substrate and spun at 1300 rpm for between 30 seconds and 2 minutes. The polymer substrates used for the experiments were $4cm^2$. The process was repeated several times to produce multiple coatings.

C. Solvent Evaporation

As described earlier for the glass substrates, the solvent evaporation technique simply involved placing some tin oxide coating solution on the substrate with a Pasteur pipette, spreading it evenly across the surface and allowing it to dry at ambient temperature.

5.2.4 Annealing Techniques

The infrared furnace used for flash-annealing experiments was supplied by SFL Ltd, Bristol. It had two timers: one controlling the preheating time for the infrared lamps and the other controlling the actual time for which the samples were exposed to the IR radiation. Figure 5.2 shows a photograph of the furnace. Appendix 3 shows a diagram of the furnace.

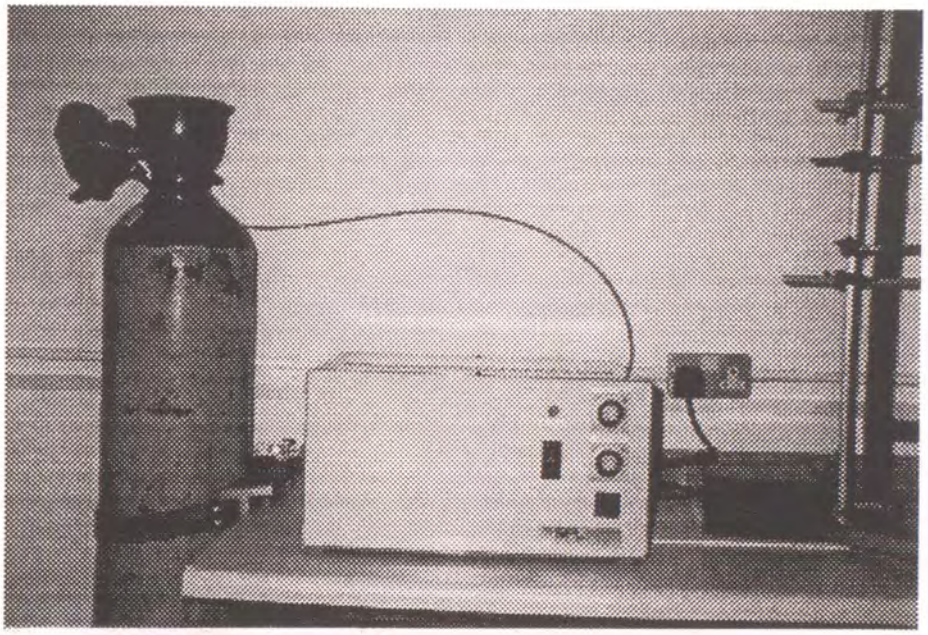

Figure 5.2: Photograph of Infrared Furnace

For the experiments discussed later in this chapter, a preheat time of 2 seconds was used and the sample exposure time varied between 4 and 10 seconds. A nitrogen gas pressure of 2.5 bar was used to operate the pneumatically controlled sample shutter.

5.2.4 Filters in the Infrared Furnace

When using the infrared furnace for heating tin oxide coated polymers, the polymer substrates were expected to become very hot after a short time. In order to try and limit the amount of heat being absorbed by the substrate to a minimum, it was decided to place an appropriate filter above the samples in the furnace to absorb some of the heat.

An absorption spectrum for tin oxide was obtained over the infrared range 7800 to 4000cm^{-1}. It displayed a broad absorption band from 5500 to 2000cm^{-1} which had a maximum absorbance at approximately 3500cm^{-1} (see figures 5.2 and 5.3 for spectra).

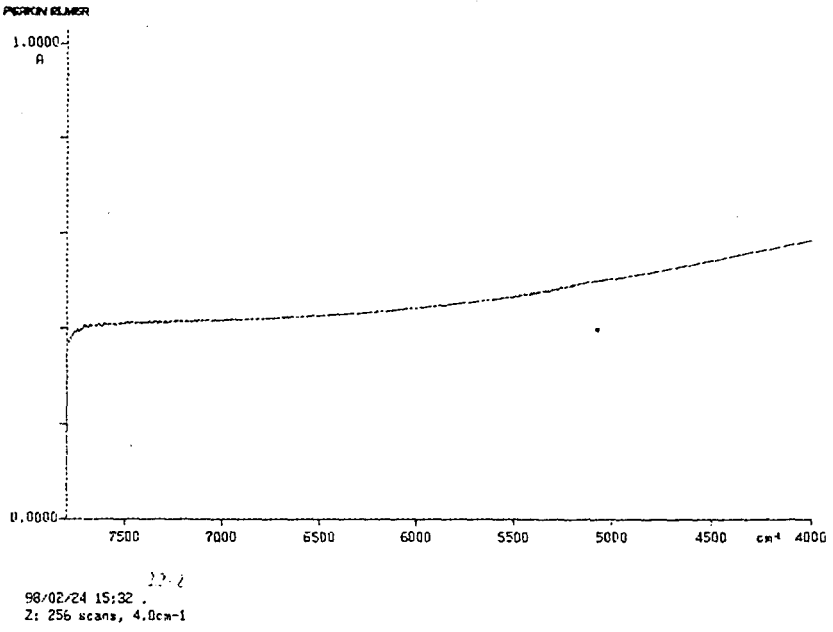

Figure 5.3: Part of Infrared Spectrum of SnO_2

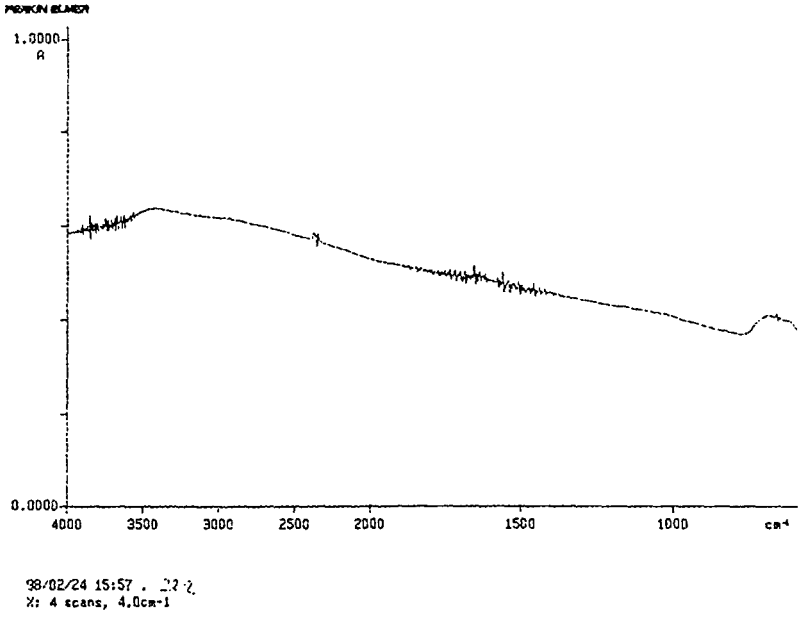

Figure 5.4: Part of Infrared Spectrum of SnO_2

Ideally, it is only necessary to allow the radiation within this absorption band to reach the SnO_2 coating, and this would lessen the heating effect on the polymer substrates. Germanium seemed suitable for use as a filter since it has a band gap energy of ~0.7eV

which corresponds to a cut-off in the IR region of ~5500cm^{-1} (see figure 5.5 for an infrared spectrum of germanium.

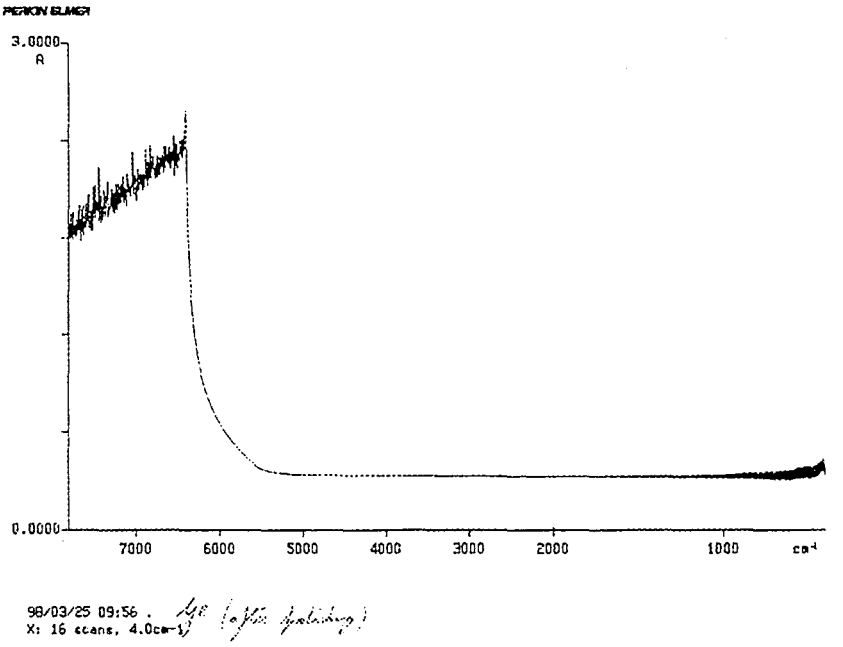

Figure 5.5: Infrared Spectrum of Germanium

5.2.5 Surface Resistance Measurements

Surface resistances of the partly-annealed SnO_2 coatings (on polymer substrates) were obtained using a Keithley 617 Programmable Electrometer with an internal voltage source. The coatings to be measured were prepared as in figure 5.6.

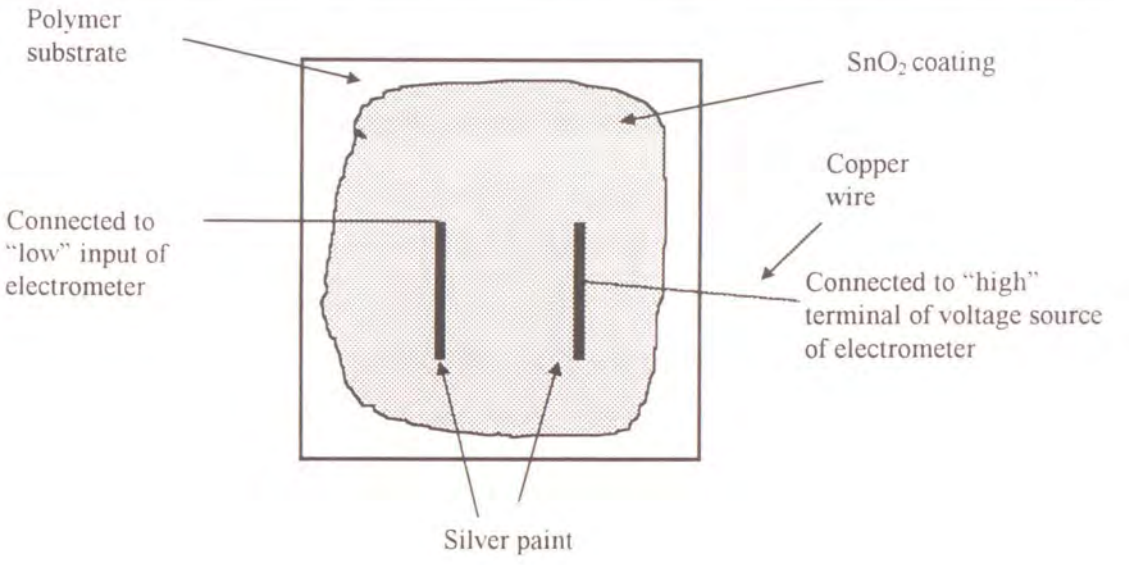

Figure 5.6: Set up for measuring surface resistances

After connection of the copper wires to the electrometer as shown, a known supply voltage (60 volts) was set. When operated, the electrometer displayed the current driven through the coating by the voltage source. The display was changed subsequently to show the resistance being measured (i.e. to calculate V/I directly).

The resistance measurements were used to calculate resistivity values using the equation:

$$\rho = \frac{RA}{l}$$

where ρ = resistivity

R = resistance

A = length of electrode x thickness of coating

l = distance between electrodes

The conductivity, σ, is simply the inverse of the resistivity.

5.2.6 Surface Profiling

The thickness of some of the coatings was measured using a "Tencor" Alpha-Step 500 Surface Profiler.

5.2.7 Photomicroscopy

Photographs were taken of tin oxide thin films on polymer substrates using a Leitz Orthoplan optical microscope with automatic camera attachment. The objective magnifications used were 2.5, 6.3, 10, 16 and 25. Photographs were taken of calibration graticules at each magnification in order to measure the features on the tin oxide coatings.

5.2.8 Percentage Transparency Measurements

UV/visible spectra of the coated polycarbonate and perspex substrates were recorded over the range 380 to 900nm using pre-cleaned and uncoated PC and PMMA substrates as the references. A Kontron Uvikon 940 spectrophotometer was used for the measurements.

5.2.9 Sample Preparation for XRD

The following samples were run in a Philips PW 1730/10 powder X-Ray Diffractometer. Some were exposed to IR heat treatments, as described below:

Polymer Substrates

1. uncoated Kaladex 2000 (Kaladex is the trade name for poly (ethylene naphthalate)
2. tin oxide coated Kaladex, unannealed (2% n-type doped sample applied by spray coating)
3. tin oxide coated Kaladex, IR annealed (2% n-type doped sample applied by spray coating; IR treatment was 12 exposures of 5 seconds each)

Borosilicate Substrates

4. tin oxide coated borosilicate, IR annealed (spray coated with 2% n-type doped sample, IR treatment was 20 exposures of 10 seconds)

Sol-Gel SnO_2 Powder

5. unannealed tin oxide powder (5% antimony doped sample, which was an air-dried powder)
6. IR annealed tin oxide powder (the dried powder from the above run was exposed to 14 exposures of 10 seconds in the infrared furnace)

5.3 Results and Discussion

5.3.1 Surface Tension Results

As discussed in the introduction, it was decided to add a non-ionic surfactant to the tin oxide coating solutions in order to try and lower the surface tension of the solutions, thereby reducing the interfacial tension between the hydrophilic tin oxide coating and the hydrophobic polymeric substrates. The ionic surfactant used was Brij-35 and it had a critical micelle concentration of 0.046mM[23].

Initially the surface tension of some antimony doped tin oxide solutions were measured and they had the values shown in table 5.4. There was no direct relationship between the antimony dopant concentration and the surface tension values.

Table 5.4

Doping Conc. (mol %)	Surface Tension (mN/m)
1	47.1
6	43.0
2	43.7
4	46.7
1	43.9

Various small concentrations of the surfactant were added to the tin oxide solutions (from the above table) and the surface tension measured. Figures 5.7 and 5.8 show examples of the changes in surface tension as the surfactant was added.

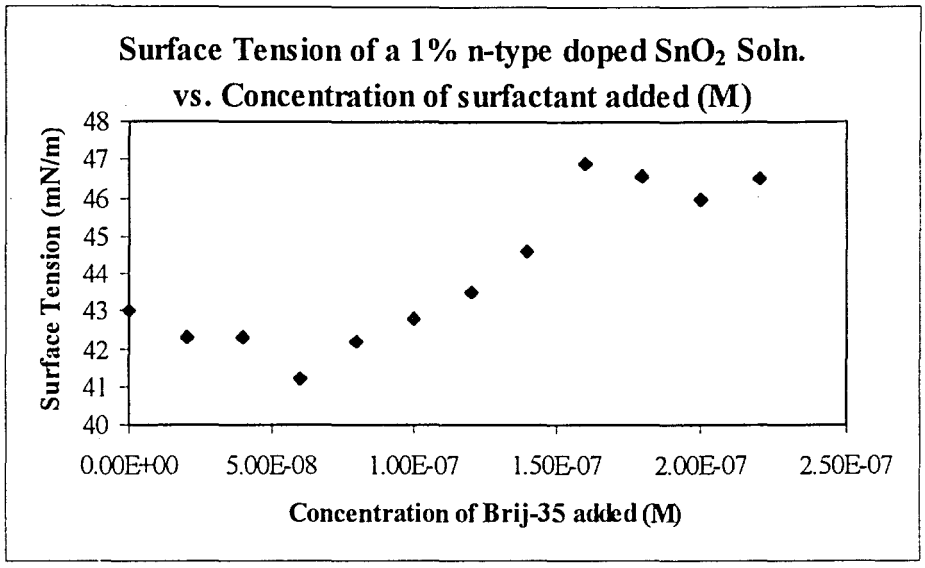

Figure 5.7: Change in the Surface Tension of a 1 % n-type Doped SnO_2 Solution as 1×10^{-6}M Brij-35 is added

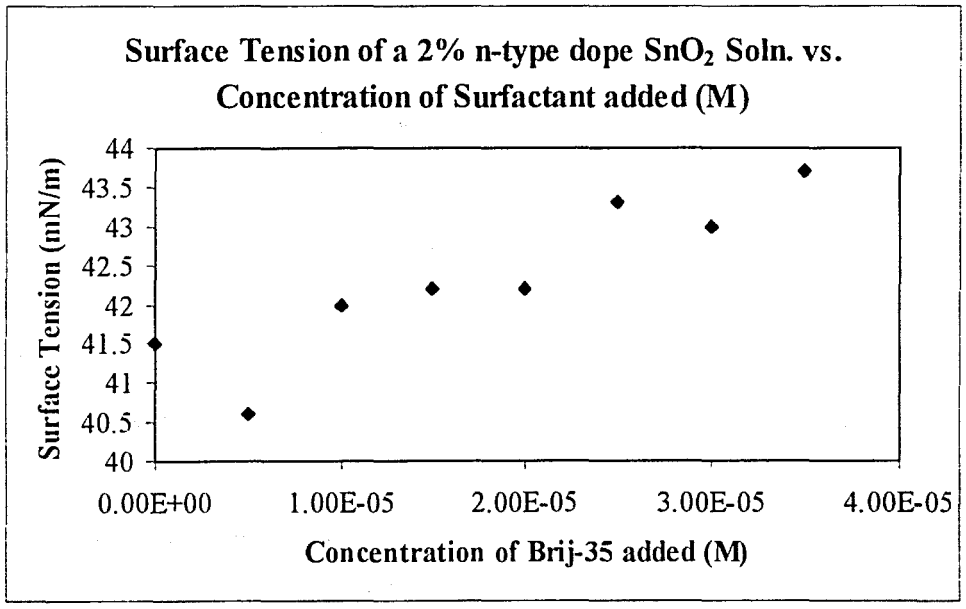

Figure 5.8: Change in the Surface Tension of a 2 % n-type Doped SnO_2 Solution as 1×10^{-4}M Brij-35 is added

It was found that in each case the addition of the surfactant caused an increase in the surface tension (by about 4 units) rather than a decrease. From the graphs, it can be seen

that in each case there was a slight dip in the surface tension before it increased. It was thought at first that the dip might correspond to the critical micelle concentration but it is not possible since the concentrations of surfactant added were much lower than the critical micelle concentration of the surfactant (0.045mM).

The increase in surface tension is presumed to be happening because the surfactant is preferentially being bound in the bulk of the solution rather than at solution-air interface. This means that the head groups of the surfactant molecules are being attracted to the tin oxide particles in solution.

Since this work did not result in a significant decrease in the surface tension of the tin oxide coating solutions, it was decided to try using a coupling agent to strengthen the bond between the substrate and the coating solutions. The results of the coupling agent work are discussed in section 5.3.4.

5.3.2 Effect of Different Coating Techniques

Spray coating, spin-coating and solvent casting techniques were used to apply tin oxide coatings to the polymer substrates. The quality of the coatings were analysed using optical microscopy and photomicroscopy. It was observed by optical microscopy that the spin-coated films and those produced by solvent evaporation were of better quality than the coatings applied by spray coating. The photos below (figures 5.9, 5.10 and 5.11) show examples of coatings produced from each coating technique. Although the coating applied by solvent evaporation is very cracked (figure 5.10), the method uniformly wets the surface of the substrate unlike the spray coated thin film (figure 5.11). The spin-coated films were particularly smooth, and figure 5.9 shows an area with small defects surrounded by a featureless surface.

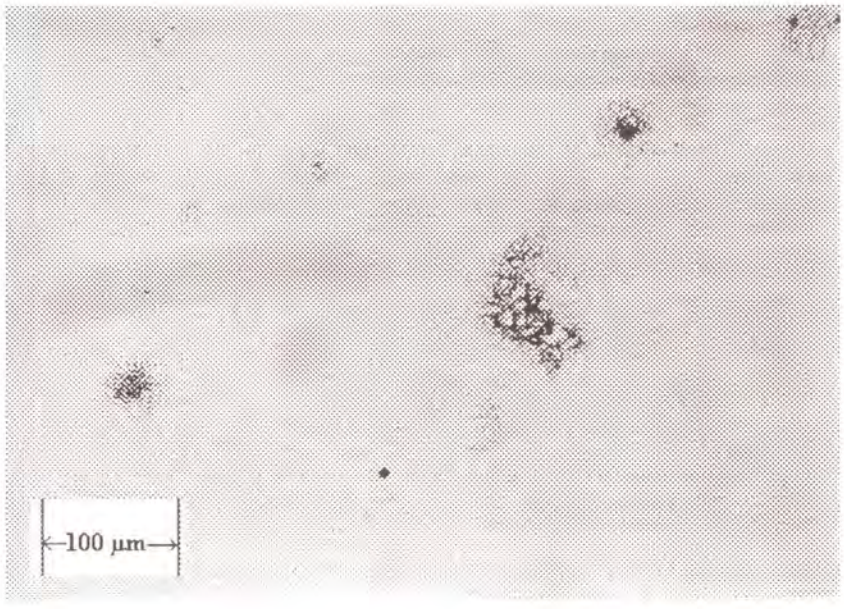

Figure 5.9: Spin coated SnO_2 Coating

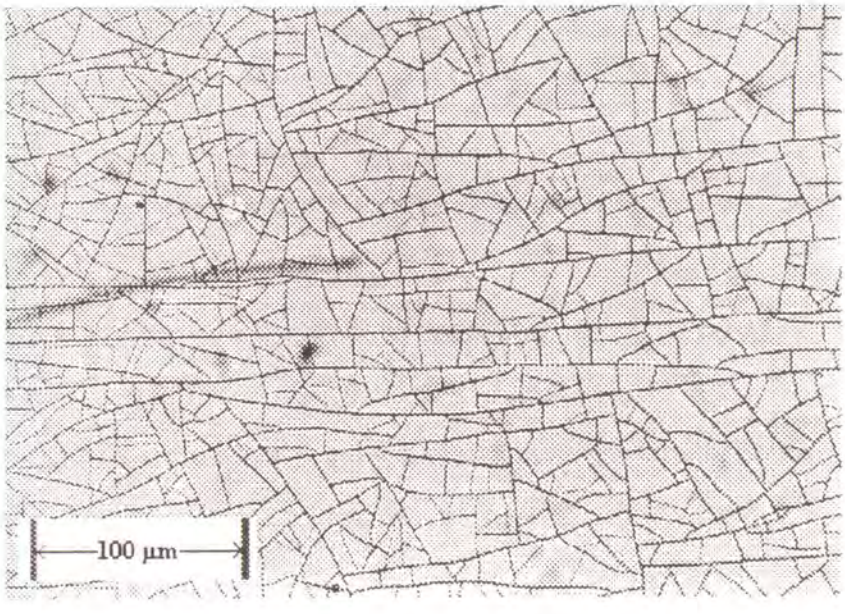

Figure 5.10: Solvent Evaporated SnO_2 Coating

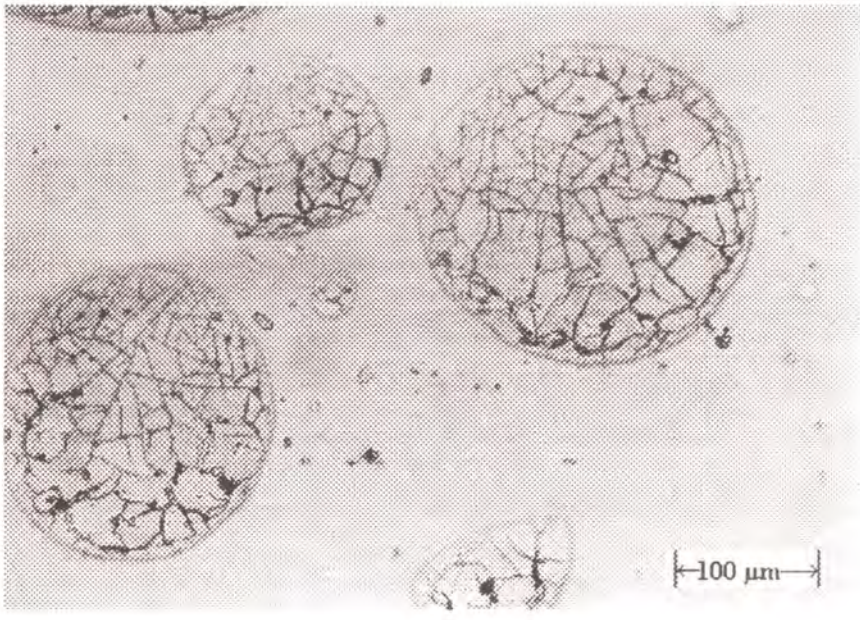

Figure 5.11: Spray Coated SnO_2 Coating

It was disappointing that the spraying experiments were not successful, as spray coating is a more useful technique for applying coatings to large sample sizes. All of the parameters (pressure, distance, time) of the spray coating were varied but it still resulted in coatings which consisted of droplets of tin oxide, rather than a uniform coating. From the photograph above, it can be seen that the droplets of tin oxide from spray coating were 50 to 100:m in radius. From the radius of the droplets, it is assumed that their thicknesses were also of the order of 50-100 microns. This is considerably thicker than the coatings produced by spin-coating or spray coating and although the polymer substrates had been surface treated to improve adhesion between the coatings and the substrates, it obviously not suitable for uniform coatings.

Topographical information was obtained for a tin oxide coating using atomic force microscopy. Figure 5.12 is a 3D image of a tin oxide thin film which had been spin-coated onto a polycarbonate substrate, and exposed to infrared treatments.

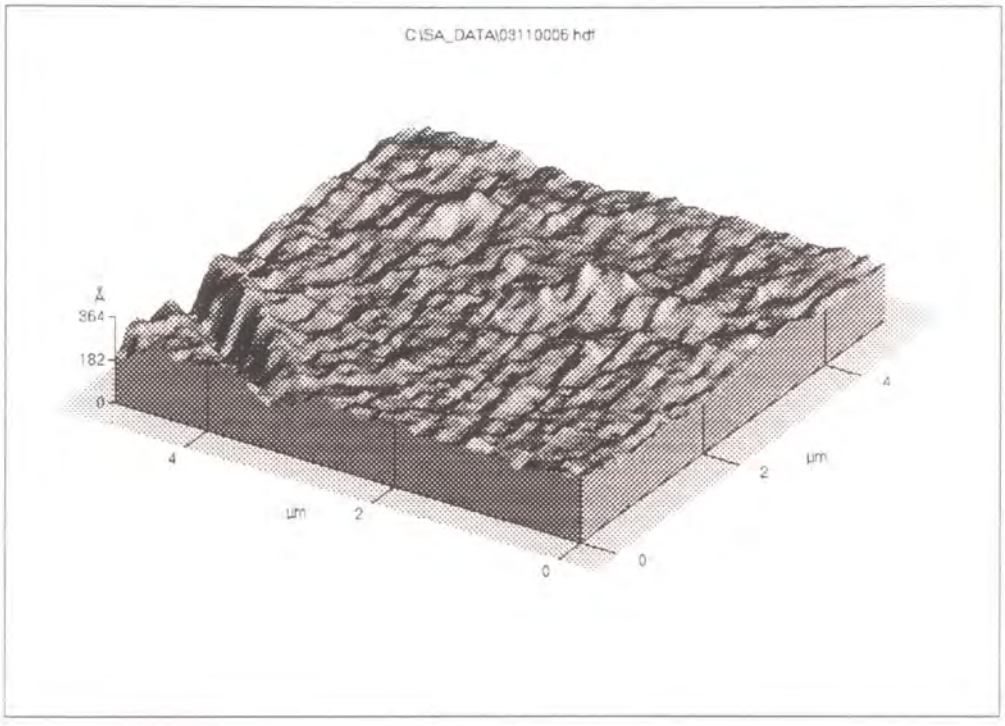

Figure 5.12: AFM Image of SnO_2 Coating on Polycarbonate

The image shows that the surface of the coating is very flat, with only ~70Å between the highest "peak" and lowest "trough" on the image. Although the image shown is only a tiny section of the entire coating, it is representative of the whole sample. Attempts were also made to obtain images of a tin oxide layer spray coated onto a polycarbonate substrate. However, it was not possible to obtain any images as the surface of the film was too uneven.

For comparison purposes, the following image (figure 5.13) shows a SnO_2 coating on a silica substrate. The coating was applied by solvent casting, and was not annealed. The average distance between the highest and lowest regions in the image (not including the cracked area) was 1170Å. The surface is a lot more uneven than that of the coating applied by spin-coating. This gives more evidence that the coatings produced by spin-coating were superior to those produced by the other coating techniques.

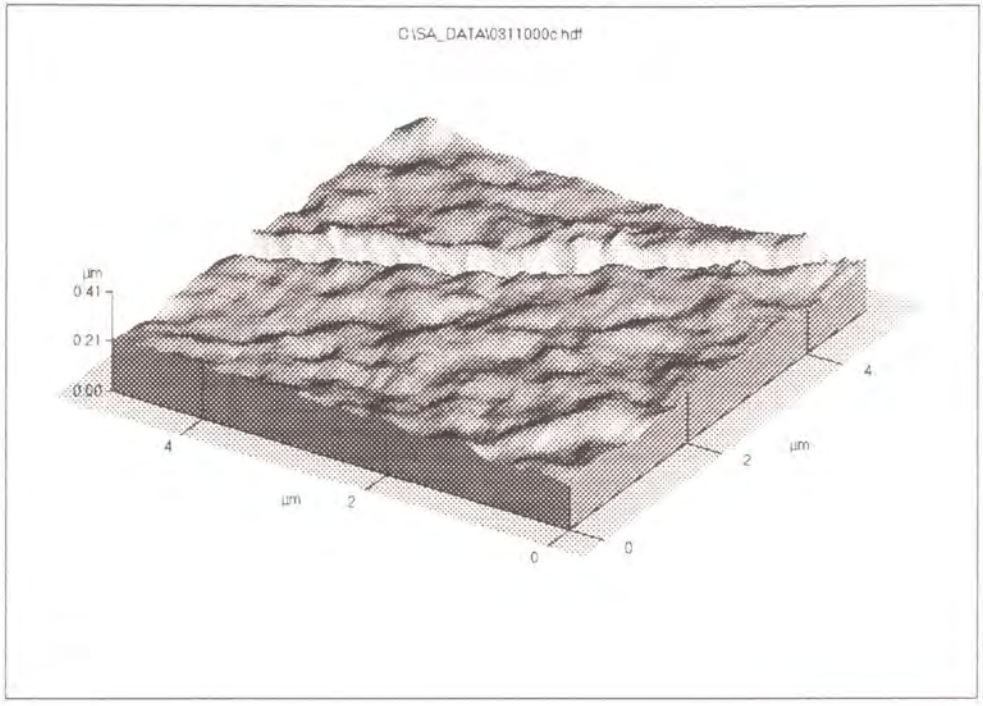

Figure 5.13: AFM Image of SnO_2 Coating on Silica

5.3.3 IR Annealing Results

This section contains the results of experiments carried out using the infrared furnace. As discussed in the introduction, it was hoped that exposing tin oxide coated polymer substrates to short periods of infrared heating would result in an improvement in the conductivities of the tin oxide coatings. The coatings described in this section did not contain coupling agents or surfactants.

The following tables outline the infrared heat treatments given to some coated samples, the number and type of coatings given, some optical microscopic observations of the coatings and the resulting conductivities. The samples described were given several consecutive heat treatments and are representative of infrared heating experiments performed on several tin oxide coated polymer substrates in the infrared furnace.

Sample IR1: *PMMA substrate spin coated with an 8 mol% n-type doped SnO_2 solution (Approximate thickness = 180 nm)*

Table 5.5

Exposure time (seconds)	No. of exposures
2	1
3	1
5	1
8	1
10	1
Observations: Optical microscopic observations (magnification x 40) of the coating at this stage showed that it was very cracked.	
10	3
Observations: It was noticed that the PMMA was beginning to bubble on one side after the last heat treatment. The sample was recoated twice using the spin-coater (1300rpm for 2 minutes). Under the microscope, the coating appeared fairly even but with many small cracks.	
8	2
Observations: Optical microscopy (x40) revealed crazy pavement type cracking, although the cracks appeared very fine. The apparent bulk conductivity was 2.1×10^{-6} Scm^{-1}.	
6	5
Observations: It was noticed that after this further series of flash-heating steps, the silver paint strips had become white and had bubbles. The apparent bulk conductivity was 4.4×10^{-8} Scm^{-1}. More silver paint strips were applied to the coating just inside the previous contacts and the new bulk conductivity was 5.3×10^{-7} Scm^{-1}.	

From the table above describing the heat treatments and results of one sample, it can be seen that cracking occurred from the early stages of heating. It was hoped that by re-coating the sample between heat treatments, it would fill in the cracks in the coating. It was also found that the PMMA substrate could withstand about 6 seconds in the infrared furnace before it started to soften. The best conductivity value achieved for the coating was ~2×10^{-6} Scm^{-1}.

Sample IR 2: *polycarbonate spin coated with a 2 mol% n-type doped SnO_2 solution (approximate thickness = 200nm)*

Table 5.6

Exposure time (seconds)	No. of Exposures
6	1
8	2
Observations: The substrate was then recoated 10 times by spin-coating.	
8	2
Observations: The polycarbonate had started to show signs of melting on one side.	
6	3
2	1
4	1
6	1
7	1
Observations: The sample was recoated 10 times by spin-coating.	
6	5
Observations: The apparent conductivity was 7.5×10^{-5} Scm^{-1}. Optical microscopy showed that the coating was cracked.	
2	1
4	1
5	1
6	2
Observations: The conductivity was 5.7×10^{-7} Scm^{-1}.	
6	4
Observations: At this stage, the silver paint strips appeared white with bubbles. New silver paint strips were applied, and the conductivity was 3.2×10^{-6} Scm^{-1}.	

IR3: *polycarbonate substrate spin-coated with a 1 mol% n-type doped SnO_2 solution (approximate thickness = 200nm)*

It was decided to try annealing a coated polymer sample several times before measuring its resistance in order to avoid the problem with heating of the silver paint electrodes. Sample

IR3 was heated 30 times for 8 seconds, allowing two minutes in between heating periods for the polymer to cool down. Looking at the coating under the microscope (magnification x 40) after the heat treatments showed that it was extremely cracked. The apparent bulk conductivity of the coating was about 5.2×10^{-7} Scm^{-1}.

Heat treatments using PET Substrates

Attempts were made to heat SnO_2 coatings on PET substrates using the infrared furnace. Unfortunately, even when using very mild conditions (2 second heating), this resulted in buckling of the polymer substrates.

It was apparent that there was a problem due to the cracking of the tin oxide coatings on the polymer substrates. This must be partly caused by the mismatch of thermal expansion between the polymers and the inorganic tin oxide thin films. The coefficients of thermal expansion for polycarbonate and indium oxide are 3.9×10^{-5} $°C^{-1}$ and 7.2×10^{-6} $°C^{-1}$ respectively so the heated films were under tension[4]. Another factor which probably contributed to the cracking problem was that of capillary forces as the gel was drying[24]. This is a common phenomenon with drying of sol-gel products and it occurs as the liquid evaporates from the pores and it exerts a stress on the surrounding gel network, which can cause fractures in the coatings. One way of avoiding capillary force problems is to use supercritical drying to dry the gels but this was not within the scope of our project.

It was decided to try and use filters above the samples in the IR furnace in order that only the tin oxide would get heated. From section 5.1.4 in the introduction, it was proposed that germanium might be a suitable filter. However, on heating the polished germanium substrates for just 4 seconds in the furnace, they became very brittle, and cracked immediately on cooling. The other idea for a filter was to place a thicker piece of PET above the substrate, with an air-gap separating them. This also did not work very well because the polymer filter heated up inside the furnace, bent and proved difficult to remove from the furnace.

More results of infrared annealing are given in the next two sections of this chapter.

5.3.4 Results of Adding Coupling Agents

As outlined in section 5.1.2 of the introduction, coupling agents were added to improve the adhesion of the n-type tin oxide coatings on the polycarbonate substrates. Table 5.7 below outlines the coating experiments carried out using coupling agent solutions (see section 5.2.2 for their preparation).

Table 5.7

Expt. No.	Coating Solution(s)	Method of Coating	Observations
1	(1) Soln. C* (2) SnO_2 (n-type doping = 8%)	Solvent evaporation	(1) Transparent Coating (2) Cloudy blotchy coating
2	(1) Soln. E* (2) SnO_2 (n-type doping = 8%)	Solvent evaporation	(1) Transparent Coating (2) Uniform coating with cloudy region in middle
3	Soln. I* (n-type doping = 2%)	Solvent evaporation	Uniform coating which is slightly opalescent
4	Soln. I* (x2) (n-type doping = 5%)	Spin-coating	Transparent Coating
5	(1) Methanol (2) Soln. F* (3) SnO_2 (n-type doping = 2%)	Solvent evaporation	(1) No effect on surface (2) Thin transparent film (3) Blotchy coating
6	(1) Soln. G* (2) SnO_2 (n-type doping = 5%)	Solvent evaporation	(1) Transparent coating (2) Uneven blotchy coating
7	Soln. J* (n-type doping = 5%)	Spin-coating	Very cracked coating
8	Soln. I* (x8) (n-type doping = 2%)	Spin-coating	Transparent coating
9	Soln. K* (n-type doping = 3%)	Spin-coating	Transparent coating

* To remind the reader, solns. C, E, F, G, I, J and K were the following mixtures:

Soln. C: IPA (5ml) and $SnCl_4$ (0.5ml); ***Soln. E:*** IPA (3ml) and $MeSiCl_3$ (80μL); ***Soln. F:*** Methanol (3ml) and $MeSiCl_3$ (80μL); ***Soln. G:*** IPA (3ml) and $Allyl(OMe)_3Si$ (80μL):); ***Soln. I:*** Soln. E (80μL) and 5% n-typed doped SnO_2 (2ml); ***Soln. J:*** Soln. G (0.5ml) and 5% n-type doped SnO_2 (3ml): ***Soln. K:*** Soln. E (180μL) and 3% n-type doped SnO_2 (4ml).

Overall, it can be seen from the table that the spin-coated samples gave more promising results. Of the coatings which were cast from solution, experiment 3 which used solution I was the most successful i.e. it gave the most uniform and transparent coating.

Infrared heating was given to four of the above coated polymers (experiments numbered 2, 4, 8 and 9). The following table shows the infrared treatment given, additional heat treatments (where applicable) and the resulting conductivities for the tin oxide coatings.

Table 5.8

Expt. No.	Coating Solution(s) used	IR* and Heat Treatments	Bulk Conductivites
2	(1) Soln. E (IPA + $MeCl_3Si$) (2) SnO_2 soln. (n-type doping = 8%)	IR x 4 exposures	$< 1 \times 10^{-8}$ Sm^{-1}
4	Soln. I (IPA + $MeCl_3Si$ +tin oxide soln. with 5% n-type doping)	IR x 6 exposures	2.9×10^{-4} Sm^{-1}
8	Soln. I (IPA + $MeCl_3Si$ +tin oxide soln. with 5% n-type doping)	(1) 1hour @ 50°C under vacuum (2) IR x 9 exposures	5.0×10^{-5} Sm^{-1}
9	Soln. K (IPA + $MeCl_3Si$ + tin oxide soln. with 3% n-type doping)	(1) 1 hour @ 80°C under vacuum (2) IR x 10 exposures	$< 1 \times 10^{-8}Sm^{-1}$

* The infrared treatments were for 6 seconds after preheating the lamp for 2 seconds.

As can be seen from the table, the best results were obtained for the samples containing coupling agent solution I (experiments numbered 4 and 8), with conductivities of 2.9×10^{-4} Sm^{-1} and 5.0×10^{-5} Sm^{-1} respectively. The coating solution used for both these samples was

a tin oxide colloid containing a very small amount of methyl trichlorosilane dissolved in isopropanol. It was found that overall, the best results were obtained when the coupling agent was applied to the surface of the substrates as part of the tin oxide coating solution i.e. when the coupling agent was partially hydrolysed.

By comparison of the conductivity results with those in the previous section of this report for samples which did not contain coupling agents, it can be seen that the addition of the coupling agents was capable of producing a substantial improvement in the surface conductivities. This was due to the reduction in cracking due to the coupling agent.

Optical microscopic observations of samples 4 and 8 showed that they were extremely uniform with no cracks. To remind the reader, samples 4 and 8 were polycarbonate substrates coated with antimony doped tin oxide solutions containing a very small amount of methyl trichlorosilane dissolved in isopropanol. Adhesion tests were carried out on the coatings by applying sellotape to the coatings and pulling it away quickly. No damage was observed in the coatings by the naked eye and only minimal damage was seen under a magnification of 30 times with an optical microscope. Figure 5.14 shows the area of a coating which had been tested by this method.

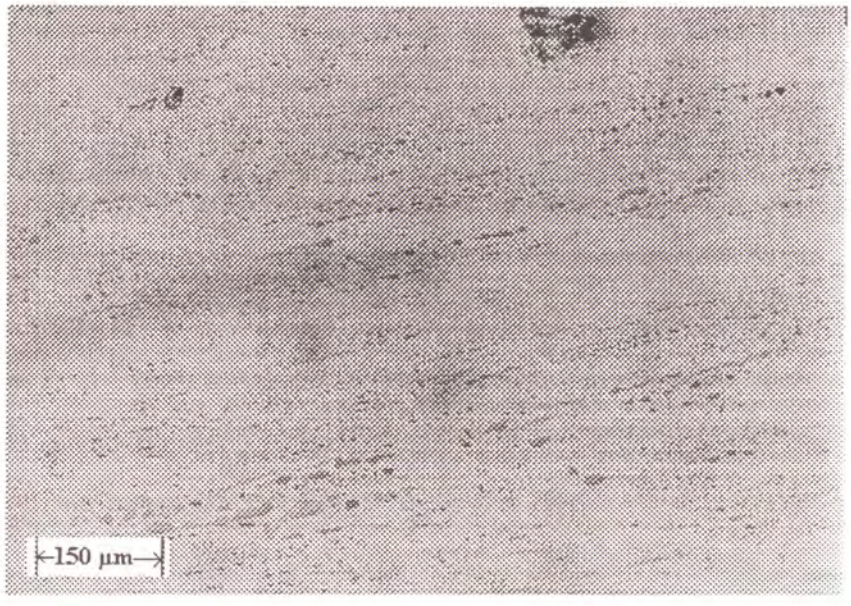

Figure 5.14: Adhesion Test Area

5.3.5 X-Ray Diffraction Results

In order to assess if the infrared heat treatment was having a positive effect on the microstructure of the tin oxide, it was decided to use XRD to investigate whether any changes had occurred in the crystallinity of the tin oxide coatings and tin oxide powder. As described in section 5.2.9 of the experimental, many samples were run in the XRD. It was hoped to compare coated and uncoated samples, and unannealed and infrared annealed samples.

The diffractograms of Kaladex (coated and uncoated) all had the same features, the only difference being that the intensities of the peaks on the uncoated polymer were far greater than on the coated ones. There was no discernible difference between the unannealed and annealed samples. The reason why the coated substrates did not show any sign of tin oxide was apparently that major Kaladex peaks roughly coincide with the main tin oxide reflections. Three diffractograms were recorded of IR-annealed tin oxide coatings on borosilicate slides. They all had a very flat baseline with little evidence of peaks.

It appears that there was not enough SnO_2 on the surface of the above samples to give appreciable X-ray scattering. The diffraction pattern of an air-dried tin oxide powder (sample 5) was recorded, and the powder (still in the XRD sample holder) was exposed to IR treatment (sample 6). For the unannealed sample, the three main characteristic peaks of cassiterite SnO_2 are identifiable, although it is essentially amorphous (see figure 5.15). The diffractograms of the infrared annealed material shows the same characteristic peaks, but they are noticeably more defined and less amorphous in appearance, and all the d-spacings are slightly diminished (figure 5.16). The Scherrer equation was used to calculate the mean crystallite size using the hkl line [100] and it was found that the crystallite size increased from 2.57nm to 5.22 nm as a result of infrared heat treatment.

These results above provide evidence that the thermal conditions achieved in pulsed IR treatment of amorphous tin oxide can cause some increase in crystallinity. Although this applied to the powder sample, it is encouraging because metal oxides are generally much better thermal conductors than are polymers, and so it was expected to be difficult to attain suitable temperatures for annealing in the bulk material.

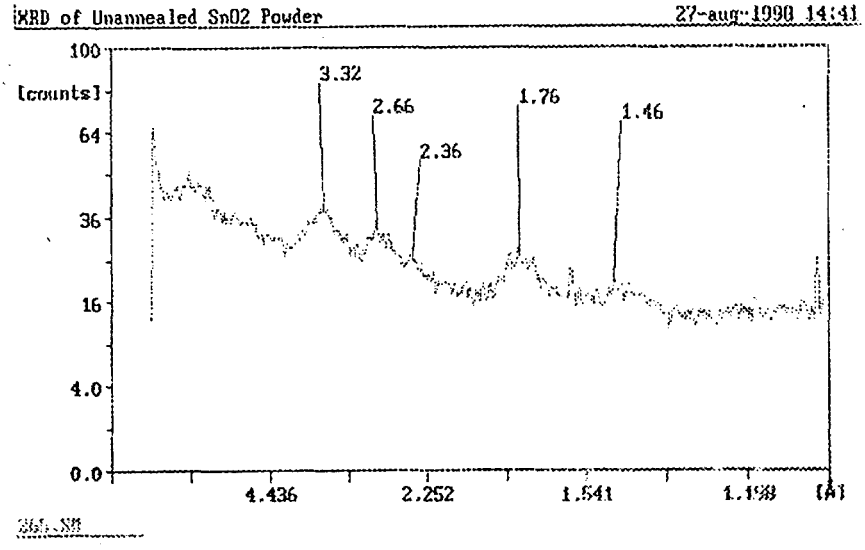

Figure 5.15: XRD of Unannealed SnO_2 Powder

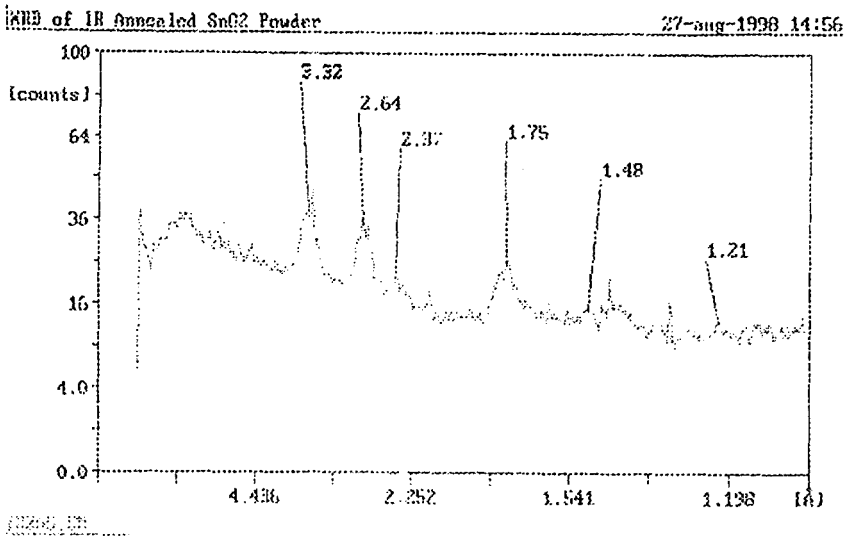

Figure 5.16: XRD of IR Annealed SnO_2 Powder

5.3.6 UV/Visible Absorbance of Coatings

The percentage transparencies of the tin oxide coatings on the polymers remained very high for all samples, over 90%. This applied even to the coatings which were infrared annealed or contained coupling agent additives. The figure below shows an example of the UV/visible spectra obtained for the SnO_2 coated polymers.

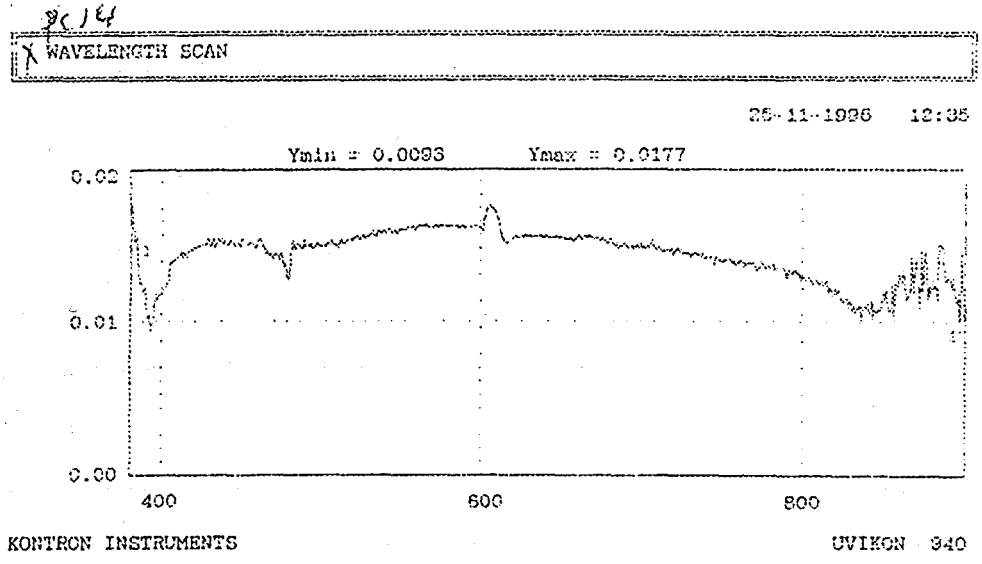

Figure 5.17: UV/visible Spectrum of SnO_2 Coating on Polycarbonate

5.4 Conclusions

Tin oxide was applied to polymer substrates using spin-coating, solvent evaporation and spray coating techniques. It was found that spin-coating gave the most uniform films.

To improve the adhesion and wetting of the tin oxide coatings, surfactants and coupling agents were added to the some tin oxide coating solutions. The addition of a non-ionic surfactant did not cause a decrease in the surface tension of the tin oxide solutions. The addition of coupling agents caused better adhesion, and this resulted in less cracked coatings and a small increase in the conductivities.

An infrared furnace was used to heat the tin oxide on the polymer substrates. The heating effect of the furnace did not improve the conductivities of the coatings. However, the annealing ability of the infrared furnace was shown through heating tin oxide powder and analysing the crystallinity increase by X-ray diffraction.

The percentage transparencies of the tin oxide coatings on polymers were very high for all samples (over 90%).

References

1. T. Minami, H. Sonahara, T. Kakumu, S. Takata, *Thin Solid Films,* **270** 37 (1995)
2. B-S. Chiou, S-T. Hsieh, W-F. Wu, *J. Am. Ceram. Soc.,* 77 1740 (1994)
3. A. Mukherjee, *Vacuum* **39** 537 (1989)
4. J. Grozdanov, *Syn. Metals,* **63** 213 (1994)
5. W-F Wu., B.-S. Chiou, *Applied Surface Sci.,* **99** 237 (1996)
6. R. Mijuntani, Y. Oono, J. Matsouka, H. Nasu, K. Kamiya, *J. Mat. Sci.,* **29** 5773 (1994)
7. M. J. Schick, *Nonionic Surfactants, Surfactant Science Series, Volume 1,* Edward Arnold Publishers (Ltd.), London (1967)
8. G. Pritchard, *Polymer Additives,* Chapman and Hall, London (1998)

9. C. A. Daniels, *Polymers: Structure and Properties,* Technomic Publishing Company Inc. (1989)

10. D. Ganz, G. Gasparro, J. Otto, A. Reich, N. J. Arfsten, M. A. Aegeter, *J. Mat. Sci. Letters,* **16** 1233 (1997)

11. D. Ganz, A. Reich, M. A. Aegeter, *J. Non-Cryst. Solids,* **218** 242 (1997)

12. U. Neta, V. Richter, R. Kalish, *Mat. Res. Soc. Symp. Proc.,* **92** 273 (1987)

13. G. Bashkov, K. Kolentsov, L. Yousukova, A. Rachkova, D. Mateava, *Mat. Sci. and Engineering,* **B30** 1 (1995)

14. G. Prasad, O. N. Srivastava, *Semicond. Sci. Tech.,* **8** 2161 (1993)

15. J. H. R. Page, *J. Material Engineering and Performance,* **4** 418 (1995)

16. A. Usami, Y. Tokuda, M. Katayama, S. Kaneshima, T. Wada, *J. Phys. Appl. Phys.,* **19** 1079 (1079)

17. N. Zabala, J. M. Barandiarán, *J. Phys. D: Applied Physics,* **28** 2607 (1995)

18. P. Gorria, I. Orue, F. Plazaola, J. M. Barandiaran, *J. Appl. Phys.,* **73** 6600 (1993)

19. C. Morón, M. C. Sánchez, E. López, P. Sánchez, C. Aroca, *J. Magnetism and Magnetic Materials,* **101** 59 (1991)

20. T. Jagielinski, *IEEE Transactions on Magnetics,* **19** 59 (1983)

21. T. Kulik, H. Matyja, *Materials Sci. and Eng.* **A133** 232 (1991)

22. T. Kulik, D. Bulik, H. Matyja, *J. Mat. Sci. Letters,* **12** 76 (1993)

23. J. H. Clint, *Surfactant Aggregation,* Chapman and Hall, New York (1992)

24. C. J. Brinker, G. C. Frye, A. J. Hurd, C. S. Ashley, *Thin Solid Films,* **201** 97 (1991)

6.1 Main Conclusions

This chapter summarises the principal findings of the current study and outlines some additional suggestions for future research.

1. Initially, known method of preparing tin oxide by a sol-gel process was used, in which the starting precursor was tin (IV) tetrachloride. Some variations were made in the procedure, and XRD analysis confirmed that cassiterite tin oxide was produced. However, the method was very time consuming and the resultant tin oxide was partially opaque and did not adhere well to glass.

2. A novel sol-gel process for the production of tin oxide was developed in which tin bis (acetylacetonate) dichloride was the main precursor. Again, XRD analysis confirmed the products were cassiterite tin oxide. P-type and n-type dopants (indium and antimony respectively) were added to the tin oxide at the beginning of the sol-gel process to effect ion concentrations of up to 13%.

3. Doped and undoped tin oxide was applied to glass and silica substrates using solvent casting and dip-coating techniques. Some of the samples were annealed, and van der Pauw measurements of the conductivity showed that annealing at 400°C caused an increase of about 4 orders of magnitude in the conductivity. However, annealing caused the percentage transparency of the tin oxide to decrease from about 80% to 40% over the visible range. It was also established that antimony doping of the tin oxide resulted in higher conductivities than doping with indium. Spectroscopic studies on the indium doped tin oxide revealed that polaronic electronic charges were contributing to its overall conductivity.

4. A method was devised for pre-treating polymer substrates in order to make them more compatible for coating with aqueous based tin oxide coatings. The poly (methyl methacrylate) substrates were treated with sodium hydroxide and the polycarbonate substrates were treated with a combination of short wavelength UV light and ozone gas. Contact angle measurements and subsequent surface energy calculations were used to determine the effect of

these treatments on the polymer surfaces. FTIR diffuse reflectance studies of the pre-treated polycarbonate substrates gave information on the chemical changes occurring on the polymer surfaces as a result of the ozonolysis.

5. The antimony doped tin oxide was applied to the pre-treated polymer substrates by spin-coating, solvent casting and spray coating techniques. Although all of the coatings had a high percentage transparency (greater than 90%), optical microscopic studies showed that spin-coating resulted in the most uniform and crack free films. The addition of a non-ionic surfactant to the coating solutions to increase the affinity between the substrate and the film did not result in a decrease in the surface tension of the solutions. However, the addition of coupling agents to the tin oxide coating solutions caused better adhesion of the coatings on the polymers and slightly improved their conductivity.

6. An infrared furnace was specially built for the purpose of giving short pulses of heat to the tin oxide coatings on the polymer substrates in order to try and anneal the tin oxide coatings and subsequently improve their conductivity with minimum damage to the polymers. Even with the use of filters in the furnace, the polymer substrates were heated and degraded whilst being heated for short periods. However, XRD analyses of tin oxide powder exposed to flash annealing showed that it resulted in a significant increase in the crystallinity of the tin oxide.

6.2 Future Work

1. The amount of acetylacetone remaining in the tin oxide gels could be determined using thermogravimetric analysis hyphenatedly linked to a Fourier transform infrared spectrophotometer. Several analyses could be done during the sol-gel process to determine the loss of acetylacetone and other organic constituents. Better understanding of the roles of residual organics should further improve the consistency of the sol-gel product.

2. Atomic force microscopy could be used on the untreated and treated polymer substrates to compare the effects that the surface treatment has on the surface morphology of the polymers. Even more importantly, the technique could be used to further characterise the micro-cracking of the tin oxide coating and to optimise the effects of coupling agents considerably more.

3. Once more effective coupling has been achieved, to investigate the effects of very short, intense bursts of flash annealing (xenon flash tube or possibly pulsed IR laser irradiation).

4. To carry out more extensive studies on the relationship between the DC conductivity and the doping concentration for the antimony doped tin oxide coatings on glass and silica substrates. To further confirm that polarons contributed to the conductivity of the indium doped tin oxide, the activation energy for the polaron motion could be estimated from transition energies found through spectroscopic means.

5. The conductivity of the tin oxide coatings could be measured at different temperatures. By plotting Ln conductivity versus reciprocal temperature, it allows the calculation of the activation energy for conduction of the tin oxide from the slope of the linear plot.

Appendix 1

Table 1: First $SnCl_4$ Experiments, no dialysis used

Sample no.	3.1(A)	3.2(A)
0.5M $SnCl_4$ (ml)	35	33
10M NH_4OH (ml)	20	30
2M NH_4NO_3 (ml)	10	-
Centrifuged	3500 rpm, 15 mins.	3500 rpm, 10 mins.
Ppt. washed with:	dil. NH_4NO_3 (50ml)	dil. NH_4NO_3 (600ml)
Refluxed	70°C for 15 mins.	70°C for 25 mins.
Result (after air-drying)	white brittle solid, no con.*	white brittle solid, no con.*

* con. = conductivity response from two-probe multimeter

Table 2: Second set of $SnCl_4$ Experiments

Sample no.	4.1(A)	4.2(A)	4.4(A)
1M $SnCl_4$ (ml)	33	19	19
6M NH_4OH (ml)	30	120	-
0.6M NH_4OH (ml)	-	-	465
Centrifuged	3500 rpm, 10 mins.	-	-
Dialysis duration	1 month	3 weeks	3 weeks
Refluxed	40°C for 10 mins.	added 0.06g $InBr_3$, 70°C for 30 mins.	added 0.04g $InBr_3$, 70°C for 15 mins.
Result (after air-drying)	crystallized white solid, no con.	semi-transparent coating, some con.	Powdery white solid, no con.

Table 3: $SnCl_4$ Experiments, varying concentration of NH_4OH

Sample no.	5.1(A)	5.2(A)	5.3(A)	5.4(A)
1M $SnCl_4$ (ml)	19	19	19	19
8M NH_4OH (ml)	50	-	-	-
0.6M NH_4OH (ml)	-	600	600	-
Centrifuged	3500 rpm, 10 mins.	3500 rpm, 10 mins.	3500 rpm, 10 mins.	3500 rpm, 10 mins.
Dialysis duration	30	3 weeks	2 months	4 weeks
Refluxed	Added 0.1g $InBr_3$, 70°C for 15 mins.	Added 0.06g $InBr_3$, 70°C for 15 mins.	Added 0.1g $InBr_3$, 60°C for 15 mins.	Added 0.02g $InBr_3$, 60°C for 1 hour
Result (after air-drying)	Particulate coating, no con.	Particulate coating, no con.	white glassy solid, no con.	white glassy solid, no con.

Table.4: First Series of $Sn(acac)_2Cl_2$ Experiments

Sample no.	1.1	1.2	1.3	1.4	1.5	1.6	1.7	1.8	1.9
$Sn(acac)_2Cl_2$ (g)	0.25	0.25	0.25	0.25	0.25	0.25	0.25	0.25	0.25
Acetone (ml)	10	10	10	10	10	10	10	10	10
H_2O (ml)	1	2	1	3	4	5	6	7	8

Table 5: Repeating Sample 1.7 with Some variations

Sample no.	3.1	3.2	3.3	3.4	3.5
$Sn(acac)_2Cl_2$ (g)	0.76	0.26	0.25	0.25	0.25
Acetone (ml)	30	10	10	10	10
H_2O (ml)	18	5.5	6	6.5	6

Table 6: Experimenting with Different Solvents

Sample no.	4.1	4.2	4.3	4.4	4.5
$Sn(acac)_2Cl_2$ (g)	0.20	0.23	0.25	0.28	0.30
Acetone (ml)	10	10	10	10	10
H_2O (ml)	6	6	6	6	6
Ethanol (ml)	10	-	-	10	10
NH_4OH (ml)	-	-	60	-	-
Ultrasonic bath (mins.)	-	-	10	-	-

Table 7: Initial Experiments adding P-type Dopant (Indium)

Sample no.	6.1	6.2	6.3	6.4	6.5	6.6
$Sn(acac)_2Cl_2$ (g)	2.502	2.5076	1.2518	0.4492	0.5097	0.4427
$InBr_3$ (g)	-	-	0.2606	0.01	0.0364	0.0656
~ % doping (mol %)	-	-	22	2	8	16
Acetone (ml)	100	100	50	20	20	20
H_2O (ml)	60	60	15	6	6	6
Ultrasonic bath (mins.)	15	-	10	-	-	-
Centrifugation	-	3500rpm for 10 mins.	-	-	-	-

Table 8: Initial Experiments Adding Indium as 1% In Br_3 in Water (w/v)

Sample no.	9.1	9.2	9.3	9.4	9.5
$Sn(acac)_2Cl_2$ (g)	0.5	0.5	0.5	0.5	0.5
1% $InBr_3$ (ml)	0.46	0.91	1.37	1.84	2.3
Doping conc. (mol %)	1	2	3	4	5
Acetone (ml)	20	20	20	20	20
H_2O (ml)	12	12	12	12	12
Rotary Evaporation	5 mins. @ 30°C	5 mins. @ 30°C	5 mins. @ 30°C	5 mins. @ 30°C	5 mins. @ 30°C

Table 9: Samples Prepared with p-type Dopant

Sample no.	11.1	11.2	11.3
$Sn(acac)_2Cl_2$ (g)	0.5	0.5	0.5
1% $InBr_3$ (ml)	0	2.73	3.22
Acetone (ml)	20	20	20
H_2O (ml)	12	9.27	8.78
Doping conc. (mol %)	0	6	7

Table 10: Samples Prepared with p-type Dopant

Sample no.	13.0	13.1	13.2	13.3	13.4	13.5	13.6	13.7
$Sn(acac)_2Cl_2$ (g)	0.5	0.5	0.5	0.5	0.5	0.5	0.5	0.5
1% $InBr_3$ (ml)	0	0.46	0.91	1.37	1.84	2.3	2.73	3.22
Acetone (ml)	20	20	20	20	20	20	20	20
H_2O (ml)	12	11.54	11.09	10.63	10.16	9.7	9.27	8.78
~ Doping conc. (mol %)	0	1	2	3	4	5	6	7

Table 11: Addition of n-type Dopant in the form of 1% $SbBr_3$ in Acetone (w/v)

Sample no.	19.0	19.1	19.2	19.3	19.4	19.5	19.6
$Sn(acac)_2Cl_2$ (g)	2	2	2	2	2	2	2
1% $SbBr_3$ (ml)	0	2.14	4.28	6.42	8.56	10.7	12.84
Acetone (ml)	100	100	100	100	100	100	100
H_2O (ml)	60	60	60	60	60	60	60
~Doping conc. (mol %)	0	1	2	3	4	5	6

Table 12: Samples Prepared for Viscosity Measurements

Sample no.	12.5	14.1	17.3	18.3
$Sn(acac)_2Cl_2$ (g)	10	10	10	10
1% $InBr_3$ (ml)	40	40	-	-
Acetone (ml)	200	200	200	200
H_2O (ml)	240	240	240	250
~ Doping conc. (mol %)	5	5	-	-
Conditions	Waterbath at 26°C	Waterbath at 26°C	Waterbath at 26°C	Waterbath at 26°C

Table 13: Samples prepared with n-type doping

Sample no.	$Sn(acac)_2Cl_2$ (g)	1% $SbBr_3$ in acetone (ml)	Acetone (ml)	H_2O (ml)	Doping conc. (% molarity)
20.1a	2.0	2.14	18.86	30	1
20.2a	2.0	4.28	15.72	30	2
20.3a	2.0	6.42	13.58	30	3
20.4a	2.0	8.56	11.44	30	4
20.5a	2.0	10.70	9.30	30	5
20.6a	2.0	12.84	7.16	30	6
20.7a	2.0	14.98	5.02	30	7
20.8a	2.0	17.12	2.88	30	8

Table 14: Samples prepared with n-type doping

Sample no.	$Sn(acac)_2Cl_2$ (g)	1% $SbBr_3$ in acetone (ml)	Acetone (ml)	H_2O (ml)	Doping conc. (Atomic %)
21.0	2.0	0	20	30	0
21.1	2.0	2.14	18.86	30	1
21.2	2.0	4.28	15.72	30	2
21.3	2.0	6.42	13.58	30	3
21.4	2.0	8.56	11.44	30	4
21.5	2.0	10.70	29.3	30	5
21.6	2.0	12.84	27.16	30	6
21.7	2.0	14.98	25.02	30	7
21.8	2.0	17.12	22.88	30	8
21.9	2.0	19.26	20.74	30	9
21.10	2.0	21.4	28.6	30	10
21.11	2.0	23.54	26.46	30	11
21.12	2.0	25.68	24.32	30	12
21.13	2.0	27.82	22.18	30	13

Table 15: Samples prepared with n-type doping

Sample no.	$Sn(acac)_2Cl_2$ (g)	1% $SbBr_3$ in acetone (ml)	Acetone (ml)	H_2O (ml)	Dopant conc. (Atomic %)
22.0	2.0	0	40	30	0
22.1	2.0	2.14	38.86	30	1
22.2	2.0	4.28	35.72	30	2
22.3	2.0	6.42	33.58	30	3
22.4	2.0	8.56	31.44	30	4
22.5	2.0	10.70	29.30	30	5
22.6	2.0	12.84	27.16	30	6
22.7	2.0	14.98	25.02	30	7
22.8	2.0	17.12	22.88	30	8
22.9	2.0	19.26	20.74	30	9

Table 16: Samples Prepared for Coulter Counter Measurements

Sample no.	Doping conc. (atomic %)	$Sn(acac)_2Cl_2$ (g)	1 % $SbBr_3$ in acetone (ml)	Acetone (ml)	H_2O (ml)
23.2A	2	2.0	4.28	35.72	30
23.2B	2	2.0	4.28	35.72	30
23.3A	3	2.0	6.42	33.58	30
23.3B	3	2.0	6.42	33.58	30
23.4A	4	2.0	8.56	31.44	30

Appendix 2

Surface Profiling Images

The surface profile images below display the edge of the SnO_2 coatings. The thickness of the coatings were taken as the average of the thicknesses between areas "a" and "b".

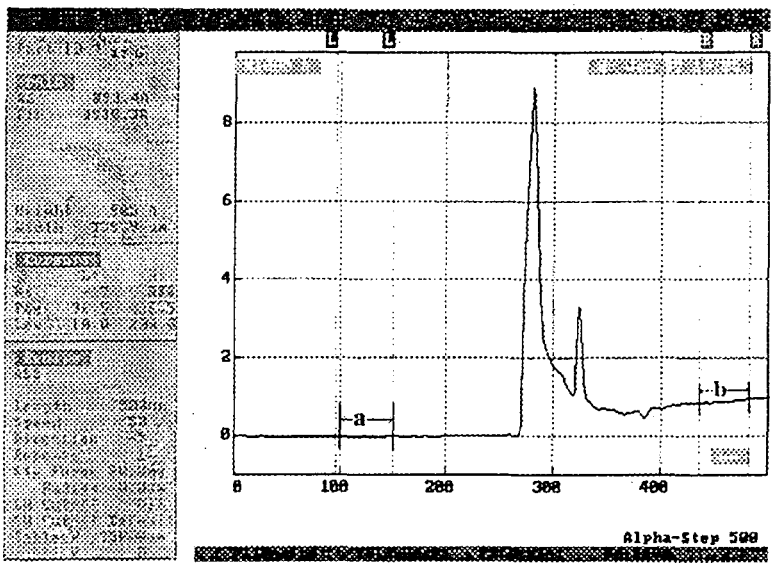

Edge of SnO_2 Coating on Silica

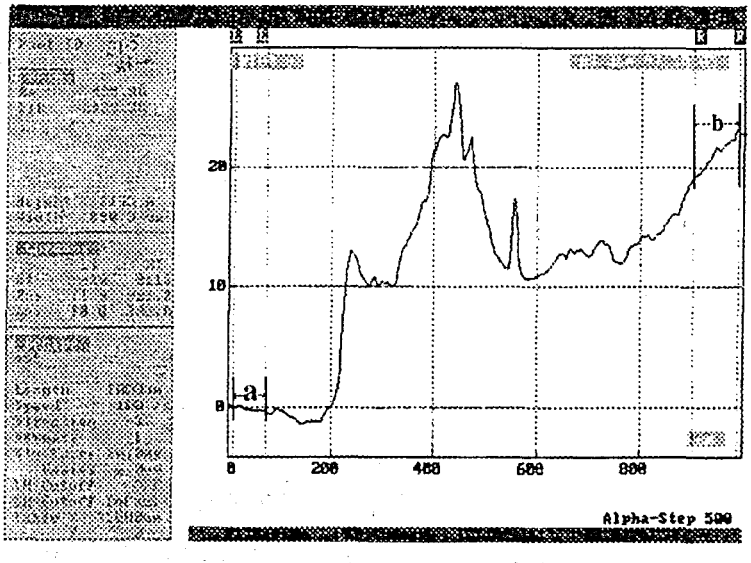

Edge of SnO_2 Coating on Silica

Calculating the Thickness of a Thin Film from Interference Patterns

To calculate the thickness of the thin film from an interference pattern, two peaks are chosen and their wavelengths determined (see the figure below which shows a schematic diagram of part of a UV/visible spectrum).

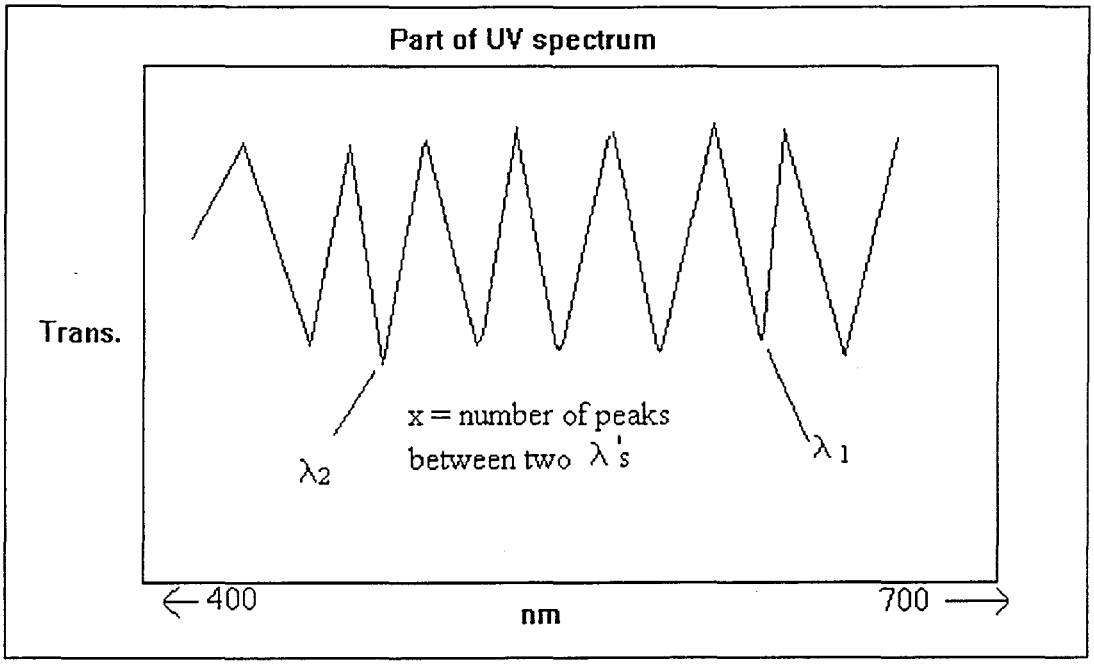

Part of a UV/visible Spectrum

Using the two wavelengths and the number of peaks between the wavelengths the following simultaneous equations[19] can be used to calculate the thicknesses of the films.

$$2nt = (m+\tfrac{1}{2})\lambda_1$$

$$2nt = (m+x+\tfrac{1}{2})\lambda_2$$

where $\lambda_1 > \lambda_2$

n = refractive index, approximately 2

t = thickness of thin film (cm)

λ = wavelength (cm)

m = constant

x = no. of peaks between two chosen wavelengths

UV/visible Spectrum Showing an Interference Pattern

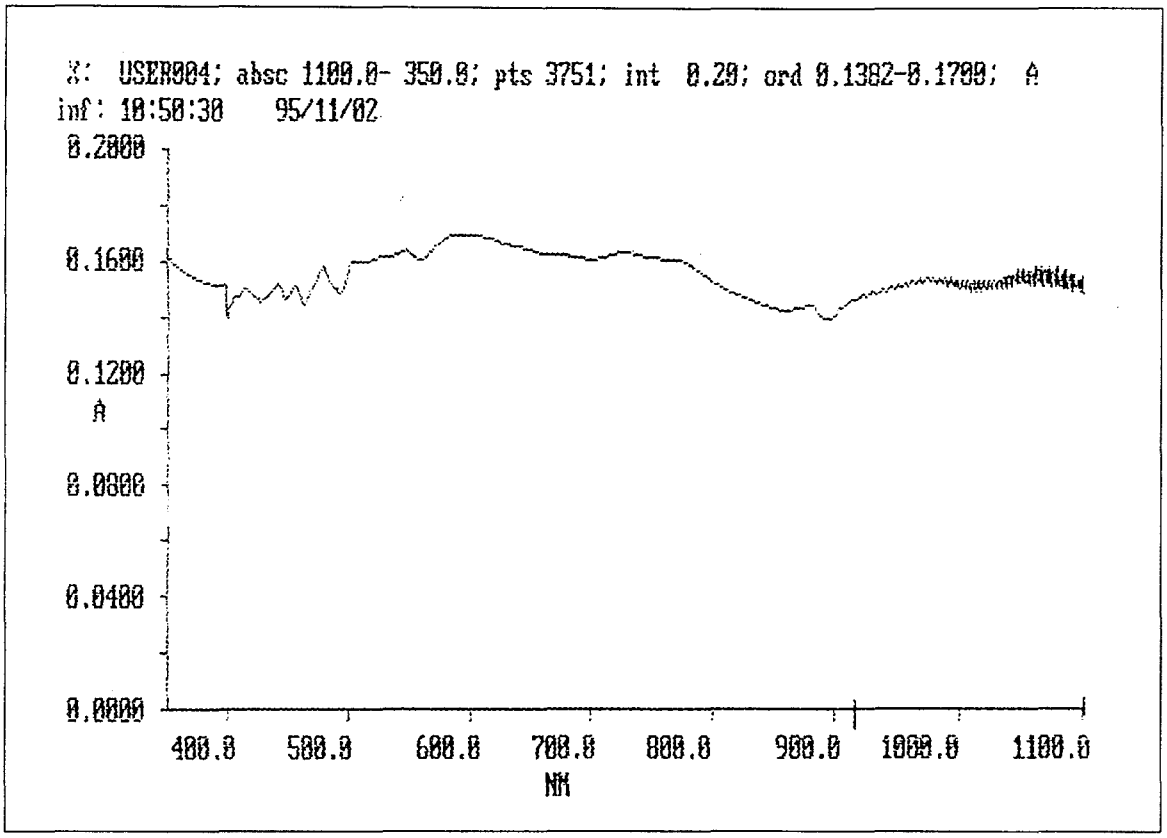

Calculation of Thickness from ICP-AES Analyses

A specimen calculation follows for a sample which had a tin content of 0.336ppm.

Total tin present = 5.38×10^{-6}g (0.336ppm x 16 since the total volume was 16ml)

Moles of Sn = 4.53×10^{-8}

Moles of O_2 = 9.06×10^{-6}

Mass of O_2 = 1.45×10^{-6}

Total Mass = 6.83×10^{-6} (mass of O_2 + mass of tin)

Volume = Mass/Density (density of SnO_2 = 6.95)

therefore volume = $6.83 \times 10^{-6}/6.95 = 9.82 \times 10^{-7}$

Volume = length (0.58cm) x breadth (0.66cm) x height/thickness (unknown)

Thickness = $9.82 \times 10^{-7}/0.58 \times 0.66 = 2.57 \times 10^{-6}$cm

The thickness measurement was then used in the calculation of the DC conductivity.

Appendix 3

Diagram of Infrared Furnace